THE UNIVERSITY *of* EDINBURGH

The Mechanical Properties of Phospholipid Coated Microbubbles

Julia Kathleen Morris

THE UNIVERSITY *of* EDINBURGH

Doctor of Philosophy
The University of Edinburgh
2014

Lay Summary

Tiny, gas-filled spheres, or microbubbles (MBs), are commonly used in medical clinics as contrast agents to improve the quality of diagnostic ultrasound images. The presence of MBs allows us to image very small vascular structures by improving the contrast between the boundary of the blood vessels and the surrounding tissue. Contrast agent MBs have developed from being simple air bubbles with hard coatings of materials like albumin, to the current products which are filled with large-molecule gases (compared to air) and soft coatings of phospholipid molecules.

Cell membranes are mostly made up of phospholipids, so they make an excellent MB coating material which is happily accepted by the body and which can be easily removed by the kidney when they are no longer useful. A MB is several microns in diameter (the smallest blood vessels are about 4 microns wide) but the phospholipid coating is much smaller, less than 5 nanometres thick. There is much interest in re-purposing these MBs for other tasks, such as targeted drug/gene delivery and uptake which would potentially allow diseases which have a localised site, like a tumour, to be treated directly in the affected area; this could greatly reduce the dosage of powerful drugs required for treatment and reduce side effects.

While a great deal is known about how MBs behave under ultrasound, much less is known about their response to direct mechanical loading, and it is this knowledge gap that this thesis seeks to address. In order to investigate the mechanical behaviour of these tiny structures, we need a technique which allows us to work on the

nanoscale. An atomic force microscope, or AFM, is well suited to this task. The AFM uses a small beam, or cantilever, which is of a similar size to a human hair, to compress the MB and monitors its response. The loads are very small, down to pico newtons, and very precisely controlled.

In this thesis, the AFM is used to investigate the mechanical properties of three different types of phospholipid coated MBs: Definity®, BR14 and Sonovue®. The MBs are individually compressed with a cantilever quite slowly, and the resulting AFM data is used to create force-distance curves which show how the MB responds to the load applied by the cantilever. This data is used in conjunction with mathematical models which predict how the MB deforms as it is loaded to estimate the Young's modulus of the MB. The models used in this study are the Reissner model, the Hertz model, Elastic membrane theory and De Jong theory; these models all have different assumptions and are theoretically applicable at different levels of MB deformation. We find that at higher deformations, the elastic membrane theory can be used but that at very small deformations, further work is needed to develop a suitable model.

Abstract

Phospholipid coated, inert gas filled microbubbles (MBs) are currently in widespread use in medical applications for the enhancement of diagnostic ultrasound images, and they are promising candidates for use in the area of targeted drug/gene delivery and uptake. As phospholipid coated MBs were developed for use with diagnostic ultrasound, their behaviour under acoustic loading is well investigated, however much less is known about their response to direct mechanical loading, which will potentially prove important as the range of uses of MBs expands. This is particularly true of the existing commercially available MB products. In this thesis, atomic force microscopy (AFM) was used to investigate the mechanical behaviour of three types of commercially produced phospholipid coated MBs, Definity®, BR14 and Sonovue®, at small deformations. Force spectroscopy was used to produce force-deformation (F-Δ) curves showing how the MBs deform under mechanical loading. Definity® MBs were deformed with tipless cantilevers at high deformations (though still less than 30% of the initial height of the MB); BR14 and Sonovue® MBs were probed with both tipless and tipped cantilevers to investigate both whole-bubble deformation and also shell indentation. BR14 was limited to low deformations; Sonovue® included both low and high deformations. The F-Δ curves were used to evaluate MB stiffness and also in combination with up to four mechanical models to predict the Young's modulus of the MBs. The suitability of Reissner, Hertz, Elastic Membrane and De Jong theories for the prediction of the Young's modulus of the MBs was explored.

In the case of Definity® MBs no correlation between MB size and stiffness was observed; however an unexpected size dependence was observed in the Young's modulus values, possibly due to variations in the thickness of the phospholipid shell. The membrane stretching component of elastic membrane theory was found to be the most applicable model on these MBs in this higher deformation regime. However, in this regime, gas compressibility could play a role and this is not included in the model.

We studied the mechanical properties of BR14 MBs at very low deformations using 'soft' cantilevers. In this regime, gas compressibility should play a minimal role and there are several mechanical models which may be used. These MBs demonstrated decreasing stiffness with increasing diameter, and little variation in Young's modulus with diameter. Hertz and De Jong theories showed more realistic Young's modulus values (compared to other models) with little observable trend.

Sonovue® MBs were used for a more comprehensive study of the small and very small deformation regimes using 'soft', 'hard' and tipped cantilevers. They showed no definitive trend in MB stiffness with MB diameter. Hertz and De Jong theory were again found to be most suitable. Analysis of curves acquired with tipped cantilevers indicated that the stiffness of a localised area of the shell membrane is similar to the overall stiffness of the MB and that the apparent Young's modulus of the membrane according to the Hertz theory is also similar to that of the MB as a whole.

Generally, considering all systems, Reissner theory was found to produce large overestimates of Young's modulus, exceeding expected values by several orders of magnitude. Hertz and De Jong theories produced underestimates, though by a much smaller margin. Elastic membrane theory worked well and produced realistic Young's modulus values only at relatively high deformation (the stretching term) in spite of the fact that gas compressibility is not taken into account. The suitability of the models is therefore very dependent on the deformation regime of the experiment. It seems that there is scope for better models at low deformation taking into account the soft shell of the MB and possibly its specific structure. Precise structural information of the MB shells does not exist; it is not trivial to attain and should certainly be a topic of future work with additional instrumentation.

Declaration

I declare that this thesis was composed by myself, that the work contained herein is my own except where explicitly stated otherwise in the text, and that this work has not been submitted for any other degree or professional qualification except as specified.

Work which has formed part of jointly authored publications has been included in this thesis as the basis of Chapter 4. Experimental work for this chapter was carried out by Dr. Emmanouil Glynos. Preliminary data analysis was carried out by Evelyn Buchner-Santos. Principal data analysis and all data interpretation were completed by me. Appropriate credit has been given within the thesis where reference has been made to the work of others

(*Julia Morris*)

Related Publication:

Buchner-Santos, E, Morris, JK, Glynos, E, Sboros, V & Koutsos, V. Nanomechanical properties of phospholipid microbubbles. Langmuir. 2012, 28, 13; 5753-5760. DOI: 10.1021/la204801u

Acknowledgments

This thesis could not have been completed without the help, support and guidance of innumerable people, though I would like to take this opportunity to acknowledge as many as I can.

First and foremost, my supervisor Dr. Vasileios Koutsos, whose guidance has been invaluable and whose scientific mind and approach I hold in the highest regard. I thank you for all of your input, scientific and otherwise, and for your patience and support throughout my research.

My second supervisor, Dr. Jane Blackford, who has been a source of both support and inspiration, I thank you for your confidence in my abilities even on days when I was not convinced they were there.

Dr. Vassilis Sboros I thank for his early guidance and experimental instruction as well as his advice on how to be an experimental researcher.

The work in Chapter 4 was initiated by a previous graduate student, Dr. Emmanouil Glynos, who collected the experimental data before the commencement of my studies. The data was subjected to a preliminary analysis by an undergraduate student, Miss Evelyn Buchner-Santos, who developed the process of fitting non-linear models by the use of non-linear axes. This preliminary analysis was extended and refined by me and was connected firmly to previous work by further

calculations; this process led to significant new insights and new interpretation exemplified by the extensive discussion of the results in the context of existing literature which was possible only after my analysis. I thank them both for their contributions.

Dr. Michail Kalloudis, Dr. Apostolos Evangelopolous, Alexandros Askounis, Ibrahim Albaijan; I thank you for making my working environment a pleasant one, and to them and every other colleague and friend who has humoured my need to understand a problem by talking it through – my gratitude is immense. This is particularly true for Tom Barraclough, who has somehow managed to put up with my ramblings for the last eight or so years and whose breadth of knowledge on just about everything, ever, will always be inspiring to me.

I thank the physics coffee room lunch crowd for brightening my darker days and offering intellectual stimulation of a different sort, Anne Pawsey for care and feeding during my writing up, and most particularly Kym Eden, always my dearest dance partner and most kindred spirit.

My thanks to my parents, for their support whenever and however I needed it, and for appreciating that asking “How is the writing up going?” will never be anything but a recipe for disaster.

Finally, there is Jo. I am without sufficient words of gratitude for everything you have done for my over the last few years; for all the ways you have supported me,

challenged me, delighted me and changed me. Perhaps I shall just say thank you for the exploding tea…

Table of Contents

List of Symbols and Abbreviations

MB	Microbubble
AFM	Atomic force microscopy
SPM	Scanning probe microscopy
UCA	Ultrasound contrast agent
PEG	Poly(ethelyne gylcol)
BBB	Blood-brain-barrier
STM	Scanning tunnelling microscopy
LVDT	Linear voltage differential transformer
MFP	Molecular force probe
INVOLS	Inverse optical lever sensitivity
F	Force
h	Shell Thickness
R_0	Initial Radius
R	Radius of scatterer
λ	Wavelength
κ	Compressibility of medium
κ_s	Compressibility of scatterer
ρ	Density of medium
ρ_s	Density of scatterer
E	Young's Modulus
υ	Poisson's Ratio
k	Stiffness
k_c	Cantilever stiffness
Δ	Deformation
ε	Relative Deformation
D_0	Initial Diameter
σ	Stress
Y	Linear Strain
F-Δ	Force – deformation
F-ε	Force – relative deformation
F-d	Force – distance
δ	Indentation

Chapter 1: Introduction

1. Introduction

Phospholipid coated, inert gas filled microbubbles (MBs) are currently in widespread use in medical applications for the enhancement of diagnostic ultrasound images, particularly of the heart, [1] liver [2] and kidney. [3] MBs are biologically inert, stable and easily cleared from the body once a procedure is complete. They are also interesting as a potential mechanism for drug/gene delivery. [4, 5] While a great deal of research has focused on the acoustic behaviour of MBs under diagnostic ultrasound, [6] less is known about the mechanical properties and response of phospholipid MBs to directly applied forces. In order for the technology to bridge the gap between contrast agent and delivery vehicle, a more complete understanding of how MBs respond to directly applied loads, such as they might be subjected to during circulation, is required. It is this gap in knowledge that this thesis seeks to address.

Atomic force microscopy is one of several techniques in the area of scanning probe microscopy (SPM), a field widely concerned with surface analysis. With an AFM it is possible to characterise surface topography with atomic resolution, [7] measure the forces required to break intermolecular bonds [8] and conduct compression/indentation experiments with contact areas ranging from square nanometres to square microns. This technique is therefore well suited to the investigation of small, relatively delicate structures such as phospholipid coated MBs.

This thesis presents a systematic investigation into the mechanical properties and behaviour of three different types of commercially developed phospholipid coated MBs. Atomic force microscopy is used to gather information about the mechanical response of the microbubble to directly applied mechanical loading, and mechanical models are used to estimate Young's modulus values.

Chapter 2 contains a brief summary of the history and uses of phospholipid coated MBs as ultrasound contrast agents, the principles behind atomic force microscopy and force spectroscopy, and the theoretical background supporting the mechanical models used to calculate Young's modulus from the experimental force spectroscopy data.

Chapter 3 describes the experimental and analytical procedures used to gather force – distance curves and apply the mechanical models to evaluate estimates of Young's modulus.

Chapter 4 comprises a study of Definity® MBs investigated by force spectroscopy with tipless cantilevers at small deformations. The apparent microbubble stiffness is evaluated. Mechanical models are used to estimate the microbubble Young's modulus and the potential suitability of these models as descriptors of microbubble mechanical properties is discussed. In addition in this chapter, we explain the different deformation regimes and we define low and high deformations (within the small deformation regime).

Chapter 5 is a study of BR14 MBs at very small deformations. Force spectroscopy data gathered with tipless cantilevers is used to evaluate stiffness and mechanical models applied to estimate Young's modulus values. The suitability of the models and the difference between the low and very low deformation regime is discussed. Data from tipped cantilever experiments is also presented, and the membrane stiffness and Young's modulus values are estimated.

In Chapter 6 a final study on Sonovue® MBs is presented. This study involves force spectroscopy data with tipless cantilevers analysed at both small and very small deformations, and tipped cantilever data at low deformations. The whole microbubble and membrane stiffness are evaluated, and the mechanical models are used to estimate Young's modulus values. The suitability of the various models in the appropriate deformation regime is discussed, and comparisons are drawn between Sonovue®, BR14 and Definity® MBs.

Chapter 7 contains the final conclusions and suggestions for potential future work.

References

[1] Kaufmann BA, Wei K, Lindner JR. Contrast echocardiography. Current Problems in Cardiology. 2007;32:51-96.

[2] Lamuraglia M, Escudier B, Chami L, Schwartz B, Leclere J, Roche A, et al. To predict progression-free survival and overall survival in metastatic renal cancer treated with sorafenib: Pilot study using dynamic contrast-enhanced Doppler ultrasound. European Journal of Cancer. 2006;42:2472-9.

[3] Quaia E. Microbubble ultrasound contrast agents: an update. European Radiology. 2007;17:1995-2008.

[4] Bekeredjian R, Grayburn PA, Shohet RV. Use of ultrasound contrast agents for gene or drug delivery in cardiovascular medicine. Journal of the American College of Cardiology. 2005;45:329-35.

[5] Unger EC, Hersh E, Vannan M, Matsunaga TO, McCreery M. Local drug and gene delivery through microbubbles. Prog Cardiovasc Dis. 2001;44:45-54.

[6] Sboros V. Response of contrast agents to ultrasound. Advanced Drug Delivery Reviews. 2008;60:1117-36.

[7] Binnig GK. Atomic-Force Microscopy. Physica Scripta. 1987;1987:53.

[8] Janshoff A, Neitzert M, Oberdorfer Y, Fuchs H. Force spectroscopy of molecular systems - Single molecule spectroscopy of polymers and biomolecules. Angew Chem-Int Edit. 2000;39:3213-37.

Chapter 2: Background and Theory

2 Background and Theory

2.1 Phospholipid Coated Microbubbles

While a great deal of research has focused on the acoustic behaviour of MBs under diagnostic ultrasound, [1] less is known about the mechanical properties and response of phospholipid MBs to directly applied forces; this thesis seeks to address aspects of this knowledge gap, specifically in the case of existing commercially available products. The following section will introduce the phospholipid coated MB in more detail, describing its development, structure and the underlying physics which make the phospholipid MB both useful and versatile.

2.1.1 Ultrasound Contrast Agents

The use of gas MBs as ultrasound contrast agents (UCAs) was first reported by Gramiak and Shah [2] as an explanation for an accidental discovery on the part of Dr Claude Joyner in the late 1960s. While studying cardiac output, Joyner reported an increased ultrasound signal immediately following the injection of a dye into the ventricle of a patient. [3] Gramiak and Shah suggested and demonstrated that this effect was due to gas MBs forming at the tip of the injection needle. [4] From this initial discovery, the use of MBs as UCAs for clinical use has broadened into a wide field of study.

Ultrasound imaging works on the principle of applying an ultrasound pulse at a specific site and recording how the signal is reflected or scattered. The reflection/scattering signal is then used to create an image of the area under investigation. The presence of MBs in a biological system improves ultrasound imaging contrast because the gas bubble is less dense than the surrounding tissue. The density change at the boundary causes a decrease in velocity of an incident ultrasound wave passing from tissue into a MB. This change in acoustic impedance between the MBs and the surrounding tissue increases the scatter of the ultrasound signal, making the area more clearly visible and defined in the resulting image. A material having the ability to significantly increase ultrasound scatter is said to have a high scattering cross section. Linear scatterers which are much smaller than the incident ultrasound wavelength have a scattering cross section σ, as given below:[1]

$$\sigma = \left(\frac{4}{9}\pi R^2 (kR)^4\right)\left(\left(\frac{\kappa_s - \kappa}{\kappa}\right)^2 + \frac{1}{3}\left(\frac{3(\rho_s - \rho)}{2\rho_s - \rho}\right)^2\right) \qquad [1]$$

R is the radius of the scatterer (>>λ), λ is the wavelength, (k=2π/λ) is the wavenumber, κ_s is the compressibility of the scatterer, κ is the compressibility of the surrounding medium, ρ_s is the density of the scatterer, and ρ is the density of the surrounding medium. From this equation it can be calculated that gas MBs have a greater scattering cross section than either solid or liquid particles. [5] It must also be noted MBs interact strongly with an applied ultrasound wave; rather than remaining static they may oscillate, jet, coalesce or fragment. [1]

While simple air MBs have a good scattering cross section, they do not have a long circulation time in the blood, collapsing very quickly due to the effects of surface tension. Epstein and Plesset [6] calculated that an unencapsulated air bubble with a diameter of 10 μm would dissolve in less that 7 seconds even in an air-saturated water solution (less than 2 seconds if the solution was degassed); a timeframe which is too short for clinical applications. The discovery that coatings on the MBs could counter the effects of surface tension [7] allowed for the development of commercial UCA systems, the first of which, Albunex®, used serum albumin as the MB coating agent. The lifetime of these MBs was still quite short due to the relatively swift diffusion of air through the albumin coating. [8] To counter this, subsequent systems filled the MBs with a high molecular weight gas such as a perfluorocarbon or sulphur hexafluoride, [9] further improving the MB lifetime. Albumin as a coating material is relatively stiff, and tends to rupture permanently if a critical strain is exceeded, [10] so other materials such as polymers and phospholipids were developed as potentially more robust coating materials. Phospholipid coatings in particular were found to be effective MB stabilisers, as well as being more flexible and significantly more resistant to rupture than their albumin counterparts, even after large amplitude oscillations were applied. [11]

2.1.2 Structure and Assembly of Phospholipid Coated MBs

Phospholipids are a class of lipids which are found commonly in biological contexts; particularly as the major component of cell membranes. A phospholipid molecule comprises a hydrophilic headgroup containing a phosphate group and a glycerol

molecule connected to two hydrophobic tails of long chain fatty acids, usually hydro- or fluourocarbon chains. A schematic example of a phospholipid molecule can be seen in Figure 2.1.

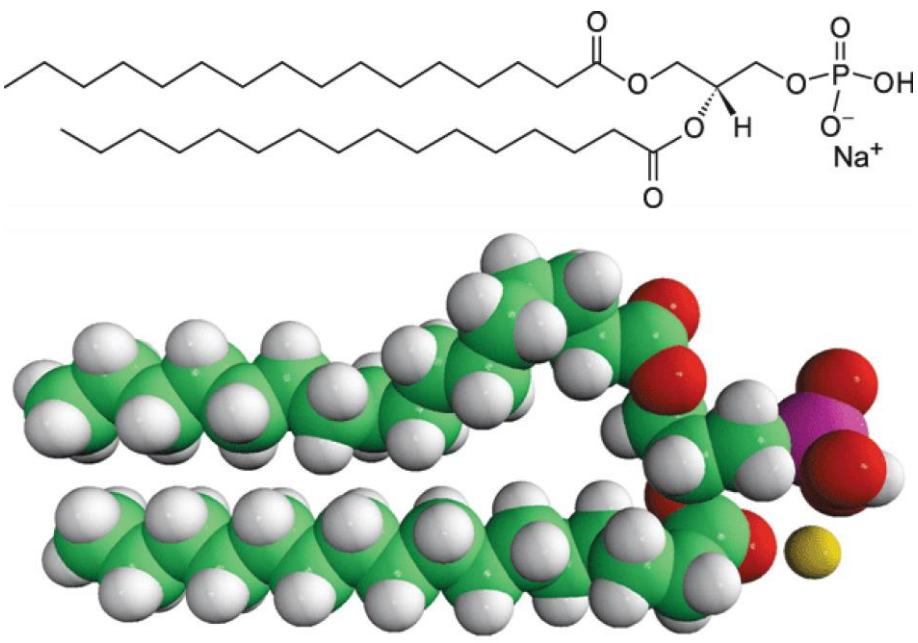

Figure 2.1 Example of a typical phospholipid molecule, dipalmitoylphosphatidic acid DPPA. Images obtained from Avanti Polar Lipids, Inc [12]

Due to their amphipatic character, when agitated in an aqueous solution the phospholipids will either self assemble into bilayer structures, or at a liquid – gas interface (such as the surface of a MB) phospholipids may orient themselves so that the hydrophilic heads face the water and the hydrophobic tails point into the gas region. Whether a bilayer or a monolayer is formed at an interface depends on the details of the individual system; the phospholipids will adopt the most energetically favourable configuration.

The details of the hydrophobic tails are very important in MB applications as altering the length of the hydrocarbon chain affects properties such as surface tension, surface viscosity, gas permeation resistance and buckling stability of the resulting shell. [13] Examples of phospholipids commonly used for MB coatings include dipalmitoylphosphatidic acid, DPPA, and dipalmitoylphosphatidycholine, DPPC.

A common feature of phospholipid MB coatings is the presence of poly(ethelyne gylcol) (PEG) groups grafted onto a proportion of the phosohplipid molecules. These long chain molecules extend from the surface of the MB forming either mushroom structures or a brush layer, depending on the proportion of PEG; this creates an exclusion zone some Angstroms (Å) thick at the membrane surface [14] which helps inhibit MB aggregation.

MBs can be formed by numerous different methods, though phospholipid MBs are most commonly produced by sonication or microfluidic processing. Of these methods, sonication is the most commonly used, particularly in the manufacture of commercial phospholipid coated UCA MBs. In this process, high intensity ultrasound is used to induce the formation of gas MBs in a suspension of the desired coating material, in our case phospholipids. [15-17] Once the MBs are formed, the phospholipids self-assemble into a coating. These coated MBs are then washed clean of excess phospholipids and re-suspended in another liquid, usually saline, before use. This method produces coated MBs across a range of sizes, the precise distribution of which depends on the properties of the applied ultrasound pulse. Any

large diameter MBs must be filtered out before use as they could potentially cause an embolism in a patient. [8]

Monodisperse solutions, or solutions having a very narrow size distribution, can be achieved with microfluidic devices. This technique is less common commercially, but is quite well established for the preparation of MB suspensions. These devices involve creating a t-junction where a gas flow meets a liquid flow, with flow rates and pressures such that the gas forms a jet which is surrounded by the liquid. Once the jet exceeds a certain distance past the meeting point, the gas-liquid interface becomes unstable and a MB is formed by a "pinch-off" process.[18] A schematic can be seen in Figure 2.2. This process produces very monodisperse MBs, but at the expense of MB yield when compared to the sonication method.

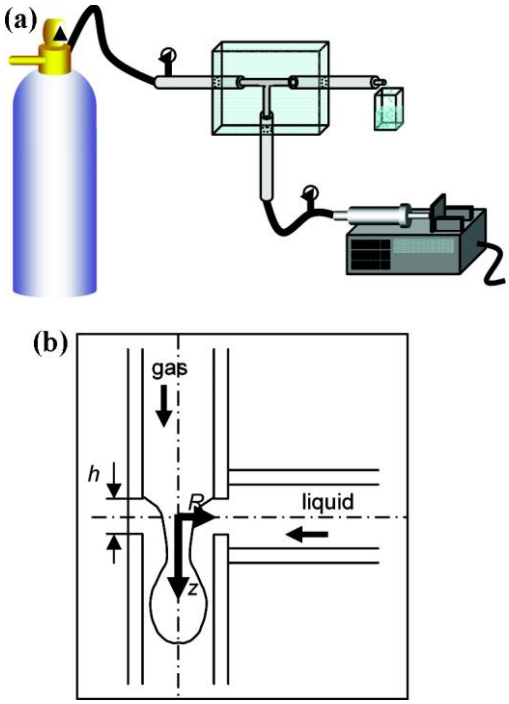

Figure 2.2 Schematic of a microfluidic T-junction device: (a) system apparatus and (b) junction geometry. Image obtained from [18]

2.1.3 Other Therapeutic Applications of MBs

There has been a great deal of interest and research into the possibility of using phospholipid coated MBs as a method of delivering drugs/genes to specific sites in the human body, as well as improving the resulting drug/gene uptake. Drugs can be incorporated into MBs in several ways, they can be enclosed within the MB, embedded in the membrane, attached to the membrane or contained in a thin oil layer on the inside of the membrane. [19] The method of incorporation/attachment depends on the type of substance to be transported. Once the MBs have been administered, ultrasound is applied to the target area in order to induce MB destruction in a process called cavitation. The payload is then released from the MB to be absorbed by the surrounding tissue. It is also possible to incorporate targeting

ligands into the membrane, [20] or onto a PEG group [21] so that MBs will be attracted to a particular site. The effectiveness of MB targeting has been demonstrated quite extensively both *in vitro* and *in vivo*. [13, 19] Even without incorporating a drug payload, the presence of MBs can increase the uptake of drugs in a region targeted by ultrasound. This is an extension of the effect of sonoporation, which is defined as "transient membrane permeabilisation and uptake of extracellular models into cells with the assistance of ultrasound and/or MBs." [22] While ultrasound alone increases membrane permeability sufficiently to improve uptake of molecules, MBs oscillating in close proximity to other membranes such as cell walls enhances this effect. Cell permeability returns to normal after the cessation of ultrasound. If a MB is subject to cavitation and consequent destruction, high velocity micro-jets may be produced which also cause the temporary rupture of nearby membranes. This effect has been utilised to allow access to areas which are normally resistant to drug uptake, such as across the blood-brain-barrier (BBB). [23-25]

2.2 Atomic Force Microscopy (AFM)

The continuing development of MB technology is dependent on building an understanding of the mechanical properties of the MBs in addition to their acoustic behavior. Various techniques to elicit a deformation of MBs are available; such as micropipette manipulation [26, 27] or osmotic swelling, [28] but it is the development of AFM which has provided us with the ability to measure the mechanical response of MBs with nanoscale force resolution. AFM has already

provided insights into the mechanical behavior of polyelectrolyte microcapsules [29] and other soft particles[30] in the size range of ultrasound contrast agent MBs.

2.2.1 General Principles of AFM

Atomic force microscopy (AFM) is the most versatile of the scanning probe microscopy (SPM) techniques, combining the principles of scanning tunnelling microscopy (STM) and stylus profilometry to enable the investigation of the surface profile of non-conducting surfaces on the atomic scale. It was invented by Binnig, Quate and Gerber, in 1986, [31] following on from their Nobel prize winning invention of the STM. There has since been further development into techniques such as Kelvin probe[32] or magnetic force microscopy, [33] but the AFM remains the most widely used technique as it is capable of investigating widely varying phenomena.

The basic principle of AFM is that a surface can be investigated by using a tiny probe attached to a soft cantilever to physically interact with or "feel" a sample surface. The cantilevers in question are of the order of 100 μm in length and 0.5 μm thick, small and soft enough to avoid damage to sensitive surfaces. The probe at the end of the cantilever may be a sharp tip, with an end radius of some nanometres, or a larger structure such as a colloid particle with a radius of a few microns. The type of probe depends on the experiment being carried out; an imaging experiment requires the sharp tip for high resolution, whereas a force experiment may require a relatively

large contact area which can be provided by the colloid. It is also possible to use a bare cantilever with no tip at all.

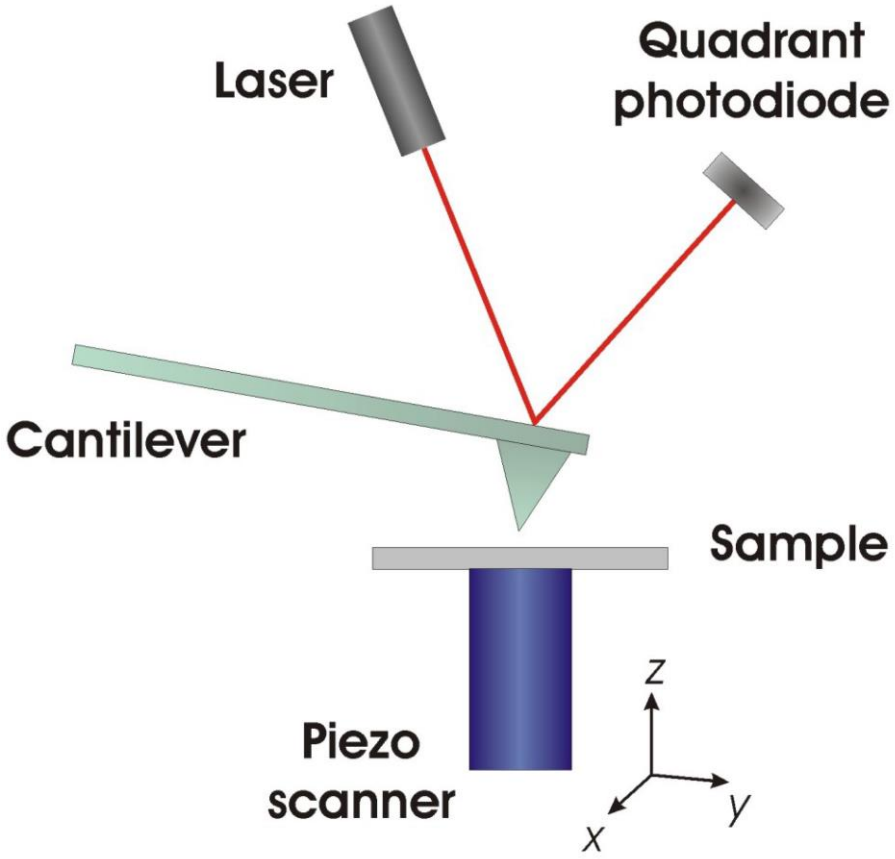

Figure 2.3 Schematic representation of an AFM configuration. Image obtained from Baclayon et al. [34]

A schematic AFM set up is illustrated in Figure 2.3. The cantilever tip is moved in and out of contact with the sample in the normal direction. Depending on the individual instrument, this is done by altering the height of either the cantilever or the sample. [35] This movement is controlled by the use of piezoelectric materials which expand or contact proportionally to an applied voltage. The size changes in these crystals are small and precise, and the response to changing voltage is very quick, making them ideal for use as actuators in an AFM. When the tip is in contact with

the sample, the cantilever will be deflected. This deflection is monitored by a laser beam which is focussed onto the end of the backside of the cantilever. The reflected beam hits a photodetector which monitors how the reflected angle of the beam changes; an indicator of the cantilever deflection. [35]

The most widespread use of AFM is for the generation of topographic images of sample surfaces. The cantilever is moved in a raster scan pattern over a surface area of up to several square microns and the height information gathered is used to produce a relief image of the surface with very high resolution. [36] During scanning, the tip can either be in continuous contact with the surface, known as contact mode, or in intermittent contact with the surface, known as tapping mode. In both cases, as the tip moves across the surface of a sample a continuous feedback system alters the voltage to the z-axis piezo crystal in response to changes in sample height, maintaining contact with the sample and preventing damage to the sample and/or the tip due to excessive loading forces. [35] This is achieved by the use of a continuous feedback system.

Contact mode measurements are the simplest to describe, as they can be likened to a gramophone needle moving across a record. The dynamics of the system are quite complicated, however, as the movement of the cantilever in the horizontal plane may subject the cantilever to significant torsional forces, particularly if the sample is quite "sticky". There is also a risk of damaging a soft sample by ploughing furrows into it with the tip. On hard surfaces, however, the resolution of the images is excellent, and

the changes in torsional loading can be used to infer boundaries between different materials on the same sample and also the coefficient of friction of the surface. [37]

In tapping mode, the cantilever is oscillated at close to its resonant frequency then brought close to the sample surface so the tip "taps" against the surface. [38] The contact between the tip and the surface is not constant, but the frequency of contact is high, several hundred kilohertz in air. This is particularly advantageous when imaging soft materials as a visco-elastic hardening effect occurs, making the sample appear harder and protecting it from damage caused by the tip. [39] Biological materials are predominantly imaged in tapping mode for this reason. In addition, the lag between the driving frequency of the piezo crystal and the measured response of the cantilever can be used to make inferences about the surface properties.[36, 40] Thoughtful use of the two basic modes of AFM has led to the development of various other techniques, including force spectroscopy; this is the technique used in this study and is described in detail in the following section.

2.2.2 Force Spectroscopy

Force spectroscopy is effectively a contact mode technique which is used to gather information about how materials respond to directly applied loads. The very small interaction area between tip and sample and the nature of the cantilever as a soft spring yields a system sensitive enough to accurately measure very small forces, down to the order of pN. This is the order of magnitude of forces required to break

intermolecular bonds such as hydrogen bonds. [35] Controlled application of this level of forces is also useful for the compression or indentation of very soft materials, including the phospholipid membranes which are the subject of this study.

During force spectroscopy measurements, the cantilever starts at a distance away from the sample, is moved into contact with the sample until a desired cantilever deflection is reached, then retracted to the original distance from the sample. The cantilever deflection is recorded throughout the approach-retract cycle and in conjunction with the piezo displacement data is used to create force – distance curves. This technique does not involve the raster scanning in the x – y direction required for imaging as the approach – retract data is gathered at a single location; however the most recently developed AFMs often use the two techniques simultaneously.[41] The data collected by an AFM is simply the piezo position at every point in the experiment, and the deflection of the cantilever tip. Knowledge of the precise elastic properties of the cantilever used to take the measurements allows us to quantify the forces applied during the experiment; the data can be transformed from deflection – position to force – distance. Figure 2.4 shows an idealised force – distance curve and highlights the main regions of importance.

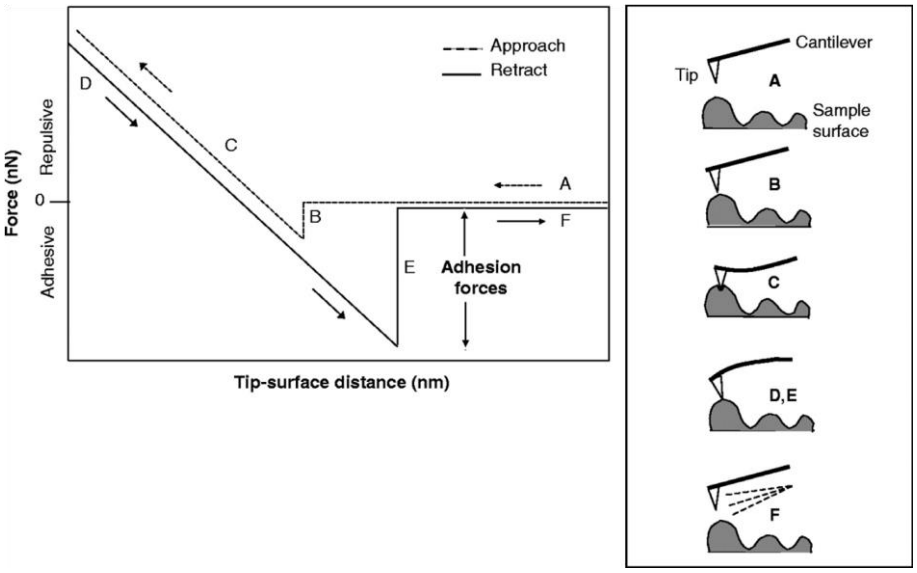

Figure 2.4 An ideal force distance curve highlighting regions of importance. A: Non-contact and approach. B: Snap in to contact. C: Approach in contact with increasing cantilever deflection. D: Retract in contact with decreasing cantilever deflection and hysteresis. E: Contact past original contact point due to adhesion forces. F: Retract out of contact. Image Obtained from Shahin et al. [42]

In region A, the cantilever is in free space above the surface at a distance exceeding the range of any surface interactions. The cantilever is then lowered by the piezo actuator, closing the gap between the cantilever and the sample. At B, the cantilever is close to the surface and attractive van der Waal's forces cause a sudden deflection of the cantilever to bring it into contact with the surface. [43] This is known as a "snap in" to contact. In region C, the piezo movement continues at a fixed rate of some microns per second until a threshold piezo position is reached. This causes a continuous increase in cantilever deflection which is ideally linear, or close to linear. In this region, the material under the cantilever is subject to compression and may be deformed or indented, depending on the relative stiffness of the material and the cantilever. In region D, the piezo motion is reversed, and the deflection of the

cantilever decreases, usually with some small hysteresis between the approach and retract curves. [44, 45] This linear change in deflection continues beyond the position of contact on the approach curve due to adhesion forces between the tip and the sample. In this region, the cantilever deflection is in the opposite direction to the deflection during contact. In the case of samples tested in air, these forces are often predominantly capillary forces which arise due to the presence of atmospheric water, particularly when tipless cantilevers are in use. [46] In aqueous conditions, adhesion forces may be attributed to the inherent "stickiness" of the sample. The size of this region varies greatly depending on the material being investigated. Once the force of adhesion is overcome, the cantilever breaks free of the surface and resumes its equilibrium position as the piezo retraction continues, as in region E. The cantilever continues to retract in region F and ends the cycle in the same position is it began, a sufficient distance from the surface to avoid any surface interactions.

The resulting force – distance curves are a composite of the behaviour of the cantilever and the surface or structure beneath it. It is therefore necessary to isolate the behaviour of the sample. This is done by subtracting the vertical deflection of the cantilever from the position of the piezo at each point along the curve. On an infinitely stiff surface, these two values will be always be equal i.e. there will be no deformation of the surface. On a material with stiffness comparable to that of the cantilever, the difference between the two values is equal to the deformation or indentation of the sample. This results in a force – deformation curve which shows the deformation behaviour of the sample alone. The change from force – distance to force – deformation is illustrated schematically in Figure 2.5.

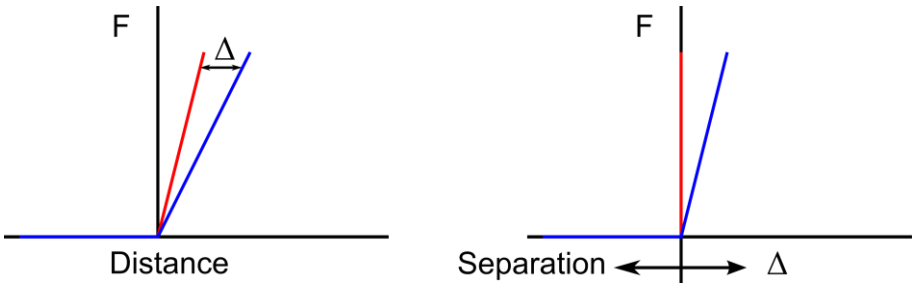

Figure 2.5 Schematic illustration of the transformation from Force – Distance to Force – Separation. Red: infinitely hard surface; Blue: soft surface.

2.2.3 Limitations and Artefacts in AFM

Whilst the AFM can be used to investigate a wide and varied range of materials, it does have limitations. In the case of force spectroscopy, the major limiting factor is in the system sensitivity. [35] When a cantilever is pressed against a hard surface, the resulting cantilever deflection should be indefinitely linear, however in actual measurements there is a limit to the measured linear region. Once a threshold deflection, δ_t, is exceeded, the force – deformation (F–Δ) curve for a hard surface gradually ceases to be linear, as illustrated in Figure 2.6.

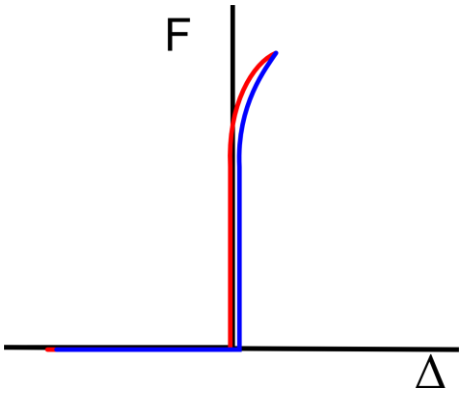

Figure 2.6 A schematic F–Δ curve of a cantilever against a hard surface showing deviation at high force. This measurement artefact can be seen on both the approach (red line) and retract (blue line) curves.

The extent of the linear region is affected by interplay between cantilever properties, the laser beam shape and the photodetector alignment; a non-circular beam shape has a large effect on system sensitivity, as does the initial positioning of the beam on the photodetector. If the cantilever is very soft, relatively large deflections of the cantilever can be incurred at relatively low forces, so these effects must not be neglected.

2.3 Theoretical Background of the Mechanical Models

The main aim of this thesis is to explore the mechanical properties of phospholipid MBs, particularly the Young's Modulus. For a simple elastic solid, the Young's modulus E can be taken as the gradient of a stress-strain (σ-Y) curve within the linear elastic region i.e.

$$E = \frac{\sigma}{\mathrm{Y}} \qquad (2)$$

In the case of thin shelled structures such as MBs, however, the situation is complicated by the system geometry and this simple relationship is no longer valid. It is necessary to use a more detailed mechanical model in order to describe the behaviour of the MBs and assess their Young's Modulus. This work focuses on several mechanical models which are used in conjunction with experimental data to investigate the Young's Modulus of phospholipid MBs. These models are: the Reissner approximation, elastic membrane theory, Hertz theory and in Chapters 5 and 6, De Jong theory. The following sections contain a description of each model and also a brief summary of their previous use in applications relevant to this thesis.

2.3.1 General Notation

In order to account for the variations in diameter of individual MBs it is convenient to define a dimensionless parameter to describe the degree of deformation which can be used to allow straightforward comparison between different bubbles. For the purposes of this thesis, the term relative deformation, ε, has been adopted. [42] It is defined as change in bubble height, ΔD, (change in diameter) divided by the initial bubble height, D_0, (initial diameter):

$$\varepsilon = \frac{\Delta D}{D_0} \qquad (3)$$

The stiffness (k_b) of a MB is obtained from the gradient of the force-deformation (F-Δ) curves, where according to Hooke's Law, k_b is a function of the applied force (F) divided by the MB deformation (Δ); i.e.

$$k_b = \frac{F}{\Delta} \tag{4}$$

2.3.2 Reissner Approximation

The first model to be considered in this investigation is the Reissner theory. When applied to stiff shelled MBs, the Reissner analytical solution has been demonstrated to be a good predictor of polymer MB properties, [48] yielding values for Young's Modulus which correlate well with those of the corresponding bulk polymer. For this reason the Reissner theory was the first model to be considered in the investigation of phospholipid shelled MBs.

This model takes as its basis the classical theory of thin shell deformation as outlined by Landau and Lifshitz. [49] This analytical solution for the mechanical behaviour of shallow spherical caps [50, 51] is applicable to isotropically-elastic thin-shelled microbubbles under small deformations. Using this analytical solution, the Young's Modulus of a thin shell MB having an initial radius R_0 and shell thickness h is described by

$$E = \frac{\sqrt{3(1-\upsilon^2)}}{4}\frac{R_0}{h^2}s \quad (5)$$

Where E is Young's modulus, υ is Poisson's ratio and s is the gradient of the linear region of the force-deformation curve. [48] This allows the YM to be calculated from the same curves as are used to calculate MB stiffness.

This expression can be modified by replacing s with F/ε and rearranging to demonstrate the relationship between applied force, F, and relative deformation as below:

$$F = \frac{4}{\sqrt{3(1-\upsilon^2)}}\frac{h^2}{R_0}ED_0\varepsilon \quad (6)$$

When simplified, the Young's modulus of the MB shell is therefore

$$E = \frac{\sqrt{3(1-\upsilon^2)}}{8h^2}\left(\frac{F}{\varepsilon}\right) \quad (7)$$

An important limitation on the application of this theory is the requirement for small deformations. Strictly speaking, the Reissner approximation is only valid where the loading of the MB is point-like, however Elsner et al. [52] showed by AFM force spectroscopy measurements of polymeric shells in conjunction with finite element

analysis the theory can be applied to systems having non-point like loads and over large contact areas. The Reissner solution has been used in studies on polymer microbubbles, [48, 53] microcapsules [48, 53, 54] and phospholipid vesicles, [55, 56] when a linear relation was observed at the initial stage of the F-Δ curves.

2.3.3 Hertz Theory

Hertz theory is a generalized solution for the elastic deformation of two homogeneous, semi-infinite spheres in contact; [57, 58] though it may be adapted for other geometries such as sphere – plate. [47] The original Hertz model describes the deformation behaviour of fully elastic, homogeneous spheres. [59, 60] The assumption of homogeneity means that a Young's modulus calculated by this method is an 'effective' Young's modulus of an equivalent sized homogeneous sphere, rather than the Young's modulus of the actual shell. This is in contrast to the other theories used in this study, which evaluate shell properties. Numerous studies on cells and vesicles have made use of the Hertz model to estimate Young's modulus, [47, 61-65] and this broad comparison range is the reason it was selected for use in this study. The basic theory can be adapted for use in different types of experiment, such as the use of colloid probes of much larger diameter than the structure under test, [47] or the use of tipped cantilevers which have a much smaller radius than the test structure.[61]

This model assumes that deformation occurs only in the area of contact and that the rest of the object remains spherical, as illustrated in Figure 2.7; this assumption holds whether or not the cantilever has a tip. It is notable that the use of Hertz theory assumes that any adhesion between tip and sample is much smaller than the applied load, which is to be expected in the case of the aqueous experiments described in this study. We expect this model to be of use only in the case of very small deformations, when the assumption of homogeneity is least egregiously violated.

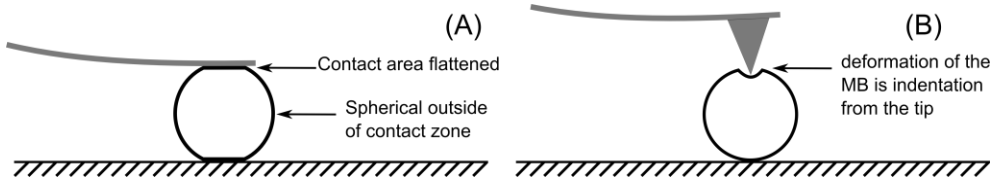

Figure 2.7 Deformation of MBs according to Hertz theory with an untipped cantilever (A) and a tipped cantilever (B).

For the case of tipless cantilevers, which approximate a sphere – plate geometry, we reference the work of Lulevich which studied the behaviour of cells and used Hertz theory to calculate the relationship between force and deformation according to the following [47]:

$$F = \frac{\sqrt{2}E}{3(1-\upsilon^2)} {R_0}^2 \varepsilon^{\frac{3}{2}} \qquad (8)$$

The Young's modulus can be obtained using the Hertz theory by taking the gradient of the linear part of the F-$\varepsilon^{3/2}$ curve. The use of non-linear axes in an F-$\varepsilon^{3/2}$ curve allows us to use linear fitting techniques and isolates very clearly the deformation

regime which is applicable us, i.e. the linear region. Linear regression is used to find the gradient of this region, and this result can be used to evaluate Young's modulus according to the following equation (a re-arrangement of equation 8):

$$E = \frac{3(1-\upsilon^2)}{\sqrt{2}R_0^{\,2}}\left(\frac{F}{\varepsilon^{\frac{3}{2}}}\right) \tag{9}$$

Experiments which make use of tipped cantilevers can also be analysed using the Hertz model. The radius of the tip is much smaller than that of the MB, so we still consider the geometry to comprise a sphere against a flat surface, however the contact region is now defined by the tip radius, so a different expression of Young's Modulus is necessary. We have chosen to use the relationship as described by Hu et al.[61].

$$F = \frac{4}{3}\frac{ER_{Tip}^{\frac{1}{2}}}{(1-\upsilon^2)}\delta^{\frac{3}{2}} \tag{10}$$

Where δ is indentation and R_{Tip} is the radius of the end of the cantilever tip. We assume in this case that all of the measured sample deformation is indentation of the contact region. We then replace δ with ε, and rearrange (10) to give:

$$E = \frac{3}{2^{\frac{7}{2}}}\frac{(1-\upsilon^2)}{R_{Tip}^{\frac{1}{2}}R_0^{\frac{3}{2}}}\left(\frac{F}{\varepsilon^{\frac{3}{2}}}\right) \tag{11}$$

Which can be used for fitting as in the case of tipped cantilevers.

2.3.4 Elastic Membrane Theory

Elastic membrane theory has been used by others to analyse the behaviour of phospholipid shell structures [54, 66]. It relies on membrane theory and the bending and stretching energy associated with the deformation of the capsule. When used to analyse the behaviour of living cells, the assumptions of the model were in agreement with observed behaviour and the estimates of Young's modulus were similar to those produced by other methods. [47]

For the purposes of this model, the bubble is assumed to have an impermeable membrane; [47] thus maintaining constant volume during compression (assuming compression is small). This being the case, when the bubble is compressed, any increase in pressure within the bubble is homogeneous. Upon compression, initially the membrane is assumed to deform only in the approximately circular contact area between the bubble and the cantilever i.e. the membrane will bend locally in response to the applied load as in Figure 2.8 (A). Outside the contact area, the bubble will maintain its undeformed shape.

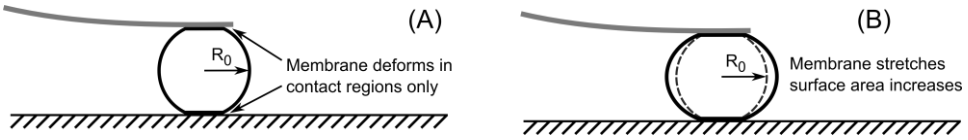

Figure 2.8 (A) Initial deformation only due to membrane bending in the contact regions. (B) As deformation continues, the membrane out of the contact region stretches, increasing the surface area of the MB.

As the applied load increases, the deformation becomes more global, with a homogeneous increase of pressure within the bubble. This increase in pressure is countered by stretching of the bubble shell i.e. increased MB surface area as shown in Figure 2.8 (B). It is then possible to balance the forces in the system using the following [47]:

$$F_m = F_{stretching} + F_{bending}$$

$$F_m = 2\pi \frac{E_m}{1-\upsilon_m} h R_0 \varepsilon^3 + \pi \frac{E_m}{2\sqrt{2}} h^2 \varepsilon^{\frac{1}{2}} \qquad (12)$$

where F_m is the applied force and E_m and υ_m are the Young's modulus and Poisson's ratio of the membrane. It is possible to calculate the ratio between bending and stretching terms of equation 12 as follows:

$$\frac{F_{bending}}{F_{stretching}} = \frac{h}{R_0} \frac{1-\upsilon}{4\sqrt{2}} \frac{1}{\varepsilon^{\frac{5}{2}}} \qquad (13)$$

From this ratio, it is possible to predict whether the membrane deformation is predominantly bending or stretching. It can be seen from Figure 2.9 that initially, the

deformation is almost exclusively membrane bending, however as relative deformation increases, the contribution of membrane bending decreases compared to that of membrane stretching up to a critical value for ε beyond which the ratio $F_B/F_S < 0.05$ and the contribution of membrane bending can be considered negligible. It can also be seen that there will be a region where both membrane bending and stretching must be considered. In cases where membrane bending is the predominant mode of deformation, when $F_S/F_B < 0.05$ membrane stretching can be neglected.

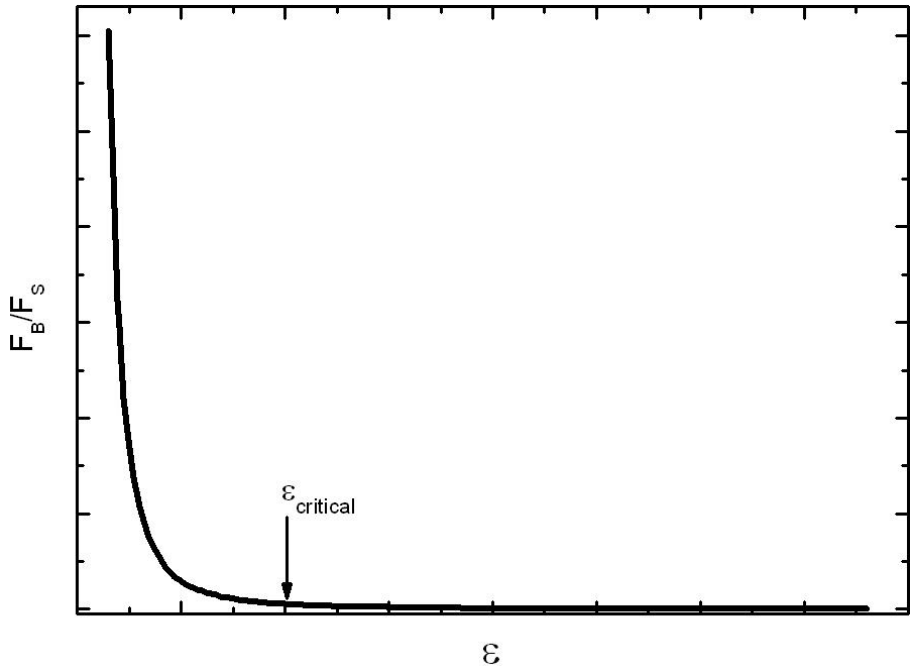

Figure 2.9 The relationship between relative deformation, ε and the ratio of membrane bending to membrane stretching. $\varepsilon_{critical}$ is defined as the point where $F_B/F_S < 0.05$.

In order to apply this theory, we select the most appropriate deformation regime and rearrange equation 12 to extract the Young's Modulus. This yields the two following expressions, one for each regime:

$$E_{Stretching} = \frac{(1-\upsilon)}{2\pi R_0 h}\left(\frac{F}{\varepsilon^3}\right) \quad (14)$$

$$E_{Bending} = \frac{2\sqrt{2}}{\pi h^2}\left(\frac{F}{\varepsilon^{\frac{1}{2}}}\right) \quad (15)$$

As using these expressions directly would involve non-linear fitting, we use the same method as described in Section 2.3.3, transforming the F–d curves into F–ε^3 or F–$\varepsilon^{1/2}$ curves as appropriate, then fitting by linear regression.

This model shares a limitation with the Reissner approximation in that it accounts only for the properties of the bubble membrane, and not at all for the bubble contents.

These three models have been applied in the following experimental chapters; however Chapters 5 and 6 include an additional mechanical model.

2.3.5 De Jong Theory

De Jong and coworkers [67] have proposed a model which describes the acoustic properties of MBs that includes a term developed from an earlier work by Reismann [68] explicitly defining the contribution of the shell assuming constant shell thickness and perfect elasticity. The shell elasticity is calculated from a relationship

between the change in MB radius and the difference in pressure inside and outside of the MB. When $h << R_0$ (as in the case of phospholipid coated MBs) the term can be simplified and the Young's modulus is linked to MB stiffness (k_B) by the following [67]:

$$k_B = \frac{8\pi E h}{(1-\upsilon)} \tag{16}$$

This can be rearranged to the form:

$$E = \frac{(1-\upsilon)}{8\pi h} k_B \tag{17}$$

This is a linear expression which can be applied directly to a Force – deformation curve in the same way as the Reissner theory.

References

[1] Sboros V. Response of contrast agents to ultrasound. Advanced Drug Delivery Reviews. 2008;60:1117-36.

[2] Gramiak R, Shah PM. Echocardiography of the aortic root. Invest Radiol. 1968;3:356-66.

[3] Feigenbaum H, Stone JM, Lee DA, Nasser WK, Chang S. Identification of Ultrasound Echoes forom Left Ventricle by Use of Intracardiac Injections of Indocyanine Green. Circulation. 1970;41:615-21.

[4] Kremkau FW, Gramiak R, Carstens.El, Shah PM, Kramer DH. Ultrasonic Detection of Cavitation at Catheter Tips. American Journal of Roentgenology Radium Therapy and Nuclear Medicine. 1970;110:177-83.

[5] de Jong N, Cornet R, Lancée CT. Higher harmonics of vibrating gas-filled microspheres. Part one: simulations. Ultrasonics. 1994;32:447-53.

[6] Epstein PS, Plesset MS. On the Stability of Gas Bubbles in Liquid-Gas Solutions. Journal of Chemical Physics. 1950;18:1505-9.

[7] Feinstein SB, Tencate FJ, Zwehl W, Ong K, Maurer G, Tei C, et al. Two-Dimensional Contrast Echocardiography. 1. In Vitro Development and Quantitative-Analysis of Echo Contrast Agents. Journal of the American College of Cardiology. 1984;3:14-20.

[8] Stride E, Edirisinghe M. Novel microbubble preparation technologies. Soft Matter. 2008;4:2350-9.

[9] Riess JG. Fluorocarbon-based injectable gaseous microbubbles for diagnosis and therapy. Current Opinion in Colloid & Interface Science. 2003;8:259-66.

[10] Stride E, Saffari N. On the destruction of microbubble ultrasound contrast agents. Ultrasound in Medicine and Biology. 2003;29:563-73.

[11] Borden MA, Kruse DE, Caskey CF, Zhao SK, Dayton PA, Ferrara KW. Influence of lipid shell physicochemical properties on ultrasound-induced microbubble destruction. IEEE Transactions on Ultrasonics Ferroelectrics and Frequency Control. 2005;52:1992-2002.

[12] Avanti Polar Lipids I. Detailed Information for 830855. 2014.

[13] Ferrara K, Pollard R, Borden M. Ultrasound microbubble contrast agents: Fundamentals and application to gene and drug delivery. Annual Review of Biomedical Engineering. 2007;9:415-47.

[14] Needham D, Kim DH. PEG-covered lipid surfaces: bilayers and monolayers. Colloids and Surfaces B: Biointerfaces. 2000;18:183-95.

[15] Unger EC, McCreery TP, Sweitzer RH, Caldwell VE, Wu YQ. Acoustically active lipospheres containing paclitaxel - A new therapeutic ultrasound contrast agent. Investigative Radiology. 1998;33:886-92.

[16] Zhao YZ, Liang HD, Mei XG, Halliwell M. Preparation, characterization and in vivo observation of phospholipid-based gas-filled microbubbles containing hirudin. Ultrasound in Medicine and Biology. 2005;31:1237-43.

[17] Christiansen C, Kryvi H, Sontum PC, Skotland T. Physical and Biochemical-Characterization of Albunex (TM), A New Ultrasound Contrast Agent Consisting of Air-Filled Albumin Microspheres Suspended in a Solution of Human Albumin. Biotechnology and Applied Biochemistry. 1994;19:307-20.

[18] Pancholi K, Stride E, Edirisinghe M. Dynamics of Bubble Formation in Highly Viscous Liquids. Langmuir. 2008;24:4388-93.

[19] Unger EC, Porter T, Culp W, Labell R, Matsunaga T, Zutshi R. Therapeutic applications of lipid-coated microbubbles. Advanced Drug Delivery Reviews. 2004;56:1291-314.

[20] Sboros V, Glynos E, Ross JA, Moran CM, Pye SD, Butler M, et al. Probing microbubble targeting with atomic force microscopy. Colloids Surf B Biointerfaces. 2010;80:12-7.

[21] Abou-Saleh RH, Peyman SA, Critchley K, Evans SD, Thomson NH. Nanomechanics of Lipid Encapsulated Microbubbles with Functional Coatings. Langmuir. 2013;29:4096-103.

[22] van Wamel A, Kooiman K, Harteveld M, Emmer M, ten Cate FJ, Versluis M, et al. Vibrating microbubbles poking individual cells: Drug transfer into cells via sonoporation. J Control Release. 2006;112:149-55.

[23] Hynynen K, McDannold N, Vykhodtseva N, Raymond S, Weissleder R, Jolesz FA, et al. Focal disruption of the blood-brain barrier due to 260-kHz ultrasound bursts: a method for molecular imaging and targeted drug delivery. Journal of Neurosurgery. 2006;105:445-54.

[24] McDannold N, Vykhodtseva N, Hynynen K. Use of ultrasound pulses combined with definity for targeted blood-brain barrier disruption: A feasibility study. Ultrasound in Medicine and Biology. 2007;33:584-90.

[25] Hynynen K, Burgess A, Ayala-Grosso CA, Ganguly M, Jordao JF, Aubert I. Targeted Delivery of Neural Stem Cells to the Brain Using MRI-Guided Focused Ultrasound to Disrupt the Blood-Brain Barrier. Figshare. 2011;1.

[26] Evans EA, Waugh R, Melnik L. Elastic Area Compressibility Modulus of Red-Cell Membrane. Biophysical Journal. 1976;16:585-95.

[27] Ratanabanangkoon P, Gropper M, Merkel R, Sackmann E, Gast AP. Mechanics of streptavidin-coated giant lipid bilayer vesicles: A micropipet study. Langmuir. 2003;19:1054-62.

[28] Rutkowski CA, Williams LM, Haines TH, Cummins HZ. The Elasticity of Synthetic Phospholipid-Vesicles Obtained by Photon-Correlation Spectroscopy. Biochemistry. 1991;30:5688-96.

[29] Vinogradova OI, Lebedeva OV, Kim BS. Mechanical behavior and characterization of microcapsules. Ann Rev Mater Res. 2006;36:143-78.

[30] Liu K-K. Deformation behaviour of soft particles: a review. Journal of Physics D: Applied Physics. 2006;39:R189.

[31] Binnig G, Quate CF, Gerber C. Atomic Force Microscope. Physical Review Letters. 1986;56:930-3.

[32] Nonnenmacher M, O'Boyle MP, Wickramasinghe HK. Kelvin probe force microscopy. Applied Physics Letters. 1991;58:2921-3.

[33] Hartmann U. Magnetic Force Microscopy. Annual Review of Materials Science. 1999;29:53-87.

[34] Baclayon M, Wuite GJL, Roos WH. Imaging and manipulation of single viruses by atomic force microscopy. Soft Matter. 2010;6:5273-85.

[35] Butt H-J, Cappella B, Kappl M. Force measurements with the atomic force microscope: Technique, interpretation and applications. Surface Science Reports. 2005;59:1-152.

[36] Alessandrini A, Facci P. AFM: a versatile tool in biophysics. Measurement Science and Technology. 2005;16:R65.

[37] Attard P, Stiernstedt J, Rutland MW. Measurement of friction coefficients with the atomic force microscope. Journal of Physics: Conference Series. 2007;61:51.

[38] Tamayo J, García R. Deformation, Contact Time, and Phase Contrast in Tapping Mode Scanning Force Microscopy. Langmuir. 1996;12:4430-5.

[39] Putman CA, van der Werf KO, de Grooth BG, van Hulst NF, Greve J. Viscoelasticity of living cells allows high resolution imaging by tapping mode atomic force microscopy. Biophysical Journal. 1994;67:1749-53.

[40] Scott WW, Bhushan B. Use of phase imaging in atomic force microscopy for measurement of viscoelastic contrast in polymer nanocomposites and molecularly thick lubricant films. Ultramicroscopy. 2003;97:151-69.

[41] Chopinet L, Formosa C, Rols MP, Duval RE, Dague E. Imaging living cells surface and quantifying its properties at high resolution using AFM in QI™ mode. Micron. 2013;48:26-33.

[42] Shahin V, Ludwig Y, Schafer C, Nikova D, Oberleithner H. Glucocorticoids remodel nuclear envelope structure and permeability. Journal of Cell Science. 2005;118:2881-9.

[43] Burnham NA, Colton RJ, Pollock HM. Interpretation issues in force microscopy. Journal of Vacuum Science & Technology A. 1991;9:2548-56.

[44] Vinogradova OI, Butt H-J, Yakubov GE, Feuillebois F. Dynamic effects on force measurements. I. Viscous drag on the atomic force microscope cantilever. Review of Scientific Instruments. 2001;72:2330-9.

[45] Hoh JH, Engel A. Friction Effects on Force Measurements with an Atomic-Force Microscope. Langmuir. 1993;9:3310-2.

[46] Müller DJ, Engel A. Chapter 13 - Conformations, Flexibility, and Interactions Observed on Individual Membrane Proteins by Atomic Force Microscopy. In: Bhanu PJ, Hörber JKH, editors. Methods in Cell Biology: Academic Press; 2002. p. 257-99.

[47] Lulevich V, Zink T, Chen HY, Liu FT, Liu GY. Cell mechanics using atomic force microscopy-based single-cell compression. Langmuir. 2006;22:8151-5.

[48] Glynos E, Sboros V, Koutsos V. Polymeric thin shells: Measurement of elastic properties at the nanometer scale using atomic force microscopy. Materials Science and Engineering B-Advanced Functional Solid-State Materials. 2009;165:231-4.

[49] Landau LD, Lifshitz EM. Theory of Elasticity. 3 ed. Oxford: Pergamon Press; 1986.

[50] Reissner E. Stresses and Small Displacements of Shallow Spherical Shells .1. Journal of Mathematics and Physics. 1946;25:80-5.

[51] Reissner E. Stresses and Small Displacements of Shallow Spherical Shells .2. Journal of Mathematics and Physics. 1946;25:279-300.

[52] Elsner N, Dubreuil F, Weinkamer R, Wasicek M, Fischer FD, Fery A. Mechanical properties of freestanding polyelectrolyte capsules: a quantitative approach based on shell theory. Characterization of Polymer Surfaces and Thin FIlms. 2006;132:117-23.

[53] Glynos E, Koutsos V, McDicken WN, Moran CM, Pye SD, Ross JA, et al. Nanomechanics of Biocompatible Hollow Thin-Shell Polymer Microspheres. Langmuir. 2009;25:7514-22.

[54] Fery A, Weinkamer R. Mechanical properties of micro- and nanocapsules: Single-capsule measurements. Polymer. 2007;48:7221-35.

[55] Dieluweit S, Csiszár A, Rubner W, Fleischhauer J, Houben S, Merkel R. Mechanical Properties of Bare and Protein-Coated Giant Unilamellar Phospholipid Vesicles. A Comparative Study of Micropipet Aspiration and Atomic Force Microscopy. Langmuir. 2010;26:11041-9.

[56] Leonenko Z, Cramb D, Amrein M, Finot E. Atomic Force Microscopy: Interaction Forces Measured in Phospholipid Monolayers, Bilayers, and Cell Membranes. Biosystems Investigated by Scanning Probe Microscopy. 2010:505-32.

[57] Johnson KL, Kendall K, Roberts AD. Surface Energy and Contact of Elastic Solids. Proceedings of the Royal Society of London Series A-Mathematical and Physical Sciences. 1971;324:301-&.

[58] Weisenhorn AL, Khorsand M, Kasas S, Gotzos V, Butt H-J. Deformation and height anomaly of soft surfaces studied with an AFM. Nanotechnology. 1993;4:106.

[59] Hertz H. On the contact of Elastic Solids. Journal für die reine und angewandte Mathematik. 1882;92:156-71.

[60] Yun T-Q. The Exact Integral Equation of Hertz's Contact Problem. Applied Mathematics and Mechanics. 1991;12.

[61] Hu MQ, Wang JK, Zhao HX, Dong SS, Cai JY. Nanostructure and nanomechanics analysis of lymphocyte using AFM: From resting, activated to apoptosis. Journal of Biomechanics. 2009;42:1513-9.

[62] Radmacher M, Fritz M, Kacher CM, Cleveland JP, Hansma PK. Measuring the viscoelastic properties of human platelets with the atomic force microscope. Biophysical Journal. 1996;70:556-67.

[63] Laney DE, Garcia RA, Parsons SM, Hansma HG. Changes in the elastic properties of cholinergic synaptic vesicles as measured by atomic force microscopy. Biophysical Journal. 1997;72:806-13.

[64] Liang XM, Mao GZ, Ng KYS. Mechanical properties and stability measurement of cholesterol-containing liposome on mica by atomic force microscopy. Journal of Colloid and Interface Science. 2004;278:53-62.

[65] Lulevich V, Shih YP, Lo SH, Liu GY. Cell Tracing Dyes Significantly Change Single Cell Mechanics. Journal of Physical Chemistry B. 2009;113:6511-9.

[66] Lulevich VV, Andrienko D, Vinogradova OI. Elasticity of polyelectrolyte multilayer microcapsules. Journal of Chemical Physics. 2004;120:3822-6.

[67] de Jong N, Hoff L, Skotland T, Bom N. Absorption and Scatter of Encapsulated Gas Filled Microspheres - Theoretical Considerations and Some Measurements. Ultrasonics. 1991;30:95-103.

[68] Reismann H, Pawlik PS. Elasticity: Theory and Application. New York, USA: John Wiley & Sons Inc.; 1980.

Chapter 3: Experimental Apparatus and Procedures

3 Experimental Apparatus and Procedures

This chapter describes in detail the experimental procedure used to carry out the MB compression experiments which form the basis of this investigation, and also the analytical procedure used to interrogate the resulting data. These procedures remain broadly the same even when the MBs under investigation vary; it is therefore convenient to describe the overall process in detail at this point. Subsequent chapters will detail experiments on three distinct formulations of phospholipid coated MB and additional specifics of both experimental and analytical procedures are detailed there.

3.1 Sample Preparation

In order to conduct compression experiments on MBs, it is necessary to immobilise them on a surface. This can be done either mechanically, which is the method used here, or chemically. [1] In our procedure, the first step is to coat the bottom surface of an appropriate cell culture dish with a 1:10 solution of poly-L-lysine (v/v) (Sigma-Aldrich Co., St. Louis, MO). The surface chemistry of the dish is important as standard dishes are hydrophobic and resistant to wetting by the poly-L-lysine. For this reason we used treated dishes such as Greiner Cellstar® (Greiner Bio-One GmbH, Germany). The excess poly-L-lysine is then washed away with deionised water. The next step takes advantage of the natural buoyancy of the gas-filled MBs to attach the MBs to the surface of the dish. A bowl larger than the prepared cell culture dish is filled with deionised water (resistivity 18 MΩ cm) and approximately 0.3 ml

of MB suspension is added. The cell culture dish is then inverted, and placed gently on the surface of the water. Details of the preparation of the different MB suspensions can be found in subsequent chapters. The floating MBs then come into contact with the poly-L-lysine coated surface of the cell culture dish, where they become gently stuck in place. A schematic of this procedure can be seen in Figure 3.10. The dish can be repositioned every few minutes to vary the section of the dish which is in contact with the MBs. An incubation time of around ten minutes is ideal to generate a sufficient area of adsorbed MBs. Excess, mobile MBs are then removed by gentle washing with deionised water and saline is added to a depth sufficient to cover the MBs and the AFM tip, ready for the compression experiments.

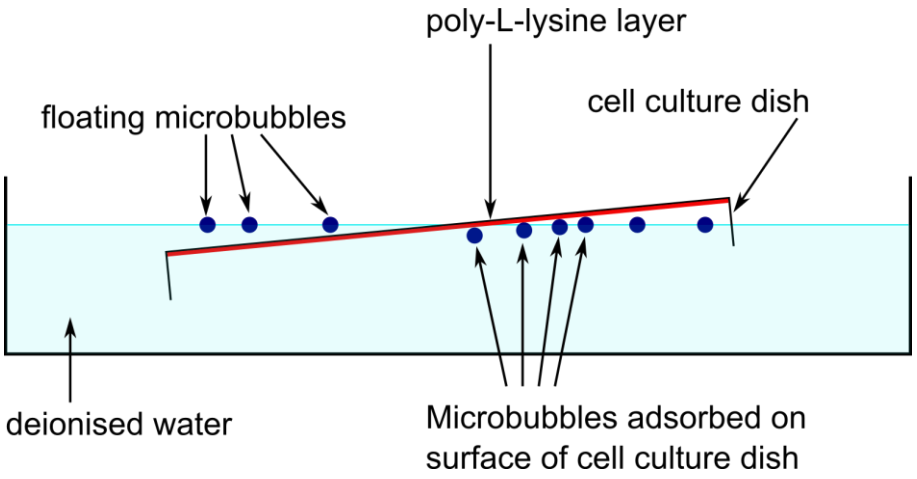

Figure 3.10 Schematic of MBs being attached to a poly-L-lysine coated petri dish

3.2 Apparatus

Figure 3.11 is an image of the experimental apparatus used throughout this investigation. The main components are indicated on the image and are described in more detail below.

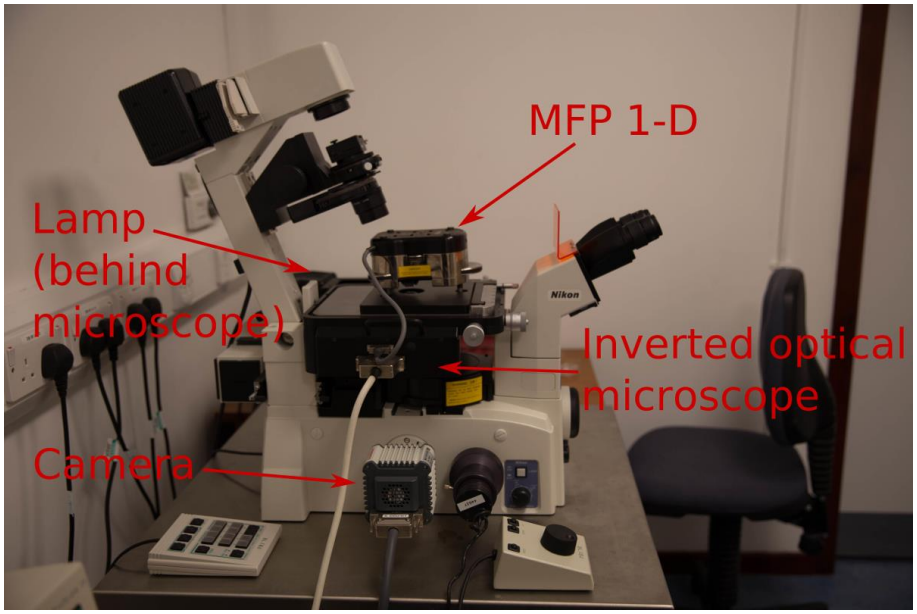

Figure 3.11 Image of experimental apparatus, MFP 1-D mounted on an inverted optical microscope

All the MB compression experiments were conducted using the molecular force probe (MFP 1-D) (Asylum Research, Santa Barbra, CA). This instrument is specifically designed to carry out accurate and precise force experiments and as such it does not have the capacity for raster scanning which is present in AFMs which produce surface images.

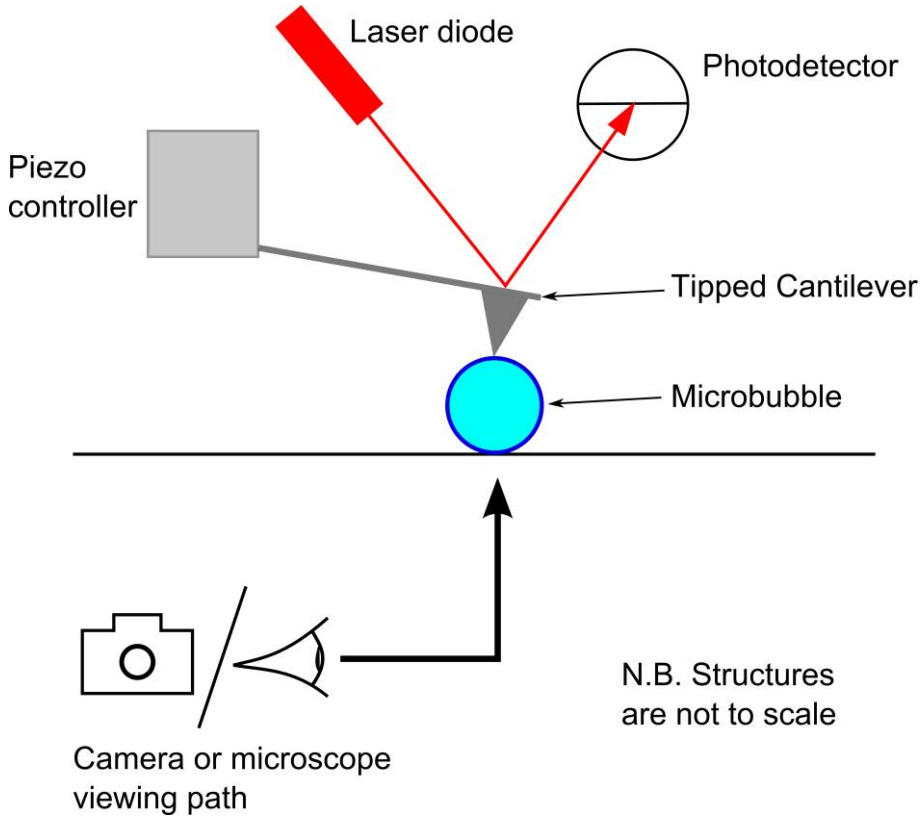

Figure 3.12 Schematic of MFP 1-D during a MB compression experiment.

Figure 3.12 is a schematic representation of the MFP 1-D during an experiment. A piezoelectric actuator raises and lowers the fixed end of the cantilever vertically with respect to the surface being investigated and the vertical deflection of the free end of the cantilever is measured by a photodetector which records changes in the incident angle of the laser beam reflected off the back surface of the cantilever. The data output from the MFP-1D is therefore the linear voltage differential transformer (LVDT) position in nm (i.e. the piezo position) and the photodetector voltage (i.e. a measure of cantilever deflection). This data is interrogated using the MFP 1-D software which runs in IGOR Pro v.4.0 data analysis software. The photodetector voltage is automatically converted to a vertical deflection, subject to cantilever calibration, which is discussed in section 3.2.1. Within the IGOR software it is

possible to control the behaviour of the MFP-1D during the experiment, and control variables such as the 'length' of the curve (the vertical distance through which the piezo actuator lowers the cantilevers), the data sampling rate and the speed of cantilever approach. It is also possible to impose a 'dwell' time where the cantilevers are kept stationary either between curves, or mid-curve while the cantilever is in contact with the surface/structure being tested.

The MFP-1D is mounted on an inverted optical microscope (Nikon TE2000U, Nikon UK Limited, Surrey, U.K.), used in reflection mode. The microscope can then be used to position MBs relative to the AFM cantilever for compression experiments. Attached to the optical microscope is a digital camera (Orca-ER C4742-80, Hamamatsu Photonics, Hamamatsu, Japan) which allows images of the MBs to be captured at high resolution. Image analysis software IPLab v3.7 (BD Bioscience Bioimaging, Rockville, MD) is used to process images of the MBs. Images recorded using the 60× objective are used to calculate MB diameter with approximately half-micrometer accuracy. [2]

3.2.1 Cantilevers and Calibration

All tipless cantilevers used in this investigation were supplied by Mikromasch (Talinn, Estonia). They are manufactured from silicon nitride with a shiny aluminium coating on the back side in order to maximise the reflected laser light during AFM

experiments. The typical layout and dimensions of these cantilevers are illustrated in Figure 3.13.

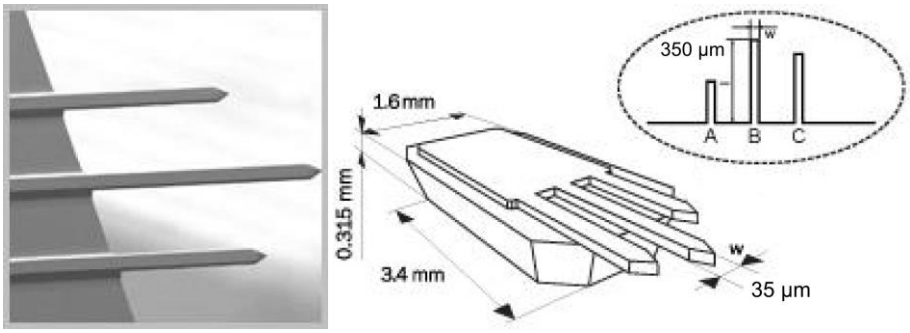

Figure 3.13 SEM images and schematic layouts of Mikromasch tipless cantilevers. Images obtained from Mikromasch catalogue [3]

The tipped cantilevers were supplied by Veeco (now Bruker) (Camarillo, CA). Their typical dimensions and layout are shown in Figure 3.14.

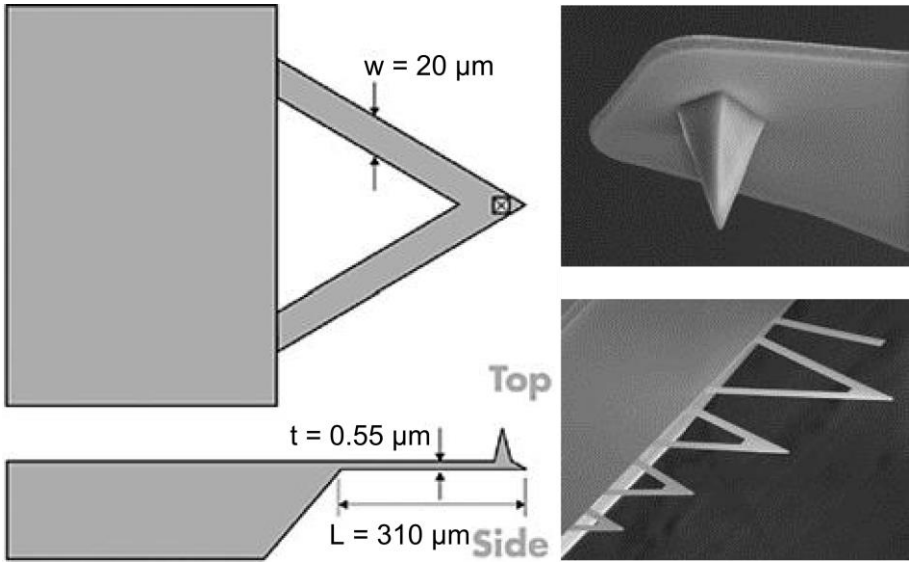

Figure 3.14 SEM images and schematic layouts of Veeco cantilevers. Images obtained from datasheet. [4]

In the case of both tipless and tipped cantilevers, the manufacturer's data sheet provides information about nominal resonant frequency and spring constant, k_c. It is necessary, however, to calculate the exact spring constant of each cantilever prior to conducting experiments. This is done in two stages. The first is to establish the sensitivity of the cantilever i.e. the change in photodetector voltage which corresponds to a given change in piezo position. This is done by taking a position – deflection curve against an infinitely stiff surface (a glass microscope slide). When the cantilever is deflected by a hard surface, we can say that the vertical deflection of the cantilever free end upwards is equal to the change in the position of the fixed end downwards, as illustrated in Figure 3.15. This known deflection can then be equated with the measured change in voltage at the photodetector. i.e. for a change in piezo position of 100 nm, the resulting change in measured voltage indicates a cantilever vertical deflection of 100 nm. If the measured change in voltage over this region was 1 V, the sensitivity of the lever would be 100 nm/V. This operation is carried out by a protocol in the IGOR Pro software. Once the level sensitivity (Inverse Optical Lever Sensitivity, INVOLS) is known, the thermal tuning method of Hutter and Bechhoefer [5] is used to calculate the cantilever spring constant. This calculated value will not change when the cantilever is placed into an aqueous environment or during the experiment (assuming no damage to the cantilever occurs), but it is necessary to recalculate the INVOLS at regular intervals before and during the experiment to ensure the accuracy of the recorded deflections.

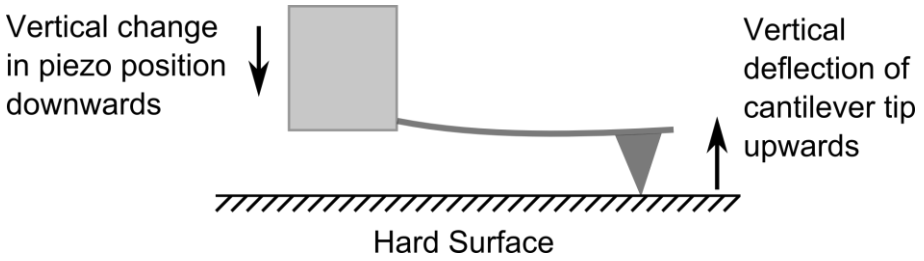

Figure 3.15 In contact with a hard surface, piezo displacement downwards is equal to cantilever vertical tip deflection

3.3 Experimental Procedure

A prepared sample is positioned under the MFP 1-D and above the microscope objective. At this point the calibrated cantilevers are submerged in saline and the change in refractive index causes a change in the laser position at the cantilever free end which must be corrected. The cantilever spring constant is now known, but the INVOLS must be recalculated by taking a curve against the hard surface of the sample dish as during cantilever calibration. A MB is then positioned under the cantilever and photographed at 60× magnification as in Figure 3.16.

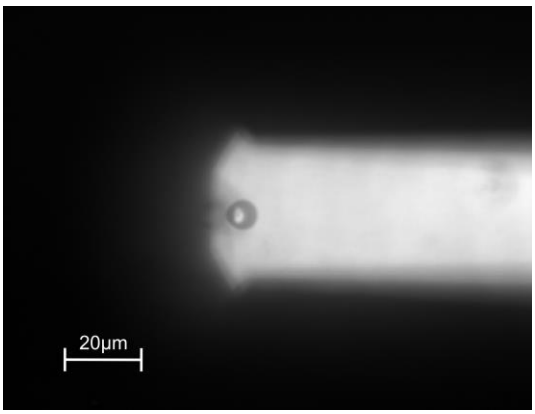

Figure 3.16 Image of a MB positioned under an untipped cantilever before compression experiment

In the case of tipless cantilevers, the cantilever width (~ 35 μm) is significantly larger than the MB diameter (> 10 μm), and the MFP height is set such that the cantilevers are roughly parallel to the top surface of the MB; it is therefore assumed that contact will occur at MB poles. In the case of tipped cantilevers, the microscope image is used to ensure the tip is centred over the MB pole. The MB diameter is then calculated from the mean of four diameter measurements. The cantilever is then lowered into contact with the MB by the piezo actuator, and the resulting LVDT-deflection curves are recorded. The length of the curve is set at 3 μm to allow for potentially large MB deformations while ensuring that the cantilever will be out of contact with the MB between curves. The speed of approach is set at 3 μm/s, which is slow enough to avoid the deformation of the MB due to a rapidly changing hydrodynamic pressure as the cantilevers displace water on approach. The initial contact curve is kept small (low measured deflection, >200 nm) to minimise the chance of damage to the MB, but changes to the maximum induced deflection can be made over the course of the experiment to investigate different deformation regimes. Specific details can be found in the relevant results chapter. After the compressions are completed and recorded, the MB is then visually assessed to verify that it remained immobile for the duration of the experiment. A new MB is then located and the process repeated.

3.4 Analytical Procedure

The data recorded by the MFP-1D comprises the LVDT and vertical deflection measurements. The resulting curves are a composite of the behaviour of the cantilever and the behaviour of the MB. This data must be processed to generate force-deformation curves where the deformation profile of the cantilever has been separated from that of the MB. The stages of this process are illustrated in Figure 3.17. Image (a) shows the position – deflection data as produced by the MFP. Image (b) shows this data translated such that the non-contact region has zero deflection, and that the contact point shows zero separation. At this point the cantilever is just in contact with the MB, and no deflection of the cantilever occurs. Graph (c) shows the change in the y-axis from vertical deflection to force. This is done by applying Hooke's law F=kx; the deflection is multiplied by the cantilever spring constant. In step (d) the deformation profile of the cantilever is removed. This is done by subtracting the deformation profile of the cantilever against a hard surface from the combined profile of the cantilever and the MB (i.e. the experimental data). The cantilever – hard surface profile can either be a recorded INVOLS curve gathered during the experiment or it can be generated mathematically using the calibrated cantilever spring constant and Hooke's law, producing an expected cantilever deflection for every applied load.

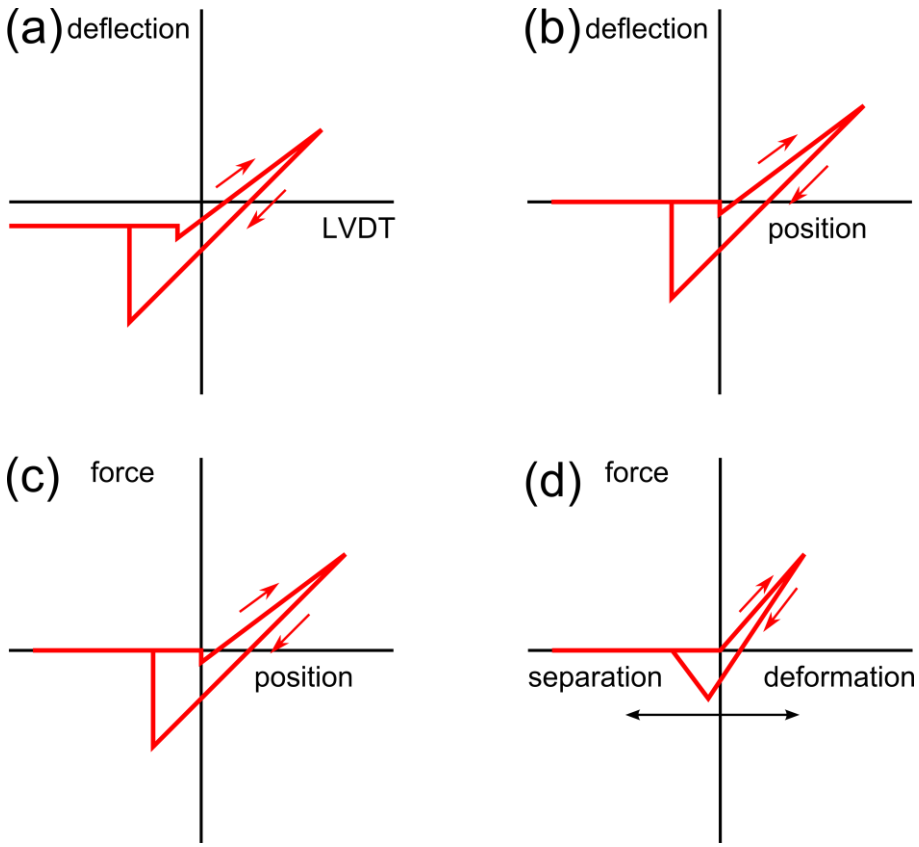

Figure 3.17 The transformation from deflection – LVDT position to force - deformation. (a) Raw data (b) Translation so contact point is zeroed (c) transformation from vertical deflection to force (d) change to MB deformation.

Once the force – deformation curves of the MB have been produced, they are used to evaluate the MB stiffness and test the effectiveness of mechanical models at predicting the MB Young's modulus. The effective stiffness of the MB is the gradient of the linear region of the force-deformation curve and is straightforward to evaluate. The linear models (Reissner and De Jong) use this effective stiffness directly so the calculation of Young's modulus is straightforward. The non-linear models are more complicated, particularly due to their varying regions of suitability and the potential complexity of non-linear curve fitting, particularly in the case of the full elastic membrane theory. A previous member of the group devised a way to

rationalise this fitting procedure by re-plotting the force – deformation curve in terms of relative deformation, ε, with non-linear axes. Linear regression can then be used to calculate the gradient of the linear region of the resulting curves, and these values can in turn be fitted into the equations governing each model to yield Young's modulus values.

References

[1] Abou-Saleh RH, Peyman SA, Critchley K, Evans SD, Thomson NH. Nanomechanics of Lipid Encapsulated Microbubbles with Functional Coatings. Langmuir. 2013;29:4096-103.

[2] Glynos E, Sboros V, Koutsos V. Polymeric thin shells: Measurement of elastic properties at the nanometer scale using atomic force microscopy. Materials Science and Engineering B-Advanced Functional Solid-State Materials. 2009;165:231-4.

[3] Mikromasch. SPM Probes and Test Structures. 2013.

[4] Bruker. MLCT Product Description. 2014.

[5] Hutter JL, Bechhoefer J. Calibration of Atomic Force Microscope Tips. Review of Scientific Instruments. 1993;64:1868-73.

Chapter 4: An Investigation of the Nanomechanical Properties of Definity®

4 An Investigation of the Nanomechanical Properties of Definity®

4.1 Introduction

The development of MB technology is dependent on building an understanding of the mechanical properties of the MBs in addition to their acoustic behavior. Various techniques to elicit a deformation of MBs are available; such as micropipette manipulation [1, 2] or osmotic swelling, [3] but it is the development of atomic force microscopy (AFM) which has provided us with the ability to measure the mechanical response of MBs with nanoscale force resolution. AFM has already provided insights into the mechanical behavior of polyelectrolyte microcapsules [4] and other soft particles[5] in the size range of ultrasound contrast agent (UCA) MBs. This research group has previously introduced AFM as a powerful tool for the investigation of polymer-based MBs, conducting a detailed investigation into the nanomechanical properties and behavior of MBs with a view to evaluating their Young's moduli. [6, 7] These studies revealed important information about the nanomechanical properties of MBs; Glynos et al. [6] in particular showed results which explain a possible cause of a failure of UCA technology. Using AFM, they found a variation of the Young's modulus of the shell with thickness at the nano scale (1 – 1000 nm), which contradicts the presumption that the Young's modulus is a constant material property, independent of size or shape. However, this finding is specific for polymeric MBs; it does not imply that other thin shell structures based on different

materials will behave in the same way and other types of MB must be investigated for possible nanoscale size-dependent effects. This is very relevant in the case of the much more compliant phospholipid-coated MBs which are the basis of many current UCA systems.

Previous work by this group on phospholipid MBs focused on MB imaging [8] and force measurements exploring stiffness and adhesive properties, as well as exploring the possibility of phospholipid MB targeting via avidin-biotin surface chemistry. [9, 10] Recently AFM has been used by others to measure the stiffness of in-house fabricated lipid coated MBs [11] and also to investigate the effect of temperature on their visco-elastic behavior. [12] The mechanical properties of phospholipid MBs have yet to be accurately specified; however studies exist describing the properties of similar phospholipid membrane systems, such as vesicles, cells and supported lipid bilayers. Many previous studies have investigated the mechanical properties of phospholipid vesicles, [2, 3, 13-15] which can be found in more than one size scale, with diameters from <100 nm up to the micron range and are filled with incompressible liquid rather than gas. The membrane of a living cell is composed of phospholipids and cholesterol and in addition to incompressible liquid; cells also contain organelles which may affect their mechanical behavior. A great deal of research into cell mechanical properties has been carried out, relating to both membrane properties [16-18] and global cell properties. [18-20] Supported lipid bilayer systems exploit the useful properties of the phospholipid membrane whilst removing the influence of the spherical geometry of a MB.

This chapter uses force spectroscopy data gathered with the MFP – 1D to analyze the mechanical properties of Definity® MBs, a commercially available UCA product which is used widely in clinical imaging applications. In particular, we evaluate the MB stiffness (k_b), the Young's modulus (E) of the phospholipid shell, and also the whole-bubble effective Young's modulus. The gradients of force-deformation (F-Δ) curves are used to calculate the stiffness of the MBs and specific mechanical models are used for the calculation of the Young's moduli. Two of the three mechanical models chosen for this study extract the Young's modulus of the MB shell; the third calculates the effective Young's modulus of the whole MB as a homogeneous sphere. The models are described and the results of our analysis are presented. The suitability of each of the three mechanical models is then discussed within the context of existing literature describing similar and comparable systems such as vesicles, cells and lipid bilayers.

4.2 Materials and Methods

4.2.1 Materials

This study uses Definity® MBs (Lantheus Medical Imaging, Inc., N. Billerica, MA). Definity® MBs are enclosed by a phospholipid shell, comprising three different types of phospholipids, Dipalmitoylphosphatidylcholine (DPPC), Dipalmitoylphosphatidic acid (DPPA), and dipalmitolyphosphatidylethanolamine–PEG5000 (DPPE–PEG5000). Each 0.75 mg of the lipid blend consists of 0.045 mg DPPA, 0.401 mg DPPC, and 0.304 mg MPEG5000 DPPE. [21] The filling gas is octafluoropropane. All the lipids are saturated and in order to improve stability, the MBs are negatively charged. [22] The Poisson's ratio was assumed to be 0.5 (highly elastic) which is standard for studies of structures of this type. [13, 16, 18] The mean MB diameter is 1.1 – 3.3 um. [21] The reported thickness values for Definity® vary from 1 to 4 nm. [23-27] We have assumed a shell thickness of 5 nm; which includes an allowance for a PEG structure in addition to the phospholipid membrane thickness. [28]

4.2.2 Sample Preparation

Since the AFM experiments require the interrogated objects to be still, the MBs were attached to Petri-dishes coated with a film of poly-l-lysine (Sigma–Aldrich Co., St. Louis, MO) formed by using a 1:10 solution of poly-l-lysine (v/v) in ultra-pure

deionized water with resistivity of 18.2 MΩ cm. This process is described in detail in Chapter 3. The preparation process ensured that the MBs adhered to the dish were at all times wetted to minimize structural or mechanical damage. All measurements were performed with MBs attached to the bottom of Petri-dishes within deionized water. [7]

4.2.3 Force Spectroscopy

We used the molecular force probe (MFP – 1D) (Asylum Research, Santa Barbara, CA), to perform force measurements, as described in Chapter 3. The MB diameters recorded during the experiment were between 2.1 μm and 4.2 μm.

For this study we carried out the force-spectroscopy using tipless/flat cantilevers (Mikromash, Tallinn, Estonia) with aluminium back coating and spring constants, k_c, 0.25 N/m and 0.07 N/m to investigate the MB deformation caused by small compressive loads i.e. before the onset of permanent deformation. The cantilever surface was aligned parallel to the petri-dish so that the force was exerted close to the MB's poles; though an exact parallel configuration cannot be guaranteed. The cantilever speed during approach/retraction was kept constant at approximately 6 μm/s. [7] The raw data obtained is the measurement of the piezoelectric vertical position and the deflection of the cantilever. The compressive force F, which is applied to the MB, is the product of k_c and the deflection of the cantilever. The deformation of the MB can be found from the difference between the piezoelectric actuator position and the deflection of the cantilever, i.e. the parameters measured by

the MFP – 1D. These values, now independent from the cantilever deflection, were plotted into force-deformation curves, or F-Δ curves which were used to evaluate the effective stiffness of the MBs. The MBs returned to their original height and therefore shape after cantilever retraction, indicating that the deformation was mainly elastic; it was therefore possible to apply multiple compressive forces to the same MB in order to check the repeatability of the behavior. For this study, only the approach curves were used in the analysis, earlier work having shown this to be an appropriate methodology; [6, 7] however the complete experimental data includes an approach curve and a retract curve. The retraction curves were inspected to ensure that minimum adhesion was generated by the contact between cantilever and MB. This in conjunction with the repeatability of the deformation profile of the MB over multiple measurements indicates that no shell material was lost or adhered to the cantilever during the experimental procedure.

The cantilever was initially set up to be relatively distant from the MB (~ 3 μm), so that the cantilever was not disturbed by any interaction between the two bodies. [29] The contact between the MB and the cantilever commences at the inflection point of the curve. It was important to accurately determine this initial contact point, i.e. the point of the first measurable force. During the experiments, the measured cantilever deflection was varied i.e. a range of forces were applied to each MB. The initial force was kept low to prevent MB damage, and then varied. The force applied to the MBs ranged between 5 nN and 56 nN, which is a deformation between approximately 160 nm and 1 μm. This equates to a maximum ε between 0.05 and 0.35. Typically, the initial region of the F-Δ graphs showed a non-linear relationship due to roughness

[30] and surface forces such as electrostatic double-layer and van-der-Waals forces. [31] Hence, the initial deflection was not taken into account when calculating the shell stiffness. In each case, the region used for a fitting was selected visually, and confirmed to be linear when the R^2 value of the linear fit over that region exceeded 0.98. In order to be considered viable for analysis, a curve was required to have more than 125 data points and the linear region used for fitting had to exceed 90 data points. If these two criteria were not met, the curve was deemed unsuitable for further analysis. The stiffness of each MB (k_b) was calculated from the gradient of corresponding F-Δ curves (according to Equation 4). Furthermore, we plotted the F-ε, F-$\varepsilon^{3/2}$ and F-ε^3 curves in order to evaluate the Young's modulus based on the Reissner, Hertz and elastic membrane theories, respectively. Unless otherwise stated, statistical uncertainty is taken to be one standard deviation of the measured dataset.

4.3 Results

4.3.1 Stiffness

The stiffness values, k_b, of 10 different MBs (D = 2.1 - 4.2 μm) were calculated. The gradient of the F-Δ curve was taken after the initial non-linear section up to the point where the curve could no longer be approximated by a straight line. Examples can be seen in Figure 4.18. This resulted in mean k_b values ranging from 0.016 ± 0.001 to 0.039 ± 0.003 N/m (Figure 4.19).

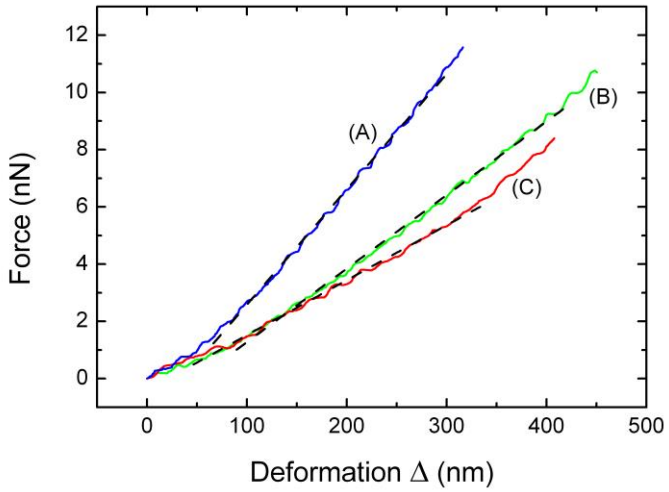

Figure 4.18 *F*-Δ curves for three different MBs. The blue curve (A) represents a MB with *D* = 2.9 µm, and stiffness (k_b) 0.040 N/m. The green curve (B) shows MB with *D* = 3.0 µm and k_b=0.026 N/m. The red curve (C) is the most compliant MB, with diameter 2.1 µm and k_b=0.019 N/m.

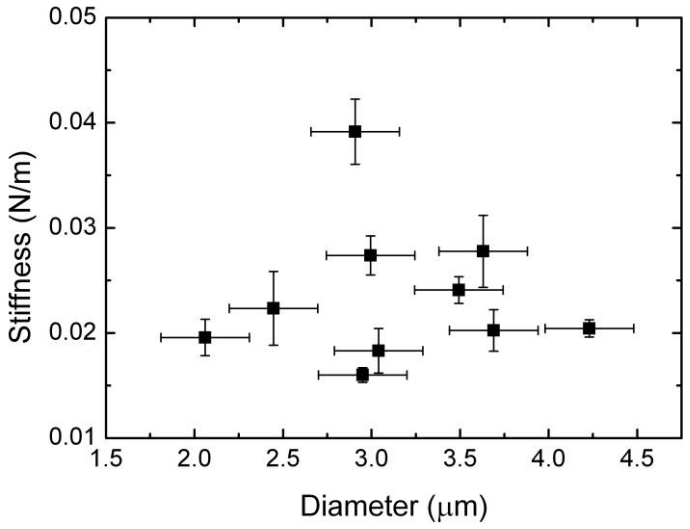

Figure 4.19 Effective stiffness for a set of 10 MBs ranging in diameter from 2.1 – 4.2 µm. The average bubble stiffness was found to be 0.026 ± 0.010 N/m.

4.3.2 Reissner Theory

Figure 4.20 (a) shows a typical F-ε curve, not linear initially, however becoming linear at approximately $\varepsilon = 0.03$ and remaining so up to approximately $\varepsilon = 0.13$. The gradient of this linear region was used to evaluate the Young's modulus of the shell according to the Reissner theory (Equation 7); yielding a value of 570 MPa.

Over the dataset of 10 bubbles, the linear region was located between $\varepsilon = 0.024 \pm 0.017$ and $\varepsilon = 0.121 \pm 0.047$. The Young's modulus of the MB shell calculated using this method was between 302 ± 27 MPa and 854 ± 68 MPa with an average of 558 ± 204 MPa (Figure 4.20(b)).

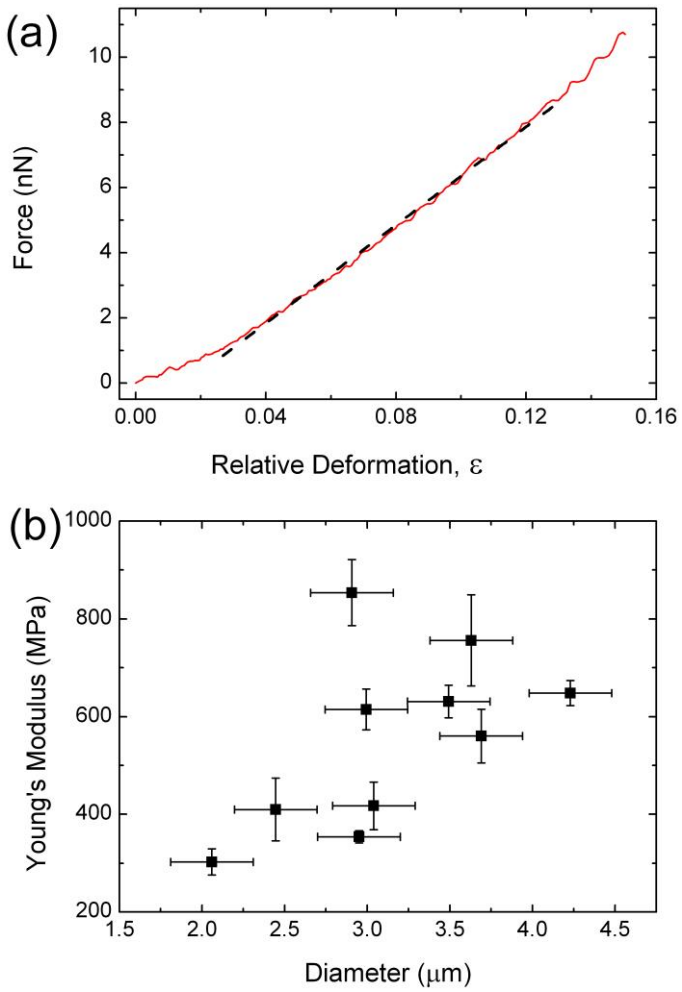

Figure 4.20 (a) *F*-*ε* curve for a MB with a diameter of 3.0 μm. The straight dashed line shows the linear region of the curve and its gradient is used in order to obtain the Young's modulus according to the Reissner Theory. (b) Young's modulus values for the shells of 10 different MBs with a diameter ranging from 2.1 to 4.2 μm calculated using the Reissner theory.

4.3.3 Elastic Membrane Theory

In Figure 4.21(a) we present a typical F-ε^3 curve; not linear in the initial region but becoming linear with further deformation. The linear region begins at approximately $\varepsilon^3 = 0.000858$, or $\varepsilon = 0.095$ and continues over the remainder of the curve to a

maximum of ε^3 = 0.00327, or ε = 0.148. The gradient of the linear part of the curve was calculated and substituted into Equation 14. The Young's modulus of the MB shell calculated from this curve was found to be 21 MPa.

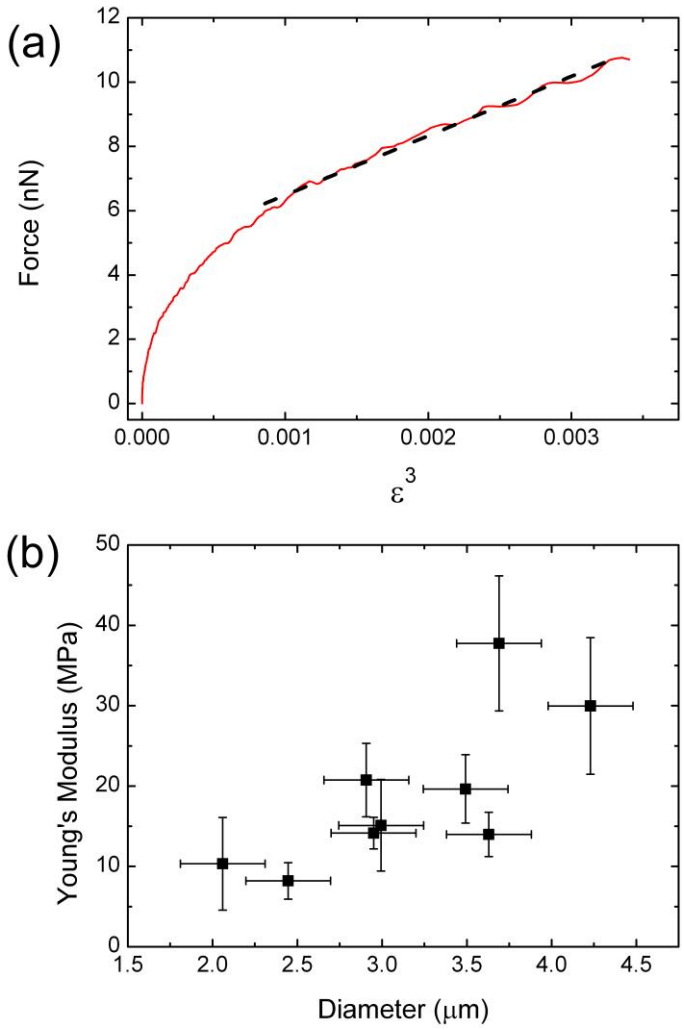

Figure 4.21 (a) F-ε^3 curve for a MB with a diameter of 3.0 µm. The straight dashed line shows the linear region of the curve, and its gradient is used in order to obtain the Young's modulus of the shell from the elastic membrane theory. (b) Young's modulus values for 9 different MBs with diameter ranging from 2.1 to 4.2 µm. The results were analyzed using the stretching term of the elastic membrane theory.

In the analysis of the whole dataset, there were few cases where the deformation range within the linear region was not sufficiently large to facilitate analysis, and noise and large fluctuations were predominant. Such curves were therefore discounted; leading to one MB being excluded from the elastic membrane analysis. In two cases, when analyzed with elastic membrane theory the Young's modulus decreased over successive curves; in these cases, only the initial few curves were considered.

Over the dataset of 9 MBs, the linear region was located between $\varepsilon = 0.122 \pm 0.042$ to $\varepsilon = 0.188 \pm 0.063$. Analysis using this method yielded a shell Young's modulus of between 8 ± 2 MPa and 38 ± 8 MPa with an average of 19 ± 9 MPa (Figure 4.21(b)). A possible positive correlation was noted between Young's modulus and MB size.

4.3.4 Hertz Theory

In Figure 4.22(a) we present a representative F-$\varepsilon^{3/2}$ curve. The gradient of the linear region of the curve was determined and substituted into Equation 9. The linear region begins at $\varepsilon^{3/2} = 0.002$, which corresponds to a relative deformation of $\varepsilon = 0.017$. The curve remains linear until $\varepsilon^{3/2} = 0.046$, or $\varepsilon = 0.128$. The effective Young's modulus calculated from this curve is 131 kPa.

Over the dataset of 10 MBs, the linear region was located between $\varepsilon = 0.043 \pm 0.025$ to $\varepsilon = 0.164 \pm 0.075$. The effective Young's modulus for all the MBs calculated

using this method was between 93 ± 10 kPa and 233 ± 30 kPa with an average of 133 ± 59 kPa (Figure 4.22(b)).

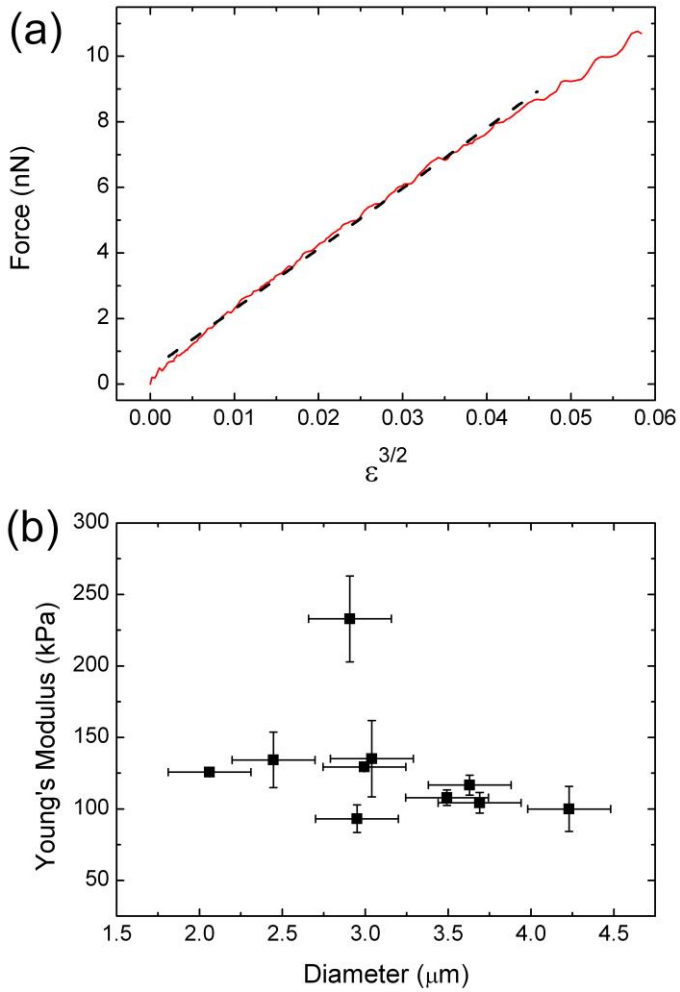

Figure 4.22 (a) F-$\varepsilon^{3/2}$ curve for a MB with a diameter of 3.0 µm. The dashed black line shows the linear region of the curve, and the gradient of this region is used in order to obtain the effective Young's modulus from the Hertz Theory. (b) Effective Young's modulus values for 10 different MBs with a diameter ranging from 2.1 to 4.2 µm analyzed using the Hertz theory.

4.3.5 Hysteresis

Some of the MBs showed minor to moderate instabilities during a compression cycle, visible in the *F*-Δ curves as 'steps' (Figure 4.23). After each step, the MB recovered and no permanent deformation was apparent. Often the following approach curve showed a residual (smaller) instability at approximately the same level of deformation. From Figure 4.23 it can also be noted that instabilities occurred during cantilever retraction. The width of the instabilities ranged from 0.4 nm to 2.9 nm.

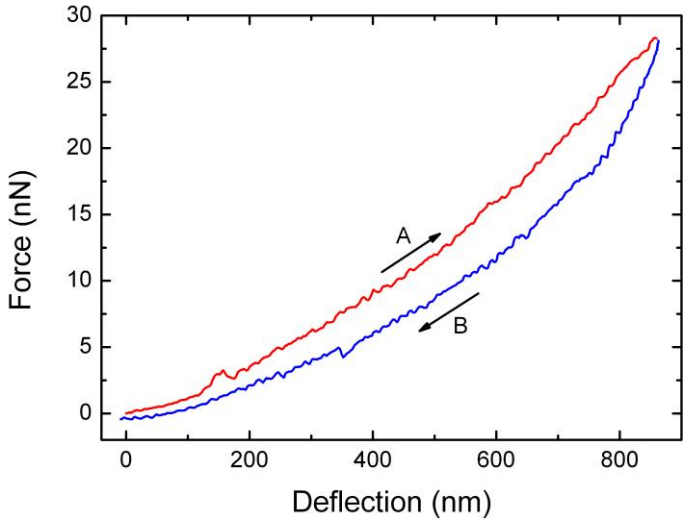

Figure 4.23 MB (*D* = 3.63 µm) showing instability during approach (red curve, A). Normal equilbrium behaviour was recovered after the instability. Another smaller instability can be seen on during retraction (blue curve, B). Hysteresis is also evident.

All of the curves showed a very small and reproducible hysteresis between the approach and retract sections of the *F*-Δ curves; however when curves also showed instability this hysteresis was more significant.

4.3.6 Results Summary

The following tables summarise the key results from this study.

Cantilever Type	Cantilever Spring Constant (N/m)	MB Spring Constant (N/m)	Size Dependence Y/N
Tipless	0.07 – 0.25	0.016 – 0.039	N

Table 4.1 Summary of Stiffness Results for the Experimental Examination of Definity® MBs

Mechanical Model	Deformation Regime	Shell / Sphere	Size Dependence Y/N	Young's Modulus
Reissner	Low	Shell	Y	302 – 854 MPa
Membrane Stretching	High	Shell	Y	8 – 38 MPa
Hertz	Low	Sphere	N	93 – 233 kPa

Table 4.2 Summary of Young's Modulus Results for the Experimental Examination of Definity® MBs

4.4 Discussion

The maximum deformation of the MBs ranged between 160-1000 nm (ε_{max}= 0.05-0.35). The maximum applied force on the bubbles was varied (5 nN – 56 nN) in order to investigate how maximum force affected the behavior of the MBs; though we did not observe any trend in the stiffness with increasing maximum load. We also did not see a trend for decreasing stiffness with increasing radius, as observed by McKendry et al. [11] The range of relative deformations we have used is similar to that reported in the study on T-cells (ε_{max} = 0.3), [18] giant protein vesicles (ε_{max} =

0.1) [13] and the deformation of polymeric MBs, before instabilities occur (ε_{max} = 0.2). [6] The stiffness of 0.026 ± 0.010 N/m obtained for Definity® MBs is slightly lower than the 0.056 ± 0.003 N/m reported for phospholipid based MBs of similar size (BR-14), [32] but is of the same order. This is one order of magnitude lower than the values reported for protein coated vesicles, [2] synthetic phospholipids [3] and human erythrocyte cells, [33] and is two orders of magnitude lower than observed for polyelectrolyte microspheres of similar diameter. [6] This finding indicates that we are dealing with very compliant MBs which may deform differently to previously investigated structures. It is possible that this low stiffness is due to the hollow nature of the UCA – in other structures a liquid core may contribute to the overall stiffness.

4.4.1 Reissner Theory

Reissner theory is a linear theory applicable to the initial small deformation of the MBs. Definity® MBs satisfy the requirement of the model that t/R be smaller than 1/20 [34] and the fitted regions have an average maximum relative deformation of ε = 0.120 ± 0.047 indicating that deformations can be considered small. Given that no major assumptions of the theory appear to have been breached, we can compare our result of a shell Young's modulus of 302 – 854 MPa with results from similar systems available in published literature.

Reissner theory has been used in several studies to analyze the deformation behavior of polymeric shells. In particular, Glynos, et al. [7] experimented on polymeric thin shells (t = 40 nm and D = 5 μm) with a soft gel skin (10 nm thick) using atomic force microscopy (AFM). This study used Reissner theory for the analysis and the resulting Young's modulus of the shell was found to be in the range of 1.5 – 3 GPa. Another study by Elsner et al. [35] on polyelectrolyte capsules (t = 25 nm and D = 16 μm) also used AFM and the Reissner theory for analysis and found a value of 294 ± 32 MPa. Dieluweit, et al. [13] investigated bare and protein-coated giant unilamellar vesicles (GUV) (t ~ 4.5 nm and D ~ 15 μm) using force spectroscopy and evaluated the shell Young's modulus with Reissner theory; which was found to be between 53 and 109 MPa. Despite the similarity between the shell materials of the GUVs and Definity® MBs, our results exceed reported values for GUVs and other phospholipid systems [3] by a factor of 10 or more, and are in fact considerably closer to values found for the much stiffer polyelectrolyte MBs. This leads us to the conclusion that the Reissner approximation produces overestimates which preclude it from being a useful model for the calculation of the Young's Modulus of the shell of Definity® MBs.

4.4.2 Elastic Membrane Theory

Our analysis with elastic membrane theory yielded Young's modulus values between 8 MPa and 38 MPa. As previously described, the full form of the elastic membrane theory used in this study is composed of a stretching term and a bending term, the ratio of which is given in equation 13. From this ratio it can be predicted that as the

deformation increases, the overall behavior is more dependent on the stretching term than on the bending term. While all the investigations in this thesis fall into the overall category of 'small' deformations, being less than 30% of the original MB diameter, we will henceforth separate the deformation of MBs in these experiments into two regimes, very small deformations are characterized as 'low deformation' and higher but still small deformations as 'high deformation'. The low deformation regime is taken as being the regime in which membrane bending is predicted to be the major mode of deformation; where $\varepsilon < 0.05$. The high deformation regime, throughout this thesis, refers to the region where membrane stretching should predominate, $\varepsilon > 0.05$. In this study we are therefore investigating the high deformation regime. The linear region of the F-ε^3 curve was observed to begin at relative deformations of 0.12 ± 0.04. The value for the thickness (t) in this study is assumed to be 5 nm, the Poisson ratio (ν) is 0.5 and the radius (R_0) is 1.05 – 2.1 μm. Substituting the appropriate values into equation 13, the bending / stretching ratio at the start of the linear region is generally less than 0.1, with a maximum value of 0.24. This indicates that we are considering regions where the stretching term will always be dominant and the bending term will tend towards being negligible; which is consistent with our use of the stretching term alone for fitting.

A possible correlation between bubble diameter and Young's modulus can be seen in Figure 4.21, though whether this correlation is linear or more complex is not clear at this stage; further investigation and more data points would be required to fully characterize the dependence. A possible explanation for this apparent correlation could be found in our assumption of constant membrane thickness. If larger radius

MBs actually have a thicker shell than their smaller radius counterparts, the observed Young's modulus of the larger MB shells would appear to be larger when our constant thickness calculation is applied. If we rearrange Equation 14 to make the shell thickness (t) variable and fix the Young's modulus (E) at 20 MPa, the resulting shell thickness values range from 2 nm to 9 nm, which could imply structures from a single monolayer up to perhaps 2 bilayers plus a monolayer. The scarcity of measurements of the largest radius MBs means it is difficult to assess whether there are 'steps' in the values which would point to a jump in thickness from 1 layer to multiple layers. An additional effect, particularly in the case of the smaller MBs, could be a modified conformation of the phospholipid molecules in response to the decreasing radius of curvature of the shell, leading to thinner shells which are also more compliant than thicker shells having a standard phospholipid layer conformation. A non-constant shell thickness would also explain why there is no visible correlation between stiffness and bubble radius. As shell thickness is a difficult property to assess independently, our method may be a useful way to assess shell thickness based on F-Δ measurements, which are considerably easier to acquire.

Since the elastic membrane theory characterizes the Young's modulus of the MB shell, it is useful to compare our results with existing studies on lipid bilayers and membrane structures, while remembering that our MB shell may not be comprised of a single bilayer. Künneke et al. [36] reported the Young's modulus for a supported lipid bilayers (SLB) of 1-palmitoly-2-oleoyl-*sn*-glycero-3-phosphoserine (POPS) as 20 MPa. This value was calculated from the observed sample stiffness and the

relation by Sneddon [37] linking stiffness to Young's modulus. This value agrees well with our findings using membrane stretching theory. Other studies find differently, however. Sullan et al. [38] reported values between 50 – 190 MPa for dioleoylphosphatidylcholine/egg sphyingomyelin/cholesterol (DEC) bilayers. It is possible that these larger values can be attributed to the presence of cholesterol, which has been demonstrated to significantly increase the Young's modulus of phospholipid layers. [15] Ogawa et al. [39] carried out tensile tests to analyze segmented polyurethane, as well as phospholipid polymers containing 2-methacryloyloxyethyl phosphorylcholine (MPC); the size of the segments were 12.5 mm × 2.5 mm and the thickness was 200 μm. In the molecule chain, MPC avoids cell adhesion and enhances biocompatibility and antithrombogenicity. The stress – strain curves showed a linear relationship for deformations up to 5%; so the Young's modulus was calculated using simple Hooke's law from the initial elastic region. The Young's modulus was given to be approximately 46 ± 4 MPa for both materials. While this exceeds our findings, the results are of the same order of magnitude.

The single cell AFM compression study on living Jurkat T lymphoma cells [18] which have similar t/R ratio to our system, reports Young's modulus values of 10-30 MPa for the cell membrane, which fits well with our findings; however a subsequent study on other lines of cells, namely human mammary carcinoma cells (MDA-MB-468) and immortalized human prostatic epithelial cells (MLC-SV40) [16] reported much lower values for Young's modulus, 1.5 – 4.9 MPa. In the latter case, relative deformation was very large ($\varepsilon_{max} = 0.8$) and a high degree of blebbing was noticed

during compression indicating that a different mode of deformation occurred which is not described by elastic membrane theory.

Our results are at the lower end of the 14 – 194 MPa range yielded by other studies on phospholipid vesicles which used methods other than AFM, summarized by Rutkowski et al. [3] That study also evaluated the shell Young's modulus of spherical phospholipid vesicles, with a shell thickness (t) of 4 nm and a diameter (D) of 0.1 µm using osmotic-swelling and applying the relation proposed by Li et al. [40] between the stress tensors, pressure, solute concentration, and geometry. Results of this study showed a Young's modulus of 50 MPa.

The GUV Young's modulus of 53 – 109 MPa gathered by AFM as reported by Dieluweit et al. [13] may exceed our results due to the protein coating on the vesicles which influences the properties of the bubble. Within that study, a change in protein coating altered the Young's modulus by up to 50%.

It is important to remember that this theory is designed for vesicles containing incompressible fluids, and Definity® MBs are filled with gas, as noted earlier. Currently, no mechanical model exists which takes account of the compressible gas contained inside Definity® MBs, but the agreement between our results and available literature would suggest that when the deformation is small, the gas is not compressed to an extent which would induce a change in MB volume. This being the case; shell mechanics alone can be used to predict MB properties. In addition, Grant et al. [12] observed a decreasing stiffness of lipid coated MBs with increasing

temperature, which is also consistent with the conclusion that the effect of the internal gas is neglible. We would therefore conclude for the calculation of the Young's modulus of the shell of Definity® MBs, the membrane stretching component of the elastic membrane theory is appropriate.

4.4.3 Hertz Theory

Our results produced an effective Young's modulus between 93 kPa and 233 kPa. The linear region of the F-$\varepsilon^{3/2}$ curves which could be used for analysis with Hertz theory commenced at $\varepsilon = 0.043 \pm 0.025$ and persisted to $\varepsilon = 0.164 \pm 0.075$. This was the most extensive of all the models used in this work and suggests that this model may describe MB behavior over the largest range of deformations. No dependence of Young's modulus on bubble diameter was obvious from the data.

The Hertz theory describes the deformation behavior assuming the MB to be a homogeneous sphere rather than a shell [18] and as such our results must be compared with other studies which calculate the effective Young's modulus of the whole structure. The results of the single cell compression study on T-cells (analogous to a semi-permeable membrane) [18] which uses Hertz theory showed an effective Young's modulus of 4-7.5 kPa for dead cells and 150-230 kPa for fixed cells; the latter being close to our values. However, another study performed on endothelial and cardiac cells, which also used AFM and applied the Hertz theory calculated effective Young's modulus values of 4 kPa for endothelial cells and 100 kPa for cardiac cells. [20]. This range of values, 1-100 kPa, is also found by other

cell studies of different types of isolated cultured cells. [19] It should be noted that some studies made use of tipped cantilevers, therefore measuring the effective Young's modulus associated with indentation rather than whole cell compression. In general, these results are slightly lower than our values, but well within the order of magnitude and with some overlap of the ranges. A study on vesicles [14] reported values for effective Young's Modulus from 0.2 – 1.3 MPa, analyzed using Hertz theory, which is somewhat larger than the values we have found; however the diameters of the vesicles in this study were all <100 nm; much smaller than our MBs.

The most obvious difference between the systems mentioned above and Definity® MBs is the internal contents of the structures. The cells and vesicles are filled with minimally compressible liquid, and the cell nucleus and cytoskeleton may also contribute to the mechanical behavior of cells. However; the agreement between our results and the existing work on cell [18-20] and vesicle [14] systems analyzed with Hertz theory suggests that the effect of the internal gas on the mechanical properties of Definity® MBs is small and that Hertz theory may be a useful tool to calculate the effective whole-bubble Young's modulus for applications such as the modeling of MB systems.

4.4.4 Hysteresis and Instabilities

Phospholipid MBs are widely accepted as visco-elastic materials, with recent research demonstrating that they display visco-elastic creep behavior when a load

applied by AFM is held constant over the course of a few seconds. [12] For this reason, a degree of hysteresis in all curves is to be expected. Both the instabilities and the more pronounced hysteresis visible in curves which display instabilities can possibly be explained by the specific composition of the phospholipid shell. Kim et al. [41] demonstrated with TEM that phospholipid shells of similar composition to Definity® form a polycrystalline grain structure and that deformations can be observed along the boundaries between adjacent grains producing small folds and creases in the surface at relatively low applied loads. We speculate that the instabilities we can see in our F-Δ curves may be explained by localised changes in the surface conformation due to a localisation of stress, followed by relaxation. The most abundant phospholipid in Definity® is DPPC, which has a carbon chain length of 16. It has been demonstrated that materials comprised of C_{16} chain molecules tend to behave in a visco-elastic manner with viscosity markedly dependent on surface pressure. [42]

4.5 Conclusions

This chapter has presented an experimental investigation of Definity® ultrasound contrast agent MBs of diameter 2.1 – 4.2 μm using AFM techniques focusing on the relatively 'high' deformation region (though all the deformations are still within the small deformation regime ($\varepsilon < 0.3$)). The resulting F-Δ curves were used directly to calculate the stiffness of the MBs before the onset of irreversible deformation. The resulting values range from 0.016 – 0.039 N/m. The Young's modulus of the MB shell was calculated using two different mechanical models; of which the membrane

stretching component of elastic membrane theory was most suitable, yielding an average shell Young's modulus between 8 ± 2 MPa and 38 ± 8 MPa. The deformation range under investigation and the similarity of these results with existing literature suggests that analysis using the membrane stretching component of the elastic membrane theory sufficiently describes the behavior of the MB shell without the need to incorporate membrane bending. A possible correlation between Young's modulus and MB diameter was noted in the case of membrane stretching which is attributed to variations in shell thickness and/or structure with size. This points to the need for further investigation in this area and suggests that this could be developed as a useful method to assess shell properties including thickness. Hertz theory was used to evaluate the effective Young's modulus of an equivalent homogeneous sphere having the same dimensions as the MB under test, yielding an average value of 133 ± 59 kPa. This is in broad agreement with values reported for the global Young's moduli of other phospholipid systems. While membrane stretching and Hertz theory show good agreement with existing values of Young's modulus for MB shell and global deformation behavior respectively, it is noted that both theories are designed for a membrane surrounding incompressible fluid rather than the compressible perfluorocarbon gas encapsulated in a Definity® MB. This leads us to conclude that the effect of gas pressure inside the MB does not significantly affect the mechanical properties Definity® MBs for small deformations.

Though we have demonstrated for the first time that a model exists which is a good predictor of phospholipid coated MB Young's modulus in the 'high' deformation regime, there remains a gap in knowledge of MB behaviour at low deformations,

which will be addressed in the following chapter. The low deformation regime is particularly interesting as traditionally mechanical models work well at sufficiently low deformations. In addition, for our systems the effect of the gas will be even more negligible. However, we are working at the nanoscale and at low deformations we might have influences from other sources such as intermolecular forces and even discreteness of matter. It is not certain that continuum mechanics models will work at the nanoscale.

References

[1] Evans EA, Hochmuth RM. Membrane Viscoelasticity. Biophysical Journal. 1976;16:1-11.

[2] Ratanabanangkoon P, Gropper M, Merkel R, Sackmann E, Gast AP. Mechanics of streptavidin-coated giant lipid bilayer vesicles: A micropipet study. Langmuir. 2003;19:1054-62.

[3] Rutkowski CA, Williams LM, Haines TH, Cummins HZ. The Elasticity of Synthetic Phospholipid-Vesicles Obtained by Photon-Correlation Spectroscopy. Biochemistry. 1991;30:5688-96.

[4] Vinogradova OI, Lebedeva OV, Kim BS. Mechanical behavior and characterization of microcapsules. Ann Rev Mater Res. 2006;36:143-78.

[5] Liu K-K. Deformation behaviour of soft particles: a review. Journal of Physics D: Applied Physics. 2006;39:R189.

[6] Glynos E, Koutsos V, McDicken WN, Moran CM, Pye SD, Ross JA, et al. Nanomechanics of Biocompatible Hollow Thin-Shell Polymer Microspheres. Langmuir. 2009;25:7514-22.

[7] Glynos E, Sboros V, Koutsos V. Polymeric thin shells: Measurement of elastic properties at the nanometer scale using atomic force microscopy. Materials Science and Engineering B-Advanced Functional Solid-State Materials. 2009;165:231-4.

[8] Sboros V, Glynos E, Pye SD, Moran CM, Butler M, Ross J, et al. Nanointerrogation of ultrasonic contrast agent microbubbles using atomic force microscopy. Ultrasound in Medicine and Biology. 2006;32:579-85.

[9] Sboros V, Glynos E, Pye SD, Moran CM, Butler M, Ross JA, et al. Nanomechanical probing of microbubbles using the atomic force microscope. Ultrasonics. 2007;46:349-54.

[10] Sboros V, Glynos E, Ross JA, Moran CM, Pye SD, Butler M, et al. Probing microbubble targeting with atomic force microscopy. Colloids Surf B Biointerfaces. 2010;80:12-7.

[11] McKendry JE, Grant CA, Johnson BRG, Coletta PL, Evans JA, Evans SD. Force spectroscopy of streptavidin conjugated lipid coated microbubbles. Bubble Science, Engineering & Technology. 2010;2:48-54.

[12] Grant CA, McKendry JE, Evans SD. Temperature dependent stiffness and visco-elastic behaviour of lipid coated microbubbles using atomic force microscopy. Soft Matter. 2012;8:1321-6.

[13] Dieluweit S, Csiszár A, Rubner W, Fleischhauer J, Houben S, Merkel R. Mechanical Properties of Bare and Protein-Coated Giant Unilamellar Phospholipid Vesicles. A Comparative Study of Micropipet Aspiration and Atomic Force Microscopy. Langmuir. 2010;26:11041-9.

[14] Laney DE, Garcia RA, Parsons SM, Hansma HG. Changes in the elastic properties of cholinergic synaptic vesicles as measured by atomic force microscopy. Biophysical Journal. 1997;72:806-13.

[15] Liang XM, Mao GZ, Ng KYS. Mechanical properties and stability measurement of cholesterol-containing liposome on mica by atomic force microscopy. Journal of Colloid and Interface Science. 2004;278:53-62.

[16] Lulevich V, Shih YP, Lo SH, Liu GY. Cell Tracing Dyes Significantly Change Single Cell Mechanics. Journal of Physical Chemistry B. 2009;113:6511-9.

[17] Lulevich VV, Andrienko D, Vinogradova OI. Elasticity of polyelectrolyte multilayer microcapsules. Journal of Chemical Physics. 2004;120:3822-6.

[18] Lulevich V, Zink T, Chen HY, Liu FT, Liu GY. Cell mechanics using atomic force microscopy-based single-cell compression. Langmuir. 2006;22:8151-5.

[19] Janmey PA, McCulloch CA. Cell mechanics: Integrating cell responses to mechanical stimuli. Annual Review of Biomedical Engineering. 2007;9:1-34.

[20] Mathur AB, Collinsworth AM, Reichert WM, Kraus WE, Truskey GA. Endothelial, cardiac muscle and skeletal muscle exhibit different viscous and elastic properties as determined by atomic force microscopy. Journal of Biomechanics. 2001;34:1545-53.

[21] Definity(R) Prescribing Information. Lantheus Medical Imaging, Inc., Billerica, MA; April 2013. http://www.lantheus.com/PDF/pi/DEFINITY%20Prescribing%20Information%2051 5987-0413.pdf. Accessed March 25, 2014.

[22] Unger EC, Porter T, Culp W, Labell R, Matsunaga T, Zutshi R. Therapeutic applications of lipid-coated microbubbles. Advanced Drug Delivery Reviews. 2004;56:1291-314.

[23] Chen WS, Lu XC, Liu YB, Zhong P. The effect of surface agitation on ultrasound-mediated gene transfer in vitro. Journal of the Acoustical Society of America. 2004;116:2440-50.

[24] Cheung K, Couture O, Bevan PD, Cherin E, Williams R, Burns PN, et al. In vitro characterization of the subharmonic ultrasound signal from Definity microbubbles at high frequencies. Physics in Medicine and Biology. 2008;53:1209-23.

[25] Goertz DE, de Jong N, van der Steen AFW. Attenuation and size distribution measurements of definity (TM) and manipulated definity (TM) populations. Ultrasound in Medicine and Biology. 2007;33:1376-88.

[26] Sarkar K, Katiyar A, Jain P. Growth and Dissolution of an Encapsulated Contrast Microbubble: Effects of Encapsulation Permeability. Ultrasound in Medicine and Biology. 2009;35:1385-96.

[27] Sontum PC. Physicochemical Characteristics of Sonazoid(TM), A New Contrast Agent for Ultrasound Imaging. Ultrasound in Medicine & Biology. 2008;34:824-33.

[28] Needham D, Kim DH. PEG-covered lipid surfaces: bilayers and monolayers. Colloids and Surfaces B: Biointerfaces. 2000;18:183-95.

[29] Johnson D, Hilal N, Waters K, Hadler K, Cilliers J. Measurements of Interactions between Particles and Charged Microbubbles Using a Combined Micro- and Macroscopic Strategy. Langmuir. 2009;25:4880-5.

[30] D'Agostino DP, Olson JE, Dean JB. Acute Hyperoxia Increases Lipid Peroxidation and Induces Plasma Membrane Blebbing in Human U87 Glioblastoma Cells. Neuroscience. 2009;159:1011-22.

[31] Bergeron V, Claesson PM. Structural forces reflecting polyelectrolyte organization from bulk solutions and within surface complexes. Advances in Colloid and Interface Science. 2002;96:1-20.

[32] Sboros V, Glynos E, Pelekasis N, Koutsos V. Nano-interrogation of a Lipid Shelled Microbubble. IEEE International Ultrasonics Symposium2008. p. 997-8.

[33] Daily B, Elson EL, Zahalak GI. Cell Poking - Determination of the Elastic Area Compressibility Modulus of the Erythrocyte-Membrane. Biophysical Journal. 1984;45:671-82.

[34] Gregory RD, Milac TI, Wan FYM. A thick hollow sphere compressed by equal and opposite concentrated axial loads: An asymptotic solution. Siam Journal on Applied Mathematics. 1999;59:1080-97.

[35] Elsner N, Dubreuil F, Weinkamer R, Wasicek M, Fischer FD, Fery A. Mechanical properties of freestanding polyelectrolyte capsules: a quantitative approach based on shell theory. Characterization of Polymer Surfaces and Thin FIlms. 2006;132:117-23.

[36] Künneke S, Krüger D, Janshoff A. Scrutiny of the failure of lipid membranes as a function of headgroups, chain length, and lamellarity measured by scanning force microscopy. Biophysical Journal. 2004;86:1545-53.

[37] Sneddon IN. The relation between load and penetration in the axisymmetric boussinesq problem for a punch of arbitrary profile. International Journal of Engineering Science. 1965;3:47-57.

[38] Sullan RMA, Li JK, Zou S. Direct Correlation of Structures and Nanomechanical Properties of Multicomponent Lipid Bilayers. Langmuir. 2009;25:7471-7.

[39] Ogawa R, Watanabe J, Ishihara K. Domain-controlled polymer alloy composed of segmented polyurethane and phospholipid polymer for biomedical applications. Science and Technology of Advanced Materials. 2003;4:523-30.

[40] Li W, Aurora TS, Haines TH, Cummins HZ. Elasticity of Synthetic Phospholipid-Vesicles and Submitochondrial Particles During Osmotic Swelling. Biochemistry. 1986;25:8220-9.

[41] Kim DH, Costello MJ, Duncan PB, Needham D. Mechanical properties and microstructure of polycrystalline phospholipid monolayer shells: Novel solid microparticles. Langmuir. 2003;19:8455-66.

[42] Krägel J, Kretzschmar G, Li JB, Loglio G, Miller R, Möhwald H. Surface rheology of monolayers. Thin Solid Films. 1996;284-285:361-4.

Chapter 5: An Investigation of the Nanomechanical Properties of BR14

5 An Investigation of the Nanomechanical Properties of BR14

5.1 Introduction

The previous chapter on the behaviour of Definity® MBs has demonstrated that in the high deformation regime membrane stretching is the most suitable model to describe the Young's modulus. Definity® has also been demonstrated to behave differently than stiffer polymeric MBs. The next step was to investigate the low deformation regime more fully, to ascertain if any of the other proposed models are effective in this regime. In this chapter, the MB system BR14 (Bracco Diagnostics, Geneva, Switzerland) is investigated. This chapter focuses on the low deformation regime (< 80 nm, ε < 0.04), and aims to assess the suitability of the models on BR14 MBs, which have not previously been investigated in this manner.

In addition to the three models utilised in the Definity® study, an additional model, De Jong theory, was included in the analysis of the force spectroscopy data. After the main study was completed, some of the remaining BR14 MBs were subjected to force spectroscopy experiments with tipped cantilevers with a view to examining how the deformation behaviour differs between the tipped and untipped contact geometry.

5.2 Materials and Methods

5.2.1 Materials

Phospholipid stabilized MBs of the type BR14 (Bracco Diagnostics, Geneva, Switzerland) in lyophilised powder form were reconstituted with 5 ml of 10% saline as per manufacturer's instructions, resulting in BR14 MBs in the size range 1 – 10 μm. BR14 is a research grade MB which is not in commercial use so the exact lipid composition is proprietary information; however since BR14 is a precursor product to Sonovue® the lipids in BR14 are most likely to be a mix of distearoylphosphatidylcholine (DPPC) and dipalmitoylphosphatidylglycerol (DPPG). [1, 2] The encapsulated gas is known to be perfluorobutane (C_4F_{10}). [3, 4]

5.2.2 Sample Preparation

Samples were prepared for force spectroscopy measurements as described in Chapter 3. Once the MBs were suitably dispersed across the surface of the dish, they were submerged in 10% saline solution and AFM measurements were taken in aqueous conditions.

5.2.3 Force Spectroscopy

AFM measurements were taken using the molecular force probe (MFP – 1D) (Asylum Research, Santa Barbara, CA) with Mikromasch CSC-12 tipless cantilevers (Mikromash, Tallinn, Estonia) with aluminium back coating having nominal spring constants in the range 0.03 – 0.08 N/m or Bruker (then Veeco) MLCT AUNM tipped cantilevers (Bruker AFM probes, Camarillo, CA) having nominal spring constants 0.005 – 0.01. The speed of the cantilever during approach and retract was constant at 3 μm/s. Each curve spanned a vertical distance of 3 μm (including the non-contact region). The use of a tipless cantilever (width 35 μm) against the MB (D = 4 μm) can be considered an approximate sphere – plate geometry. Multiple curves were taken for each bubble to ascertain that all deformation was elastic. The raw position – deflection data was transformed to force – distance (F-d) and subsequently to force – deformation (F-Δ) and force – relative deformation (F-ε) curves which display only the deformation behaviour of the MB (i.e. the cantilever behaviour is excluded).

5.3 Results

5.3.1 Tipless Cantilevers

Experiments were conducted on several different vials of BR14, all within 48 hours of the MBs being reconstituted. The resulting force-deformation curves were checked for repeatability; an indication that all deformation was in the elastic regime.

MBs which showed poor repeatability or anomalous behaviour were excluded. Any curves which did not meet the requirements for a minimum number of 90 points in the fitted region for MB stiffness were also excluded. These quite stringent criteria yielded a final number of eight MBs. The subsequent analysis of the MB data continued as described in Chapter 4, starting with the calculation of MB stiffness.

5.3.1.1 Stiffness

Multiple compressions (>10) were recorded on eight individual MBs ranging in diameter from 4.27 μm to 7.93 μm. In all cases the resulting F-Δ curves showed good repeatability indicating that no permanent deformation occurred as a result of the experiment. The effective stiffnesses of the MBs were calculated from the gradient of the initial linear section of the *F*-Δ curve up to a maximum of 80 nm. The first 25 nm of the measurement are excluded from the analysis as non-linear effects and surface interactions make the data unreliable in this region.

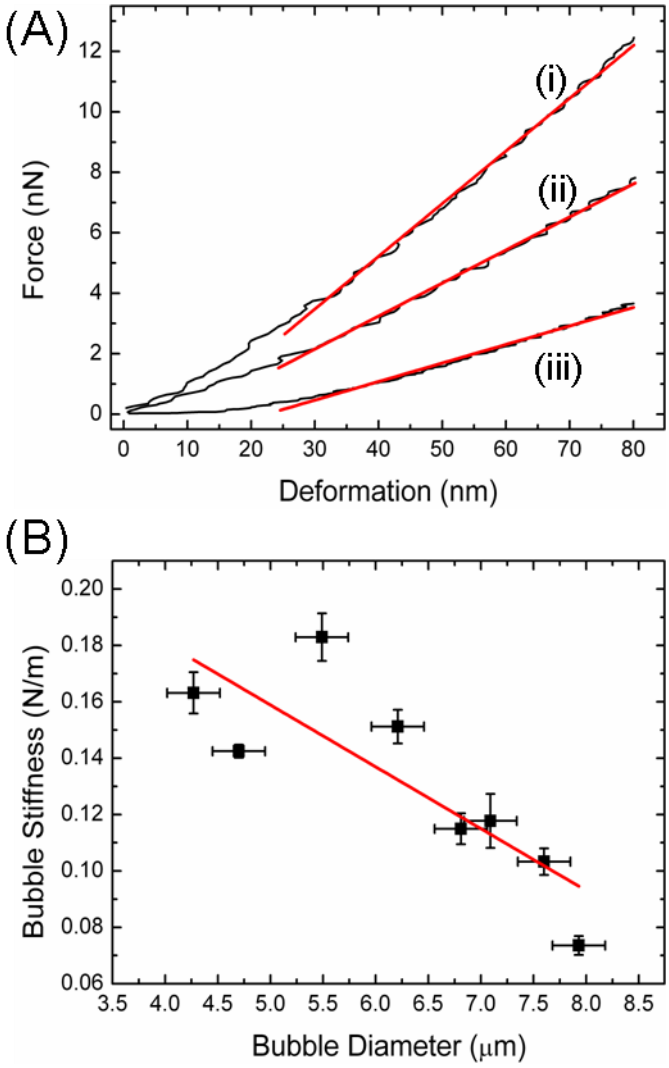

Figure 5.24 Microbubble stiffness (A) Example force – deformation curves for 3 different MBs. Curve (i) has diameter 5.49 µm and stiffness 0.183 N/m. Curve (ii) has diameter 6.81 µm and stiffness 0.115 N/m, and curve (iii) has diameter 7.93 µm and stiffness 0.074 N/m. (B) Effective stiffness values for 8 individual MBs ranging in diameter from 4.27 µm to 7.93 µm.

Figure 5.24 (A) shows individual curves from three different MBs, having diameters 7.93, 6.81 and 5.49 µm and stiffnesses of 0.074 ± 0.003, 0.115 ± 0.010 and 0.183 ± 0.008 N/m respectively. The curves can be seen to be quite linear after an initial unstable region up to the cut off of 80 nm. Figure 5.24 (B) shows the range of

stiffnesses from 0.074 – 0.183 N/m and the link between MB diameter and stiffness. A clear trend can be seen, showing a linear decrease in stiffness with increasing MB diameter.

5.3.1.2 Mechanical Models

Assuming that the MB shell has constant thickness, a value of t = 5 nm was selected. Figure 5.25(A) shows the values of Young's modulus for each bubble as calculated using Reissner and elastic membrane theories. The Reissner values fall in the range of 4.37 ± 0.200 to 7.58 ± 0.329 GPa.

In order to use the elastic membrane model, the upper limit of 80 nm deformation was used to calculate the upper value of relative deformation, ε_{max}, for each MB. The range of ε_{max} was found to be 0.010 – 0.019. For these values of ε_{max}, the inverse of Equation 13 (F_s/F_b) gives values smaller than about 0.2 which shows that stretching can be neglected and membrane bending should be the predominant mode of deformation. Further analysis used membrane bending only. Taking the gradient of the F–$\varepsilon^{1/2}$ curves from the experiment and substituting them into membrane bending equation produces Young's modulus values in the range 2.34 ± 0.008 to 6.08 ± 0.65 GPa. Fitting using linear regression shows that there is very little change in modulus with radius for either the Reissner or membrane bending models.

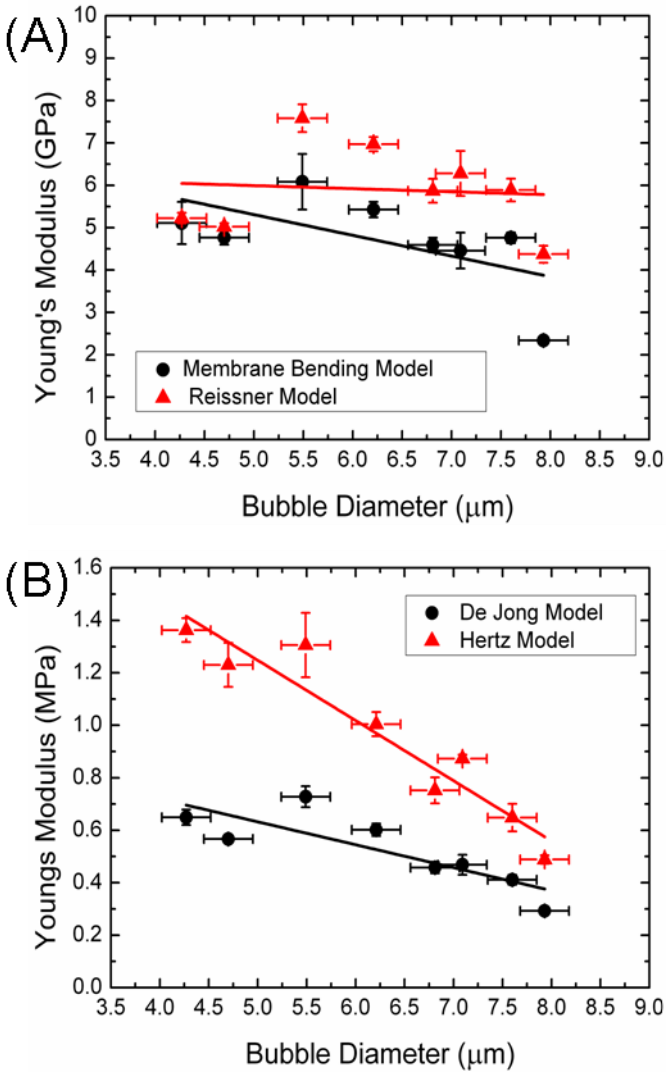

Figure 5.25 Young's Modulus of microbubbles (A) Young's modulus values as calculated with Reissner and the membrane bending component of elastic membrane theories. (B) Young's modulus values as calculated with De Jong and Hertz theories. Red lines on all graphs indicate best fit calculated by linear regression.

Taking the gradient of the F – $\varepsilon^{3/2}$ curves and applying simple Hertz theory yields Young's modulus values in the range 0.49 ± 0.016 to 1.36 ± 0.046 MPa (Figure 5.25(B)).

Using the De Jong model to calculate Young's modulus from MB stiffness, we find values in the range 0.30 ± 0.013 to 0.73 ± 0.040 MPa. Linear regression fitting of both Hertz and De Jong datasets highlights that Hertz theory shows a clear dependence on diameter, whereas the De Jong model shows a much less pronounced trend.

5.3.2 Tipped Cantilevers

These experiments were conducted on MBs exceeding 48 hours old, though the MBs appeared to remain stable for several months. Experiments over 2 days yielded data on twenty one MBs. On analysis, all results gathered on day 2 were found to have either very poor repeatability or to be too short for further analysis. Of the data gathered on day 1, five MBs were considered suitable for stiffness analysis and subsequent fitting with the Hertz model.

5.3.2.1 Stiffness

Multiple compressions (>10) were recorded on five individual MBs ranging in diameter from 3.55 μm to 7.57 μm. In all cases the resulting F-Δ curves showed good repeatability indicating that no permanent deformation occurred as a result of the experiment. The effective stiffnesses of the MBs were calculated from the gradient of the initial linear section of the F-Δ curve up to a maximum of 70 nm. The first 25 nm of the measurement are excluded from the analysis as non-linear effects and surface

interactions make the data unreliable in this region. Figure 5.26 shows the range of stiffnesses from 0.134 ± 0.004 to 0.281 ± 0.010 N/m. There is insufficient data to determine with confidence whether a correlation between MB diameter and stiffness exists.

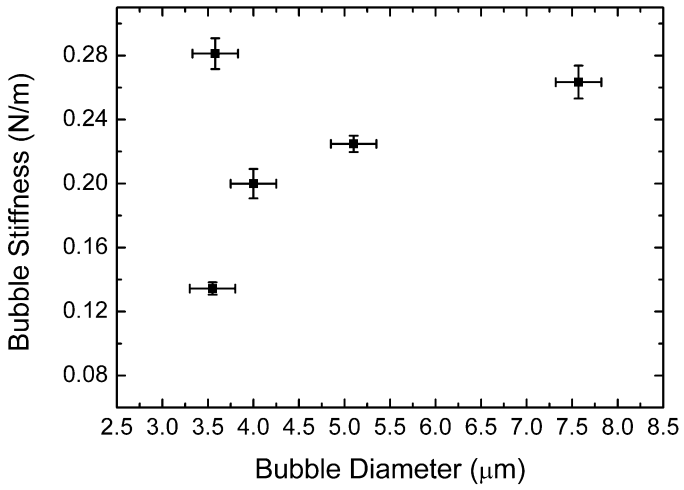

Figure 5.26 Effective stiffness values for 5 individual MBs ranging in diameter from 3.55 μm to 7.57 μm.

5.3.2.2 Hertz theory

Fitting using Hertz theory was completed in a similar manner to the analysis of tipless cantilever experiments, taking the gradient of the F-$\varepsilon^{3/2}$ curves; however in the case of tipped cantilevers the radius of interest is the radius of the cantilever tip. The nominal value of 20 nm provided by the manufacturer was used in calculations. The Young's modulus of each MB was calculated according to equation 11, a different expression of the relation used in the tipless cantilever analysis.

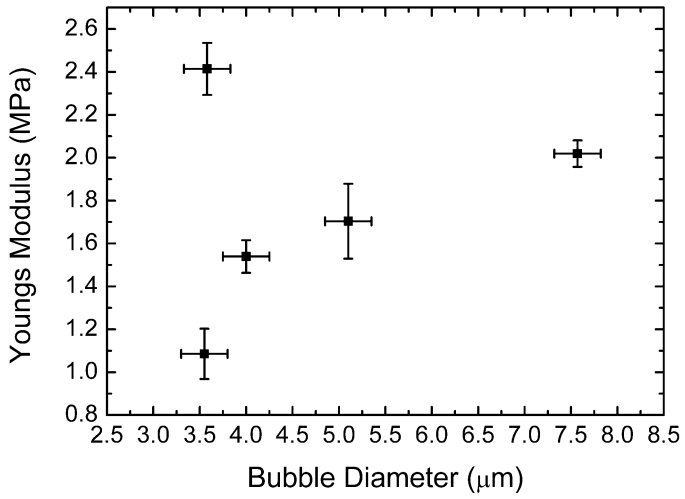

Figure 5.27 Young's modulus values of MBs as calculated with Hertz theory for tipped cantilever experiments.

Figure 5.27 shows the Young's modulus values in the range 1.09 ± 0.12 to 2.41 ± 0.12 MPa. There is insufficient data to determine with confidence whether a correlation between MB diameter and Young's Modulus is demonstrated.

5.3.3 Results Summary

The following tables summarise the key results from this study.

Cantilever Type	Cantilever Spring Constant (N/m)	MB Spring Constant (N/m)	Size Dependence Y/N
Tipless	0.03 – 0.08	0.074 – 0.183	Y
Tipped	0.005 – 0.01	0.134 – 0.281	N

Table 5.1 Summary of Stiffness Results for the Experimental Examination of BR14 MBs

Cantilever Type	Mechanical Model	Deformation Regime	Shell / Sphere	Size Dependence Y/N	Young's Modulus
Tipless	Reissner	Low	Shell	N	4.37 – 7.58 GPa
Tipless	Membrane Bending	Low	Shell	Y	2.34 – 6.08 GPa
Tipless	De Jong	Low	Shell	N	0.30 – 0.73 MPa
Tipless	Hertz	Low	Sphere	N	0.49 – 1.36 MPa
Tipped	Hertz	Low	Membrane	N	1.09 – 2.41 MPa

Table 5.2. Summary of Young's Modulus Results for the Experimental Examination of BR14 MBs

5.4 Discussion

5.4.1 Tipless Cantilevers

Figure 5.24 (B) shows the range of stiffnesses from 0.074 – 0.183 N/m and the link between MB diameter and stiffness. This is a bit higher than the previously reported average stiffness of 0.056 N/m for BR14, [5] and in addition a clear trend can be seen, showing a linear decrease in stiffness with increasing MB diameter, which is in keeping with classical mechanics for shells having constant thickness. This is in contrast to the previous work on Definity® which showed no trend, but has been demonstrated previously in work by another group which uses microfluidic devices to produce MBs with carefully controlled constant thickness. [6] Taking this trend in stiffness with MB diameter as evidence that the MB shell has constant thickness, a value of t = 5 nm was selected; this is the same value used in the calculations in Chapter 4 and it therefore makes the results of the two studies consistent. There is a marked difference in MB stiffness between the two systems, with Definity® MBs having measured stiffness values averaging around 0.026 N/m; even the most compliant of the BR14 MBs are almost 4 times stiffer. When this is combined with the fact that the measured Definity® MBs were also smaller than the measured BR14 MBs, this suggests that the stiffness difference is close to an order of magnitude. We would expect this large difference in stiffness to be borne out in the Young's modulus measurements.

Figure 5.25 (A) shows the values of Young's modulus for each bubble as calculated using Reissner and elastic membrane theories. The Reissner values fall in the range of 4 – 8 GPa, the membrane bending equation produces Young's modulus values in the range 2 – 7 GPa with very little change in modulus with radius for either model. In both cases, while the actual Young's modulus values are an overestimate by an order of magnitude, the Young's modulus is demonstrated to be almost constant, which is as one would expect for an intrinsic property of the material.

Hertz theory yields Young's modulus values in the range 0.47 – 1.6 MPa (Figure 5.27(B)). This is in keeping with values found for vesicle [7] and cell [8] systems using Hertz theory and suggests that the Hertz model has some validity in the case of very small deformations. This was initially somewhat unexpected as the principle tenet of Hertz theory – that the sphere be a homogeneous material – is not true in the case of these MBs; however the experiment is limited to very small deformations so this assumption is not excessively violated. The range of Young's modulus values exceeds that of the Definity® MBs analysed with this model, which yielded values from 0.09 to 0.23 MPa, and the trend in Young's modulus with MB radius for BR14 is also in contrast with the behaviour of Definity® MBs which did not show a trend with this model.

Using the De Jong model to calculate Young's modulus, we find values in the range 0.30 – 0.75 MPa. These values are somewhat lower than the we would expect given the results in other systems such as supported lipid bilayers [9] (20 – 190 MPa), thick segments of phospholipids [10] (46 MPa) and other vesicle studies (14 – 194 MPa);

[11] however this might be explained by the fact that we are in the low deformation regime. The original model assumes whole – bubble deformation with pressure distributed evenly across the entire MB surface, however in this study of very small deformations it is very likely that the MBs deform mostly at the poles. Linear regression fitting of both Hertz and De Jong datasets highlights that Hertz theory shows a clear dependence on MB diameter, whereas the De Jong model shows a much less pronounced trend. Since the Young's modulus should be an intrinsic property of the material, these results suggest that the De Jong model has potential to be quite useful as an indicator of MB Young's modulus; in this particular study it is the most plausible of the available models from this point of view although its absolute values are not in the expected range.

5.4.2 Tipped Cantilevers

In experiments with tipped cantilevers, stiffness ranged from 0.134 – 0.281 N/m with no observable trend with stiffness, though there are not many data points. This is in contrast to the MBs compressed with tipless cantilevers which are notably less stiff, between 0.074 and 0.183 N/m, and showed a marked trend with stiffness. Applying simple Hertz theory yields values in the range 1.09 – 2.41 MPa. Again, there is no obvious correlation between Young's modulus and MB radius, however the scarcity of data means that it is not possible to conclusively exclude any trend. These values are somewhat higher than the 0.47 – 1.6 MPa found using Hertz theory with tipless cantilevers, but there is some overlap in the range. Subsequent work (see Chpater 6)

has suggested that this difference may be due to the age of the MBs in this study. In nay case, the Young's modulus values found using tipped cantilevers are lower than those found by experiments on lipid bilayer membranes, which are more in the region of 20 – 190 MPa. [9, 12]

5.5 Conclusions

This chapter has presented an experimental investigation of BR14 ultrasound contrast agent MBs of diameter 4.27 – 7.93 μm with tipless cantilevers. The resulting F-Δ curves were used directly to calculate the stiffness of the MBs. The resulting values range from 0.074 – 0.183 N/m. The stiffness of the MB can be seen to decrease with increasing MB radius, indicating that BR14 MBs have constant thickness. The Young's modulus of the MB shell was calculated using three different mechanical models; of which De Jong theory was most suitable as there is minimal correlation between Young's modulus and MB diameter. The shell Young's modulus values calculated by this model are between 0.30 – 0.75 MPa. Hertz theory was used to evaluate the effective Young's modulus of an equivalent homogeneous sphere having the same dimensions as the MB under test, yielding values in the range 0.47 – 1.6 MPa.

From the additional experiments with tipped cantilevers, it could be concluded that the isolated membrane is stiffer than the whole MB. However, one has to note that the MBs associated with the tipped cantilevers were aged. The Hertz model appears

to provide a reasonable estimate of membrane Young's modulus; however the scarcity of data in this part of the study suggests that further experimental data with tipped cantilevers is necessary in order to check these initial findings.

References

[1] Schneider M. SonoVue, a new ultrasound contrast agent. European Radiology. 1999;9:S347-S8.

[2] Hohmann J, Müller A, Skrok J, Wolf K-J, Martegani A, Dietrich CF, et al. Detection of Hepatocellular Carcinoma and Liver Metastases with BR14: A Multicenter Phase IIA Study. Ultrasound in Medicine & Biology. 2012;38:377-82.

[3] Sboros V. Response of contrast agents to ultrasound. Advanced Drug Delivery Reviews. 2008;60:1117-36.

[4] Schneider M, Broillet A, Bussat P, Giessinger N, Puginier J, Ventrone R, et al. Gray-scale liver enhancement in VX2 tumor-bearing rabbits using BR14, a new ultrasonographic contrast agent. Investigative Radiology. 1997;32:410-7.

[5] Sboros V, Glynos E, Pelekasis N, Koutsos V. Nano-interrogation of a Lipid Shelled Microbubble. IEEE International Ultrasonics Symposium2008. p. 997-8.

[6] McKendry JE, Grant CA, Johnson BRG, Coletta PL, Evans JA, Evans SD. Force spectroscopy of streptavidin conjugated lipid coated microbubbles. Bubble Science, Engineering & Technology. 2010;2:48-54.

[7] Laney DE, Garcia RA, Parsons SM, Hansma HG. Changes in the elastic properties of cholinergic synaptic vesicles as measured by atomic force microscopy. Biophysical Journal. 1997;72:806-13.

[8] Lulevich V, Zink T, Chen HY, Liu FT, Liu GY. Cell mechanics using atomic force microscopy-based single-cell compression. Langmuir. 2006;22:8151-5.

[9] Künneke S, Krüger D, Janshoff A. Scrutiny of the failure of lipid membranes as a function of headgroups, chain length, and lamellarity measured by scanning force microscopy. Biophysical Journal. 2004;86:1545-53.

[10] Ogawa R, Watanabe J, Ishihara K. Domain-controlled polymer alloy composed of segmented polyurethane and phospholipid polymer for biomedical applications. Science and Technology of Advanced Materials. 2003;4:523-30.

[11] Rutkowski CA, Williams LM, Haines TH, Cummins HZ. The Elasticity of Synthetic Phospholipid-Vesicles Obtained by Photon-Correlation Spectroscopy. Biochemistry. 1991;30:5688-96.

[12] Sullan RMA, Li JK, Zou S. Direct Correlation of Structures and Nanomechanical Properties of Multicomponent Lipid Bilayers. Langmuir. 2009;25:7471-7.

Chapter 6: An Investigation of the Nanomechanical Properties of Sonovue®

6 An Investigation of the Nanomechanical Properties of Sonovue®

6.1 Introduction

The previous chapters on Definity® and BR14 have investigated two different types of commercially produced MBs and have highlighted significant differences between the different deformation regimes. We showed that in the relatively high deformation range the stretching term of the membrane theory works well. However, we have seen in the previous chapter that at low deformations the theories are largely unsatisfactory. In response to this, a final study was conceived which would expand the investigation to a third type of MB and be more comprehensive on the low deformation range while including the high deformation range for comparison within the same system. The overall aim was to collect a greater volume of data with different cantilever spring constants and types on a different (but still phospholipid-based) system. The MB system chosen for this final study was Sonovue®, which is a commercial product currently on the market for use in clinical applications.

This investigation includes ‘soft’, ‘hard’ and also tipless cantilevers in order to investigate whether the observed stiffness values are affected by a change in cantilever spring constant or type in the same system. Experiments are again conducted using tipped cantilevers but with recently reconstituted MBs which are

closer to their clinical usage lifetime. The increased number of experiments carried out necessitated some additions to the experimental procedure which are detailed in Section 6.2.3. The data analysis and mechanical models used were the same as those used in Chapter 5.

6.2 Materials and Methods

6.2.1 Materials

Phospholipid stabilized MBs of the type Sonovue® (Bracco Diagnostics, Geneva, Switzerland) in lyophilised powder form were reconstituted with 5 ml saline as per manufacturer's instructions. The lipids in Sonovue® are a mix of distearoyl-phosphatidylcholine (DSCP) and dipalmitoylphosphatidylglycerol sodium (DPPG.Na). The encapsulated gas is sulphur hexafluoride (SF_6). [1]

6.2.2 Sample Preparation

Samples were prepared for force spectroscopy measurements as described in Chapter 3. Once the MBs were suitably dispersed across the surface of the dish, they were submerged in 10% saline solution and AFM measurements were taken in aqueous conditions.

6.2.3 Experimental Protocol

As the range of experiments in this chapter is more extensive than previously, consideration was given to the order in which data was gathered. It was important that factors such as potential variation in batches could be monitored, though it was considered unlikely given the stability of the results on other MB systems. The potential deterioration in the MBs over time also had to be accounted for as by necessity experiments would take place over more than one day. It was decided that experiments would be conducted on three separate vials of Sonovue® MBs, with the soft, hard and tipped cantilevers used in rotation so that as many possible combinations of comparable data could be produced. The experimental timetable is shown in Table 6.1, which indicates which type of cantilever was used in force spectroscopy measurements on each day. 'Soft' refers to CSC 38 tipless cantilevers, 'hard' refers to CSC 37 tipless cantilevers and 'tipped' refers to MLCT AUNM tipped cantilevers. Day 1 is the day of MB reconstitution.

Batch Number	Day 1	Day 2	Day 3
1	Soft	Hard Tipped	Soft Hard
2	Hard	Tipped Soft	Hard Tipped
3	Tipped	Soft Hard	Tipped Soft

Table 6.1 Order of Force Spectroscopy Experiments on Sonovue® MBs

Experience suggested that results gathered immediately after MB reconstitution were often the best quality, so only one type of cantilever was used on Day 1 in order to maximise the volume of acquired data and minimise time lost due to cantilever calibration.

6.2.4 Force Spectroscopy

AFM measurements were taken using the molecular force probe (MFP – 1D) (Asylum Research, Santa Barbara, CA) with Mikromasch CSC-38 tipless cantilevers (formerly CSC-12) (Mikromash, Tallinn, Estonia) with aluminium back coating having nominal spring constants in the range 0.03 – 0.09 N/m, CSC-37 tipless cantilevers (Mikromash, Tallinn, Estonia) with aluminium back coating having nominal spring constants in the range 0.3 – 0.8 N/m, or Bruker (then Veeco) MLCT AUNM tipped cantilevers (Bruker AFM probes, Camarillo, CA) having nominal spring constants 0.005 – 0.025 N/m. The speed of the cantilever during approach and retract was constant at 3 μm/s. Each curve spanned a vertical distance of 3 μm (including the non-contact region). The raw position – deflection data was transformed to force – distance (F-d) and subsequently to force – deformation (F-Δ) and force – relative deformation (F-ε) curves which display only the deformation behaviour of the MB (i.e. the cantilever behaviour is excluded).

6.3 Results

Experiments were conducted on several different vials of Sonovue®, all within 36 hours of the MBs being reconstituted. The resulting force-deformation curves were checked for repeatability; and MBs which showed poor repeatability or anomalous behaviour were excluded as it indicated either MBs that did not adhere well (some unwanted lateral movement could be seen) or which were damaged/not well formed. The subsequent analysis of the MB data continued as described in Chapter 4. No significant variation was noted between different experimental batches and the MBs showed no deterioration over the course of each three day experiment.

6.3.1 Soft Tipless Cantilevers

Sonovue® MBs were compressed with tipless cantilevers having (measured) spring constants in the range 0.027 – 0.044 N/m. Experiments with such soft cantilevers proved tricky. After examining the recorded F–Δ curves for repeatability, 6 MBs were deemed suitable for further analysis. These MBs were spread across all three experimental batches and were included MBs tested on days 1, 2 and 3 of MB reconstitution. These MBs were subsequently analysed to determine their stiffness and the mechanical models were used to evaluate Young's Modulus.

6.3.1.1 Stiffness

Multiple compressions were recorded on six individual MBs ranging in diameter from 3.86 µm to 6.42 µm. In all cases the resulting *F*–Δ curves showed good repeatability indicating that no permanent deformation occurred as a result of the experiment. The effective stiffnesses of the MBs were calculated from the gradient of the initial linear section of the *F*–Δ curve. The first 25 nm of the measurement are excluded from the analysis. Figure 6.28 shows individual curves from three different MBs, having diameters 6.17, 4.71 and 4.10 µm and stiffnesses of 0.050 ± 0.003, 0.041 ± 0.007 and 0.020 ± 0.001 N/m respectively.

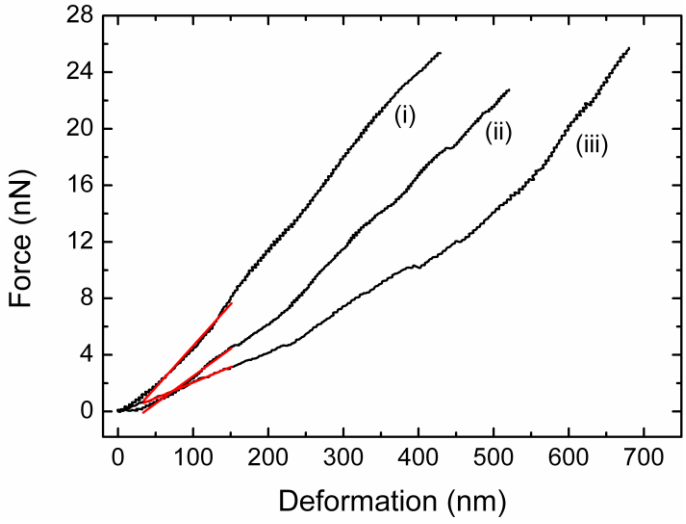

Figure 6.28 *F*-Δ curves for three different MBs. Curve (i) has diameter 6.17 µm and stiffness 0.050 N/m. Curve (ii) has diameter 4.71 µm and stiffness 0.041N/m, and curve (iii) has diameter 4.10 µm and stiffness 0.020 N/m.

Figure 6.29 shows the range of stiffnesses from 0.020 ± 0.001 to 0.050 ± 0.003 N/m. There is a suggestion for a correlation between MB diameter and stiffness.

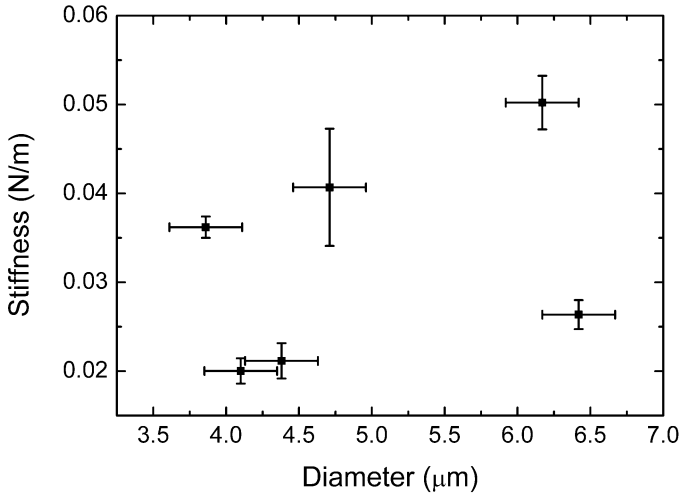

Figure 6.29 Effective stiffness values for 6 individual MBs ranging in diameter from 3.86 μm to 6.42 μm

6.3.1.2 Mechanical Models

For consistency with the other investigations, the MB shell thickness was assumed to be 5 nm. Analysis with the mechanical models was completed as in the preceding chapters. Figure 6.30 shows the values of Young's modulus for each bubble as calculated using Reissner theory. The values fall in the range of 0.62 ± 0.04 to 2.32 ± 0.13 GPa. An increase in Young's modulus with increasing MB radius can be seen.

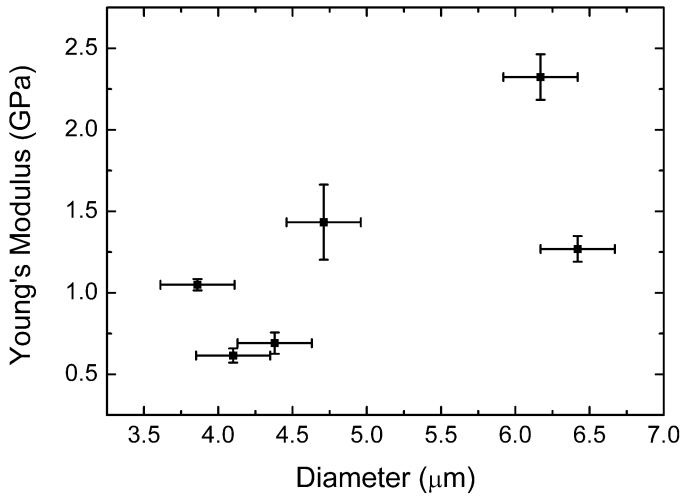

Figure 6.30 Young's modulus values for 6 MBs ranging in diameter from 3.86 µm to 6.42 µm calculated using Reissner theory

When considering the elastic membrane theory, at small deformations membrane bending should be the predominant mode of deformation. Equation 13 shows the ratio of bending to stretching; inverting this equation and setting $F_S / F_B < 0.05$ allows us to define at what value of ε stretching becomes negligible. Using equation 13, the value of ε_{crit} below which bending is the predominant mode of deformation is 0.01, so curve fitting was limited to this region. Taking the gradient of the $F–\varepsilon^{1/2}$ curves from the experiment and substituting them into membrane bending equation produces Young's modulus values in the range 0.83 ± 0.03 to 2.42 ± 0.15 GPa, as shown in Figure 6.31. Again, there is a suggestion of an increase in Young's modulus with increasing radius.

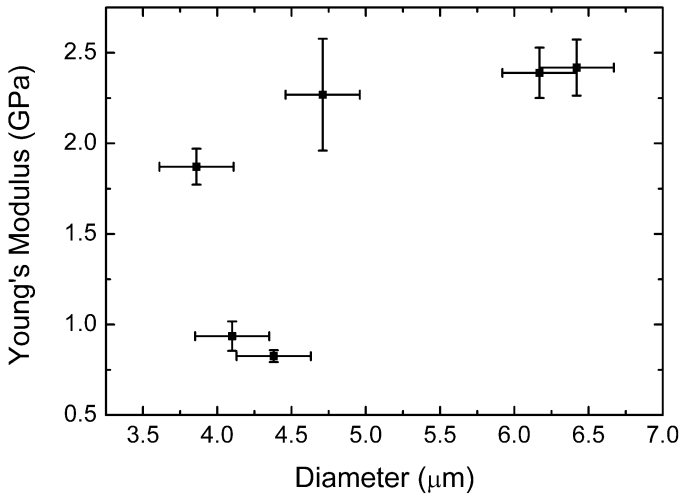

Figure 6.31 Young's modulus values for 6 MBs ranging in diameter from 3.86 µm to 6.42 µm calculated using the membrane bending component of elastic membrane theory

At larger deformations, membrane stretching should start to dominate. Setting the ratio F_B / F_S = 0.05 in equation 13 shows that the relative deformation above which bending is negligible is in the range ε_{crit} = 0.09 – 0.13. The gathered curves (with soft cantilevers) did not all exceed these thresholds, though they were close, meaning that the deformation in some cases was expected to be a mix of bending and stretching. Nevertheless, it was considered interesting to attempt fitting with membrane stretching where ε_{max} of the fitted region exceeded 0.06 (at 0.06 the contribution of the bending can be calculated theoretically to be 25% or below). The range of ε_{max} of the final data was between 0.07 and 0.16. Figure 6.32 shows the resulting Young's Modulus values ranging from 8 ± 0.5 to 72 ± 1 MPa and a visible increase in Young's modulus with increasing diameter.

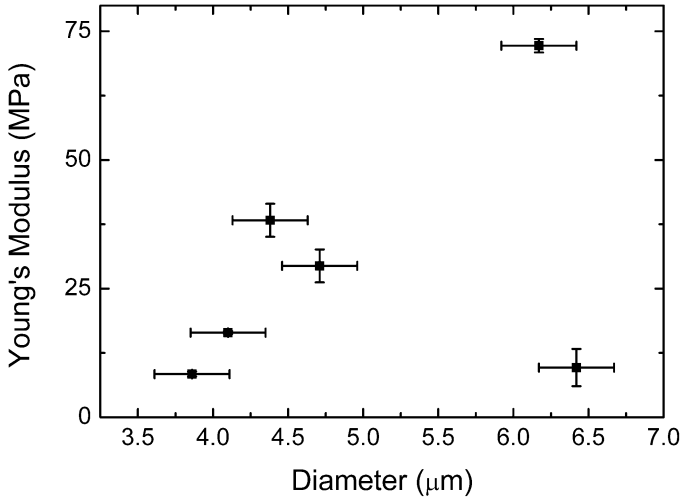

Figure 6.32 Young's modulus values for 6 MBs ranging in diameter from 3.86 µm to 6.42 µm calculated using the membrane stretching component of elastic membrane theory

Figure 6.33 shows the Young's modulus values calculated using De Jong theory in the low deformation region. The values range from 0.080 ± 0.006 to 0.200 ± 0.012 MPa. There is an indication of an increase of modulus with diameter.

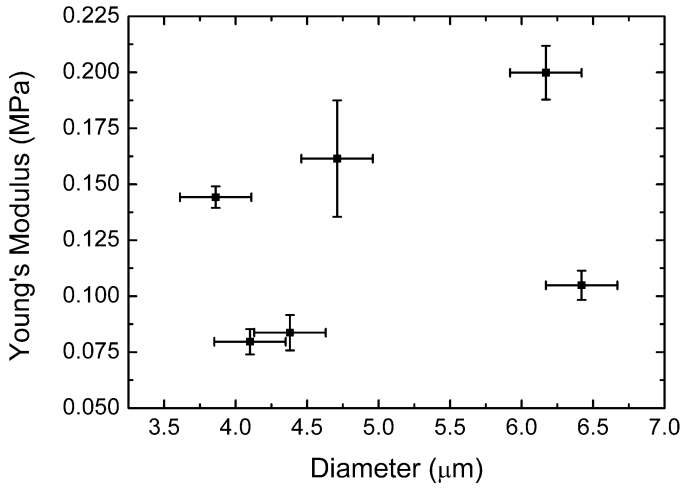

Figure 6.33 Young's modulus values for 6 MBs ranging in diameter from 3.86 µm to 6.42 µm calculated using De Jong theory.

Figure 6.34 shows the Young's modulus values calculated using Hertz theory in the low deformation region. The values range from 0.028 ± 0.001 to 0.080 ± 0.005 MPa.

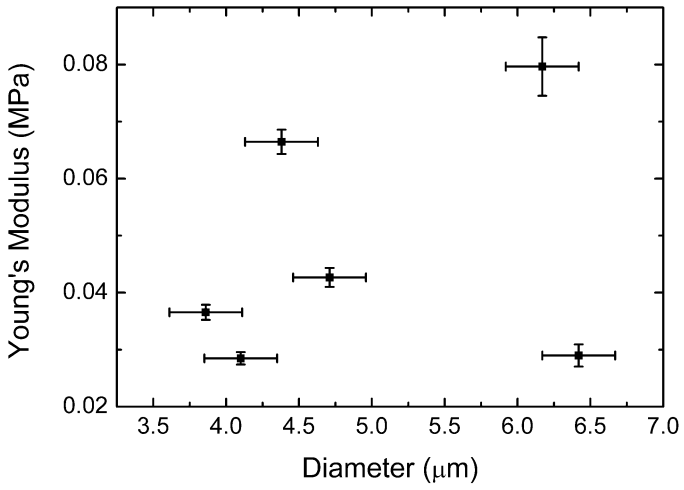

Figure 6.34 Effective Young's modulus values for 6 MBs ranging in diameter from 3.86 µm to 6.42 µm calculated using Hertz theory assuming sphere-plate geometry.

6.3.2 Hard Tipless Cantilevers

Sonovue® MBs were compressed with tipless cantilevers having measured spring constants in the range 0.247 – 0.408 N/m. After examining the recorded *F*–Δ curves for repeatability, 17 MBs were deemed suitable for further analysis. These MBs were spread across all three experimental batches and were included MBs tested on days 1, 2 and 3 of MB reconstitution. These MBs were subsequently analysed to determine their stiffness and the mechanical models used to evaluate Young's Modulus.

6.3.2.1 Stiffness

Multiple compressions were recorded on seventeen individual MBs ranging in diameter from 3.13 μm to 7.03 μm. In all cases the resulting *F*–Δ curves showed good repeatability indicating that no permanent deformation occurred as a result of the experiment. The effective stiffnesses of the MBs were calculated from the gradient of the initial linear section of the *F*–Δ curve with the first 25 nm of the curve excluded from the analysis. Figure 6.35 shows individual curves from three different MBs, having diameters 5.00, 5.75 and 3.13 μm and stiffnesses of 0.099 ± 0.002, 0.081 ± 0.005 and 0.047 ± 0.001 N/m respectively.

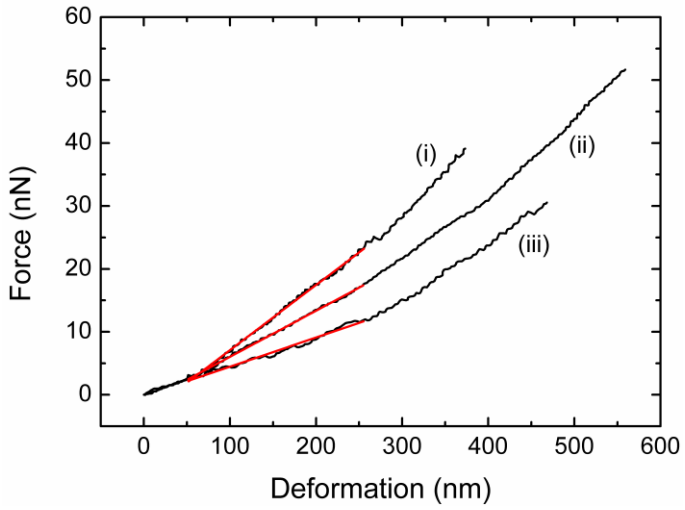

Figure 6.35 *F*-Δ curves for three different MBs. Red line shows initial linear region used to calculate MB stiffness. Curve (i) has diameter 5.00 μm and stiffness 0.099 N/m. Curve (ii) has diameter 5.75 μm and stiffness 0.081N/m, and curve (iii) has diameter 3.13 μm and stiffness 0.047 N/m. These MBs show no link between MB stiffness and initial radius.

Figure 6.36 shows the range of stiffnesses from 0.032 ± 0.002 to 0.136 ± 0.003 N/m. There no apparent correlation between MB diameter and stiffness.

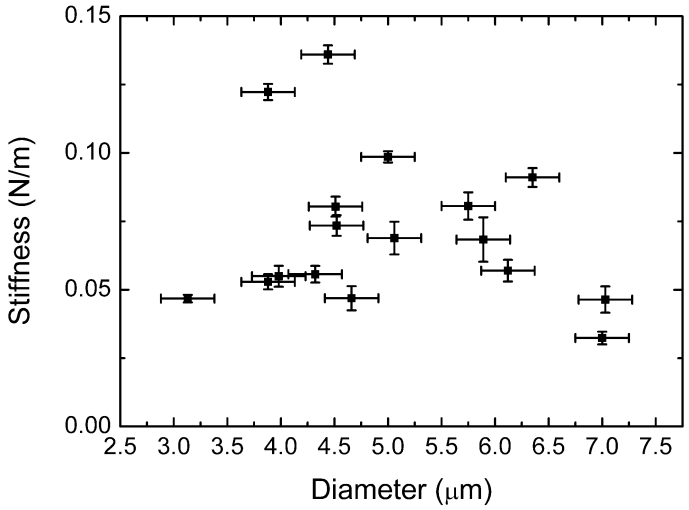

Figure 6.36 Effective stiffness values for 17 individual MBs ranging in diameter from 3.13 μm to 7.03 μm

6.3.2.2 Mechanical Models

For consistency with the other investigations, the MB shell thickness was assumed to be 5 nm. Analysis with the mechanical models was completed as in the preceding chapters. Figure 6.37 shows the values of Young's modulus for each bubble as calculated using Reissner theory. The values fall in the range of 1.08 ± 0.938 to 4.53 ± 0.112 GPa, with an indication of an increase in Young's modulus with increasing diameter.

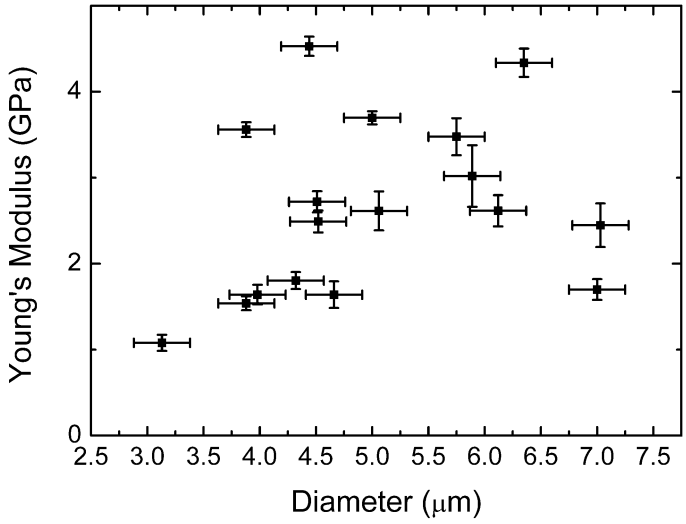

Figure 6.37 Young's modulus values for 17 MBs ranging in diameter from 3.13 µm to 7.03 µm calculated using Reissner theory

When considering the elastic membrane theory, at small deformations membrane bending should be the predominant mode of deformation. Using equation 13 as discussed in section 6.3.1.2, the value of ε_{crit} below which bending is the major mode of deformation is 0.01. Taking the gradient of the F–$\varepsilon^{1/2}$ curves from the experiment and substituting them into membrane bending equation produces Young's modulus values in the range 0.61 ± 0.06 to 4.74 ± 0.06 GPa, as shown in Figure 6.38. An increase in Young's modulus with increasing MB radius can be seen.

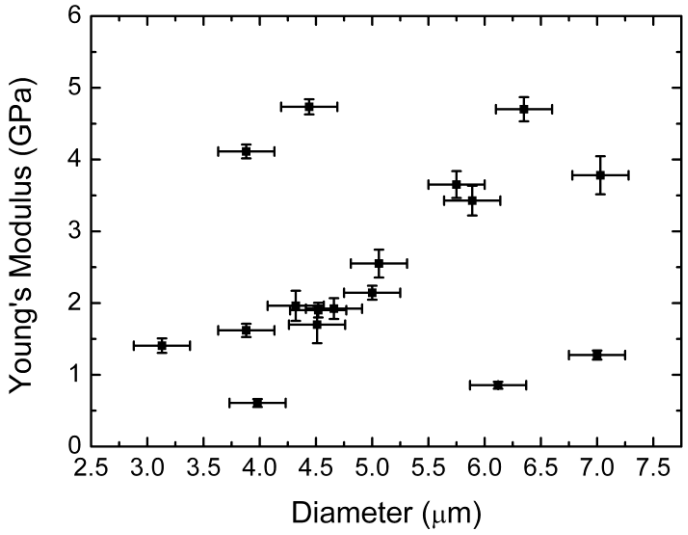

Figure 6.38 Young's modulus values for 17 MBs ranging in diameter from 3.13 µm to 7.03 µm calculated using the membrane bending component of elastic membrane theory

At larger deformations, membrane stretching should start to dominate, and the relative deformation above which bending is negligible is in the range ε_{crit} = 0.09 – 0.13. It was expected that experiments with hard cantilevers would be able to access this regime, however these MBs demonstrate more non-linear behaviour than the others studied, becoming stiffer at higher deformations. For this reason, not all of the MBs had ε_{max} values in the fitted region which exceeded the threshold for pure stretching. It was observed that the linear region of the F-ε^3 graphs did extend back into the mixed deformation regime so it was therefore still considered interesting to attempt fitting with membrane stretching where ε_{max} of the fitted region exceeded 0.05 (at 0.05 the contribution of the bending can be calculated theoretically to be 25% or below). This excluded one MB from this part of the analysis. The range of ε_{max} of the final data was between 0.07 and 0.19. Figure 6.39 shows the resulting Young's Modulus values ranging from 31 ± 2 to 233 ± 4 MPa and a visible increase

in Young's modulus with increasing diameter. It is interesting to note that the highest value (i.e. the outlier in the graph) corresponds to the lowest ε_{max} indicating that in the mixed regime this model might tend to overestimate the shell Young's modulus.

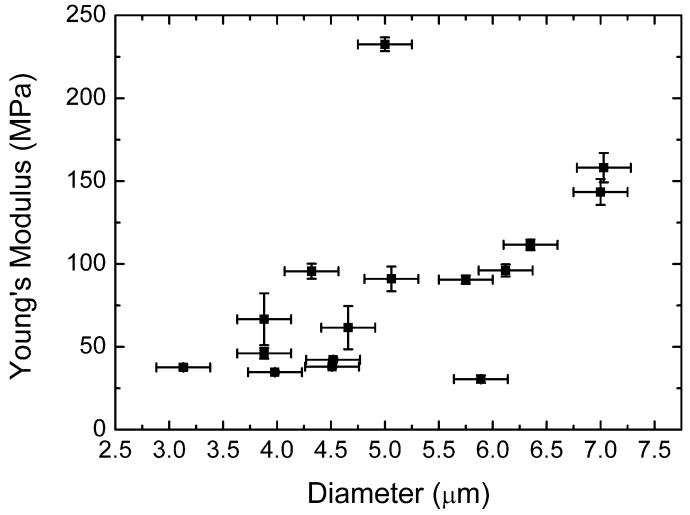

Figure 6.39 Young's modulus values for 16 MBs ranging in diameter from 3.13 µm to 7.03 µm calculated using the membrane stretching component of elastic membrane theory.

Figure 6.40 shows the Young's modulus values calculated using De Jong theory. The values range from 0.129 ± 0.009 to 0.541 ± 0.013 MPa, with no definitive trend.

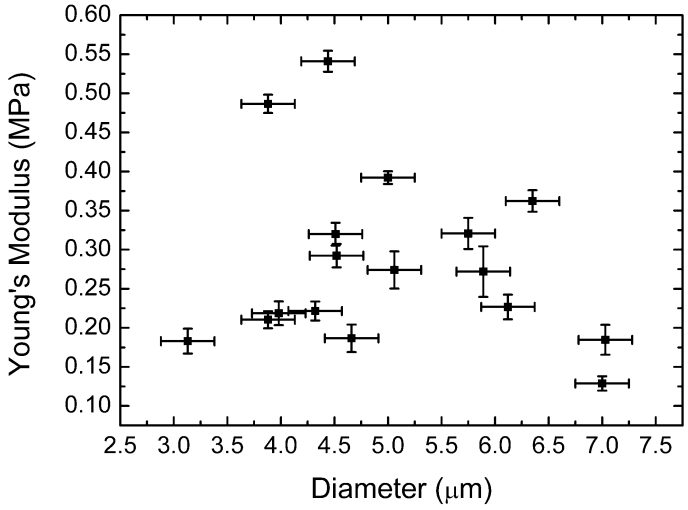

Figure 6.40 Young's modulus values for 17 MBs ranging in diameter from 3.13 µm to 7.03 µm calculated using De Jong theory.

Figure 6.41 shows the Young's modulus values calculated using Hertz theory at small deformations. The values range from 0.048 ± 0.005 to 0.219 ± 0.005 MPa, with no visible trend in Young's modulus with MB radius.

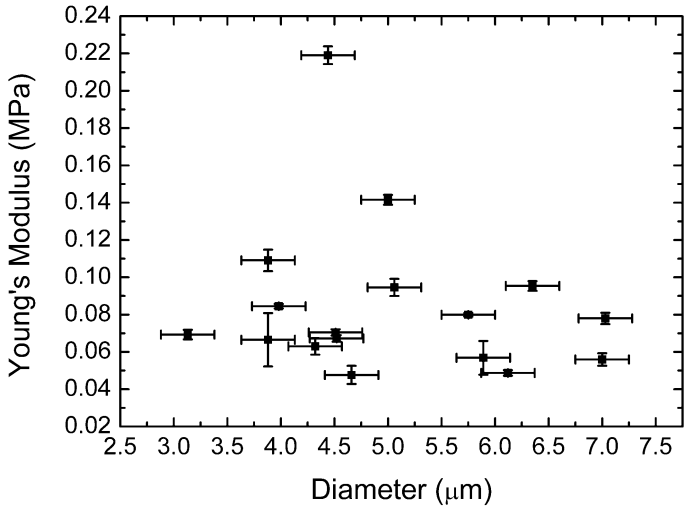

Figure 6.41 Effective Young's modulus values for 17 MBs ranging in diameter from 3.13 µm to 7.03 µm calculated using Hertz theory assuming sphere-plate geometry.

6.3.3 Tipped Cantilevers

Sonovue® MBs were compressed with tipped cantilevers having measured spring constants in the range 0.025 – 0.048 N/m. After examining the recorded *F*-Δ curves for repeatability, 15 MBs were deemed suitable for further analysis. These MBs were spread across all three experimental batches and were included MBs tested on days 1, 2 and 3 of MB reconstitution. These MBs were subsequently analysed to determine their stiffness and Hertz theory was used to evaluate the Young's modulus.

6.3.3.1 Stiffness

Multiple compressions were recorded on fifteen individual MBs ranging in diameter from 3.14 μm to 7.65 μm. In all cases the resulting *F*–Δ curves showed good repeatability indicating that no permanent deformation occurred as a result of the experiment. The effective stiffnesses of the MBs were calculated from the gradient of the initial linear section of the *F*–Δ curve. Figure 6.42 shows individual curves from three different MBs, having diameters 3.19, 5.76 and 3.40 μm and stiffnesses of 0.051 ± 0.003, 0.027 ± 0.003 and 0.015 ± 0.001 N/m respectively.

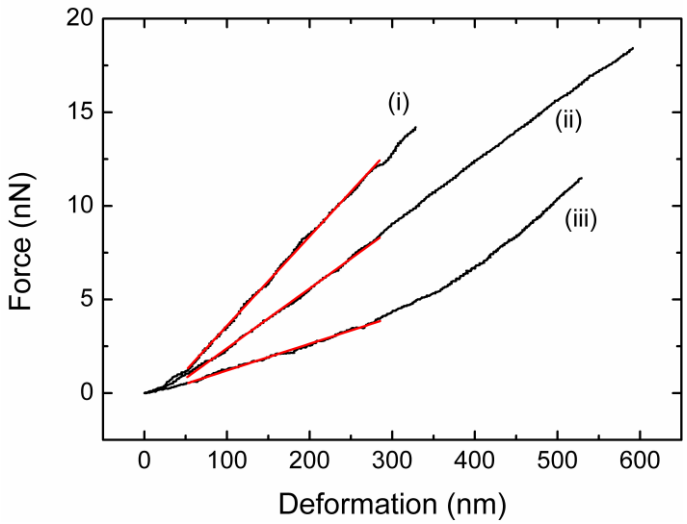

Figure 6.42 *F*-Δ curves for three different MBs. Curve (i) has diameter 3.19 µm and stiffness 0.051 N/m. Curve (ii) has diameter 5.76 µm and stiffness 0.027 N/m, and curve (iii) has diameter 3.40 µm and stiffness 0.015 N/m.

Figure 6.43 shows the range of stiffnesses from 0.013 ± 0.001 to 0.051 ± 0.003 N/m. There no apparent correlation between MB diameter and stiffness.

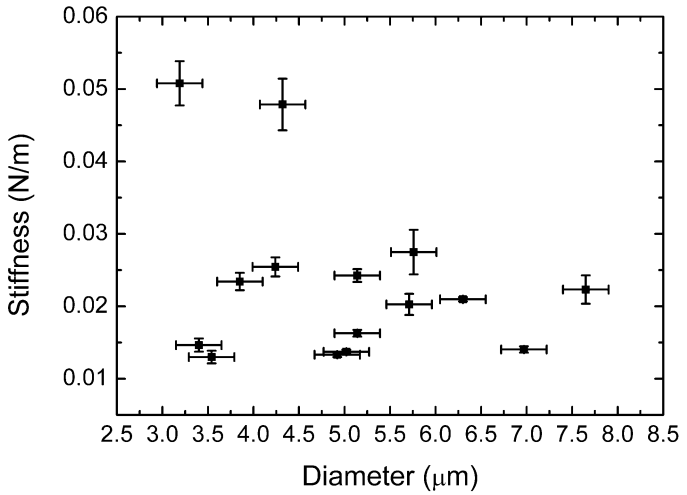

Figure 6.43 Effective stiffness values for 15 individual MBs ranging in diameter from 3.14 µm to 7.65 µm.

6.3.3.2 Hertz theory

Fitting using Hertz theory was completed assuming the geometry is best described as two spheres in contact. As it was not possible to measure the tip radius accurately, the nominal value of 20 nm provided by the manufacturer was used in calculations. The Young's modulus of each MB was calculated according to equation 11.

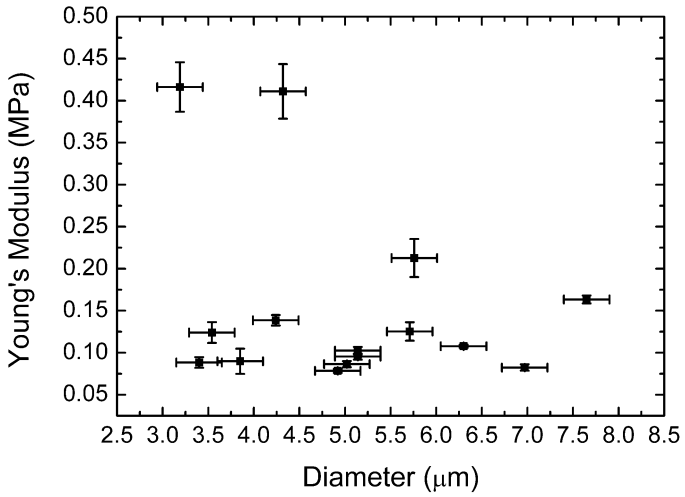

Figure 6.44 Young's modulus values of MBs as calculated with Hertz theory using sphere-sphere geometry.

Figure 6.44 shows the Young's modulus values in the range 0.078 ± 0.002 to 0.416 ± 0.030 MPa. There is no obvious correlation between MB diameter and Young's modulus.

6.3.4 Results Summary

The following tables summarise the key results from this study.

Cantilever Type	Cantilever Spring Constant (N/m)	MB Spring Constant (N/m)	Size Dependence Y/N
Tipless	0.027 – 0.044	0.020 – 0.136	N
Tipped	0.025 – 0.048	0.013 - 0.051	N

Table 6.2 Summary of Stiffness Results for the Experimental Examination of Sonovue® MBs

Cantilever Type	Mechanical Model	Deformation Regime	Shell / Sphere	Size Dependence Y/N	Young's Modulus
Tipless	Reissner	Low	Shell	Y	0.62 – 4.53GPa
Tipless	Membrane Stretching	High	Shell	Y	8 – 233 MPa
Tipless	Membrane Bending	Low	Shell	Y	0.61 – 4.74 GPa
Tipless	De Jong	Low	Shell	N	0.08 – 0.54 MPa
Tipless	Hertz	Low	Sphere	N	0.028 – 0.219 MPa
Tipped	Hertz	Low	Membrane	N	0.078 – 0.416 MPa

Table 6.3 Summary of Young's Modulus Results for the Experimental Examination of Sonovue® MBs

6.4 Discussion

The aim of this investigation was to study a third type of phospholipid coated MB, Sonovue®, with soft and hard cantilevers to comprehensively investigate both the low deformation and high deformation regimes. Tipped cantilevers were also employed to investigate how MB indentation varies from whole MB compression.

In the high deformation regime where membrane stretching dominates, the resulting Young's modulus values are in good agreement with those presented in literature for supported bilayers, [2] vesicles [3] and cells [4] which gives a collective range of 10 - 194 MPa. Our range of 31 – 233 MPa (hard cantilevers) is therefore a reasonable estimate of shell Young's modulus for this type of structure. Both the range of values and the observed trend in Young's modulus with diameter is similar to that observed in Definity® experiments, which is as we would expect given that we were operating in the same relative deformation regime, and supports our earlier findings. This similarity of results also indicates that the difference in phospholipid composition of the MB shell has a minimal impact on the mechanical behaviour.

At very small deformations the average observed MB stiffness appears to be somewhat higher for MBs compressed with hard cantilevers than with soft cantilevers, in ranges 0.032 – 0.136 N/m and 0.020 – 0.050 N/m respectively. There is significant overlap in this range, however, so the effect of cantilever stiffness on observed MB stiffness is quite small. Neither soft or hard cantilever experiments

showed a correlation between MB stiffness and MB diameter, which is a behaviour more akin to Definity® MBs than BR14. This is also in contrast to results of experiments on other constant-thickness MBs, [5] suggesting that Sonovue® MBs may also be subject to some variation in shell thickness. The behaviour of Sonovue® MBs was observed to be more non-linear than Definity® MBs at higher applied loads.

Young's modulus values at low deformations calculated with Reissner theory are in the 0.6 – 4.5 GPa range (hard and soft cantilever experiments combined range), which is a large overestimate compared to literature values of around 10 – 200 MPa [3, 6, 7] and closer to the 1.5 – 3 GPa found for polymeric capsules. [8] Soft cantilever values are slightly lower however there is good overlap between the two ranges. In both cases there is a definite increase in Young's modulus with increasing MB diameter, which is consistent with Definity® MBs.

In the low deformation regime, membrane bending is theoretically the appropriate part of the elastic membrane theory, however the 0.6 – 4.7 GPa range is again an overestimate compared to literature values in the 10 – 200 MPa range for non-AFM methods [3, 7] or the 10 – 30 MPa found using elastic membrane theory on Jurkat T lymphoma cells, though at somewhat higher deformations. [4] This probably suggests that at low deformations we have the influence of intermolecular forces (for example, repulsions from adsorbed PEG layers) that mask this mechanical term. Of course, we cannot be certain and it could be that the initial mechanism of deformation proposed in elastic membrane theory i.e. localised bending at the edges

of the contact area at the MB poles, may not match the physical behaviour of these MBs at low deformation. There is a definite increase in Young's modulus with increasing MB diameter, which is in opposition to the behaviour of BR14 MBs analysed by this method.

De Jong theory provides Young's modulus estimates in the 0.08 – 0.5 MPa range. These values are an underestimate;[3, 7] however the degree of underestimation is lower than the degree of overestimation of the previous two models. The values are very similar to those found for BR14 MBs, 0.3 – 0.75 MPa, and Sonovue® MBs show little to no trend with MB diameter, indicating that this model describes Young's modulus as an intrinsic property of the MB, even with the potential variation in MB shell thickness.

Hertz theory produces effective Young's modulus values for the MBs in the range 0.03 – 0.22 MPa. There is no trend in Young's modulus with MB diameter, which is akin to the behaviour of Definity® MBs but in contrast to BR14 which did show a link between modulus and diameter. The actual modulus values are close to those found for Definity®, which were in the range 0.09 – 0.23 MPa. They are also comparable to literature values for cells and vesicles investigated with Hertz theory.[4, 9-11] The values are lower than the values found with De Jong theory.

Tipped cantilever experiments yielded observed stiffness values between 0.013 and 0.051 N/m, which matches closely with tipless cantilever values. This suggests, as we would expect, that at low deformations the MB behaviour is dominated by the

membrane properties rather than shell geometry or the pressure of the filling gas. There is no link between stiffness and MB diameter, which supports the idea that we are probing a membrane property by means of indentation rather than a shell property by whole MB compression. The apparent stiffness of Sonovue® MBs is lower than that observed for BR14 MBs investigated with tipped cantilevers by about an order of magnitude. This may be due to the age of the BR14 MBs tested with tipped cantilevers; it seems that in fresher MBs there is better agreement between results gathered with tipless and tipped cantilevers. Analysis of tipped cantilever experiments to find values of the effective Young's modulus using Hertz theory shows no link between Young's modulus and MB radius, which is as we would expect for relatively small deformations of the membrane. The values themselves, 0.08 – 0.42 MPa, are very similar to the results from tipless cantilever experiments, 0.05 – 0.22 MPa (hard and soft cantilever results). Given that this is a comparison of two different expressions of Hertz theory, one for tipless and one for tipped cantilever experiments, the agreement between the two results is particularly noteworthy; to the best of my knowledge, this is the first time such a direct comparison has been made. The actual values are likely to be an underestimation overall; however the similarity to literature values (for Hertz theory) [4, 9-11] suggests that the model may still have some validity and could perhaps be the basis for a more comprehensive theoretical model in the future. These comparable values also support the idea that MB shell properties and membrane properties are closely related in the low deformation regime. When compared with the Young's modulus values of BR14 MBs tested with tipped cantilevers, we again see an order of magnitude difference between the two systems, with BR14 MBs having a Young's

modulus around 10 times that of Sonovue®. This is consistent with the similar finding for MB stiffness and probably due to the age of the BR14 samples at the time of testing.

6.5 Conclusions

This chapter has presented an experimental investigation of Sonovue® ultrasound contrast agent MBs using force spectroscopy with soft and hard tipless cantilevers and soft tipped cantilevers. The resulting F-Δ curves were used directly to calculate the stiffness of the MBs at low deformation. The resulting values range from 0.020 – 0.0136 N/m, with no link between stiffness and diameter. Tipless cantilever experimental data was used to calculate the Young's modulus of the MB shell using three different mechanical models. At low deformations De Jong theory was most suitable, yielding an average shell Young's modulus between 0.08 and 0.54 MPa. The other models, Reissner and the membrane bending component of elastic membrane theory, produced large overestimates of Young's modulus and showed dependence on MB diameter. Hertz theory was used to evaluate the effective Young's modulus of an equivalent homogeneous sphere having the same dimensions as the MB under test, yielding values in the range 0.028 – 0.22 MPa. Indentation experiments with tipped cantilevers yielded stiffness values and Young's modulus values from Hertz theory that were very close to those found from tipless cantilever experiments. At high deformations, the membrane stretching component of elastic membrane theory was quite effective, yielding an average shell Young's modulus

between 8 and 233 MPa. These results confirm our previous findings; as in the case of Definity®, in the high deformation regime membrane stretching yields Young's modulus values in the range we would expect, however a dependence on MB diameter has been observed which does not agree with the concept of Young's modulus as an intrinsic property, thus indicating some shell thickness variation (as with Definity). At low deformations Hertz and De Jong theories describe the MBs as having Young's modulus which is independent of MB diameter, though the values themselves are probably an underestimate.

References

[1] Schneider M. SonoVue, a new ultrasound contrast agent. European Radiology. 1999;9:S347-S8.

[2] Künneke S, Krüger D, Janshoff A. Scrutiny of the failure of lipid membranes as a function of headgroups, chain length, and lamellarity measured by scanning force microscopy. Biophysical Journal. 2004;86:1545-53.

[3] Rutkowski CA, Williams LM, Haines TH, Cummins HZ. The Elasticity of Synthetic Phospholipid-Vesicles Obtained by Photon-Correlation Spectroscopy. Biochemistry. 1991;30:5688-96.

[4] Lulevich V, Zink T, Chen HY, Liu FT, Liu GY. Cell mechanics using atomic force microscopy-based single-cell compression. Langmuir. 2006;22:8151-5.

[5] McKendry JE, Grant CA, Johnson BRG, Coletta PL, Evans JA, Evans SD. Force spectroscopy of streptavidin conjugated lipid coated microbubbles. Bubble Science, Engineering & Technology. 2010;2:48-54.

[6] Dieluweit S, Csiszár A, Rubner W, Fleischhauer J, Houben S, Merkel R. Mechanical Properties of Bare and Protein-Coated Giant Unilamellar Phospholipid Vesicles. A Comparative Study of Micropipet Aspiration and Atomic Force Microscopy. Langmuir. 2010;26:11041-9.

[7] Li W, Aurora TS, Haines TH, Cummins HZ. Elasticity of Synthetic Phospholipid-Vesicles and Submitochondrial Particles During Osmotic Swelling. Biochemistry. 1986;25:8220-9.

[8] Glynos E, Sboros V, Koutsos V. Polymeric thin shells: Measurement of elastic properties at the nanometer scale using atomic force microscopy. Materials Science and Engineering B-Advanced Functional Solid-State Materials. 2009;165:231-4.

[9] Janmey PA, McCulloch CA. Cell mechanics: Integrating cell responses to mechanical stimuli. Annual Review of Biomedical Engineering. 2007;9:1-34.

[10] Laney DE, Garcia RA, Parsons SM, Hansma HG. Changes in the elastic properties of cholinergic synaptic vesicles as measured by atomic force microscopy. Biophysical Journal. 1997;72:806-13.

[11] Mathur AB, Collinsworth AM, Reichert WM, Kraus WE, Truskey GA. Endothelial, cardiac muscle and skeletal muscle exhibit different viscous and elastic properties as determined by atomic force microscopy. Journal of Biomechanics. 2001;34:1545-53.

Chapter 7: General Conclusions and Future Work

7 General Conclusions and Future Work

7.1 General Conclusions

The purpose of this study was to use AFM force spectroscopy techniques to address a gap in the knowledge regarding the intrinsic mechanical properties of phospholipid coated MBs under direct mechanical loading. Gaining this knowledge is a necessary step in the process of adapting such MBs away from their initial function as ultrasound contrast agents into a wider variety of applications such as targeted drug/gene delivery. The systematic investigation of three different phospholipid MBs systems validates the experimental and analytical techniques which had previously only been applied MBs with a much stiffer polymeric coating.

In the high deformation regime we have demonstrated that membrane stretching is a good predictor of MB mechanical properties. This result is verified across two phospholipid MB systems. Possible variations in shell thickness were identified, which have implications for the manufacturing processes used to create these MBs.

In the low deformation regime, we have used several different models. Reissner theory is not a good predictor of MB behaviour for phospholipid MBs despite its success in the case of polymeric MBs, suggesting that it is perhaps only useful in the case of hard shelled MBs. Membrane bending is also not a very successful model. It

is possible that this is because at these very low forces where membrane bending dominates, confounding factors such as the PEG brush layer surrounding the MB affect the force-deformation behaviour observed by the AFM. De Jong theory shows potential for further development as it shows no size dependent effects, however the overall values underestimate Young's Modulus. There is also the possibility that the MB behaviour is simply quite non-linear and that they may demonstrate different Young's modulus values in different deformation regimes.

Hertz theory provides interesting information about the MB as a homogeneous sphere rather than a shell structure. The values of effective Young's modulus are likely to be underestimates but the good agreement between experiments involving tipped and untipped cantilevers suggests that Hertz theory may be a good starting point for the development of more comprehensive models in the future.

7.2 Future Work

There is still significant scope for further investigation of the mechanical properties of MBs, both experimentally and theoretically. First and foremost, the results presented in this thesis can be used as the basis of a theoretical study aiming to produce a comprehensive mechanical model of MB behaviour, particularly at low deformations. It seems that some models might contain the correct functional relationship with radius but they need further investigation as far as the coefficients

are concerned. In other words, this study shows that the continuum approach could still be relevant in this small scale but with some modifications.

In terms of further experimental work, the next step would be to expand the investigation of MB deformation under tipped cantilevers into the high deformation regime (still within the boundaries of small deformations overall) and study the mechanical behaviour up to rupture. Furthermore, one could go to large deformations ($\varepsilon > 0.3$ with tipped and tipless cantilevers) in order to provide data and develop a gas-related model. This is very important for the ultrasound applications where the range of deformation could be large and lead to rupture.

As discussed, the issue of MB thickness is very important when characterising the behaviour of the MBs. It would be advisable to attempt to conclusively demonstrate the actual thickness of the MBs used in this study experimentally. This could potentially be achieved using equipment already available within the group by collapsing bubbles onto a surface with a sharp tipped cantilever then using an imaging AFM to examine the thickness of the collapsed MB shell. Other options would require the use of other experimental techniques, but have a greater chance of producing good results. These techniques include confocal microscopy or total internal reflection (TIRF) microscopy, where a thickness could be found without having to expose the MB shell to vacuum (as would be necessary for scanning electron microscopy (SEM) or transmission electron microscopy (TEM)), which could cause structural changes in the phospholipid shell.

I would also recommend a thorough investigation of the effect of probe geometry on MB behaviour. Cantilevers with tips of decreasing radius of curvature could be used to investigate experimentally whether the use of model which assume point loading is actually acceptable. This information would be particular use to those who wish to improve the modelling of MB deformation.

Also of great potential use to MB modellers would be an investigation into the symmetry, or lack thereof, of MB deformation over the course of a compression experiment. This could potentially be achieved by the use of confocal microscopy to record the changes in contact area on both the top and bottom poles of the MB during a compression cycle.

Appendices

Appendix A: Related Publication

Buchner-Santos, E, Morris, JK, Glynos, E, Sboros, V & Koutsos, V. Nanomechanical properties of phospholipid microbubbles. Langmuir. 2012, 28, 13; 5753-5760. DOI: 10.1021/la204801u